Functional characterisation of A_{2A} receptor thermostable mutants using a yeast signalling assay

Nicolas Bertheleme

Membrane Protein Crystallography Laboratory

Department of Life Sciences

Imperial College London

Thesis submitted for the Degree of Doctor of Philosophy

2014

Abstract

G-protein-coupled receptors (GPCR) are transmembrane proteins that play a crucial role in the communication of cells with their external environment. In the last few years, several GPCR crystal structures have been solved using genetically engineered protein. The turkey β1-adrenergic receptor, the human neutrotensin 1 receptor and the adenosine A_{2A} receptor ($A_{2A}R$) structures involved the introduction of stabilizing mutations. The engineered mutant can be stabilized in an agonist or an antagonist bound conformation making the GPCR less flexible and therefore easier to crystallize. The aim of this study was to use functional characterization of the key thermostabilising mutants of the $A_{2A}R$ in order to understand the molecular basis of the thermostabilisation. The different mutants were characterized using a yeast-based growth assay, which measures down-stream signaling in response to agonist and radioligand binding analysis using both an agonist and an antagonist. Point mutations leading to a reduction/loss of constitutive receptor activity have been identified. In addition, a single point mutation abolishing the ability of receptor to bind the agonist NECA has also been identified. Conformational stabilization of the receptor is thus achieved by reducing basal activity along with modifying the ligand-binding pocket leading to inability to bind agonist. Such markers can be used to screen for stable mutants for structural characterization. Since thermostabilising mutations are not directly transferable across receptors, the yeast based growth assay could serve as a quick and inexpensive way to screen for mutations for a wide range of GPCRs.

Declarations

Declaration of originality:

I declare that the work described in this thesis is my own and that it has not been accepted in any previous application for a higher degree. All sources of information are referred to as appropriate.

Declaration of copyright:

The copyright of this thesis rests with the author and is made available under a Creative Commons Attribution Non-Commercial No Derivatives licence. Researchers are free to copy, distribute or transmit the thesis on the condition that they attribute it, that they do not use it for commercial purposes and that they do not alter, transform or build upon it. For any reuse or redistribution, researchers must make clear to others the licence terms of this work.

Acknowledgments

First, I would like to thank Dr. Bernadette Byrne, my principal supervisor for taking me on board for this project, for her unconditional help and support and in making my PhD enjoyable.

I am also very grateful to Dr. Simon Dowell, my industrial supervisor, who is always very helpful. I thank him for his very pertinent advice as well as for his patience towards me.

All my gratitude also goes to Dr. Julia Hubbard who initiated this project and showed incredible patience while guiding me through my initial training in the GlaxoSmithKline laboratories.

I am thankful to Dr. Shweta Singh and Dr. Minghao Zhang for their constant help and advice. Without their contributions my work would not have been so fruitful to say the least.

Finally, I would like to thank Dr. James Leung, Dr. David Grose, Dr. Ashley Barnes, Dr. Mike Hann, Dr Kate Smith, Dr Danuta Mossakowska for helpful discussions and precious advise. I am particularly grateful to Prof Philip Strange for his insights into models of GPCR activation. I also wish to thank Sam for looking after us in the lab and for making it a safe place to work.

Table of Contents

1 INTRODUCTION 15

1.1 OVERVIEW 16

1.1.1 G-PROTEIN COUPLED RECEPTORS 16

1.1.2 STRUCTURAL CHARACTERISTICS OF GPCRS 17

1.2 GPCR ACTIVATION AND SIGNALLING PATHWAYS 20

1.2.1 LIGAND BINDING MODELS 20

1.2.2 G PROTEIN ACTIVATION AND SIGNALLING PATHWAYS 22

1.2.3 OTHER PROCESSES IN THE GPCR ACTIVATION CYCLE 29

1.3 BIASED AGONISM AND MULTIPLE ACTIVE CONFORMATIONS 33

1.3.1 G PROTEIN INDEPENDENT SIGNALLING 33

1.3.2 BIASED AGONISM 35

1.4 STRUCTURE DETERMINATION OF GPCRS 37

1.4.1 EXPRESSION OF GPCRS 38

1.4.2 STABILISATION OF GPCRS FOR STRUCTURAL STUDIES 41

1.5 STRUCTURAL INSIGHT 53

1.5.1 COMPARISON OF CRYSTALS STRUCTURES OBTAINED USING DIFFERENT APPROACHES 53

1.5.2 THE LIGAND-BINDING POCKET OF GPCRS 57

1.5.3 STRUCTURAL CHANGES IN GPCRS UPON ACTIVATION 61

1.6 THE ADENOSINE RECEPTORS FAMILY 68

1.7 AIM OF THE STUDY 70

2 DEVELOPMENT OF THE YEAST FUNCTIONAL ASSAY 72

2.1 INTRODUCTION 73

2.2 MATERIALS AND METHODS 77

2.2.1 MATERIALS 77

2.2.2 CONSTRUCT GENERATION 77

2.2.3 EXPRESSION VECTOR OPTIMIZATION 78

2.2.4 IN-GEL FLUORESCENCE 80

2.2.5 CONFOCAL MICROSCOPY 81

2.2.6 YEAST CELL GROWTH ASSAY 82

2.2.7 OPTIMISATION OF ASSAY CONDITIONS 83

2.3 RESULTS 84

2.3.1 P306GPD VECTOR IS THE MOST SUITABLE VECTOR FOR THE YEAST FUNCTIONAL ASSAY 84

2.3.2 INCUBATION TIME AND 3AT CONCENTRATION ARE CRITICAL 86

2.4 DISCUSSION 90

3 FUNCTIONAL CHARACTERIZATIONS OF THE RAG23, RANT5, RANT21 AND SOME INTERMEDIATE MUTANTS 93

3.1 INTRODUCTION 94

3.2 MATERIAL AND METHODS 96

3.2.1 MATERIAL 96

3.2.2 SITE-DIRECTED MUTAGENESIS 96

3.2.3 EXPRESSION 97

3.2.4 MEMBRANE PREPARATION 99

3.2.5 PROTEIN CONCENTRATION 99

3.2.6 SATURATION BINDING ASSAY 100

3.2.7 COMPETITION BINDING ASSAY 101

3.2.8 YEAST CELL GROWTH ASSAY 102

3.3 RESULTS 103

3.3.1 EXPRESSION LEVELS 103

3.3.2 PHARMACOLOGICAL PROFILES OF THE WT AND MUTANTS $A_{2A}R$ 105

3.4 DISCUSSION 116

3.4.1 THERMOSTABILISATION AND FUNCTIONAL PROFILES 116

3.4.2 CONSTITUTIVE VERSUS AGONIST-INDUCED ACTIVITY 118

3.4.3 THE ROLE OF T88 IN AGONIST BINDING AND RECEPTOR ACTIVATION 120

3.4.4 THE ROLE OF V239 IN THE LOSS OF CONSTITUTIVE ACTIVITY 121

4 FUNCTIONAL CHARACTERIZATION OF THE INTERMEDIATE MUTANTS BETWEEN THE RAG23 AND THE WILD-TYPE $A_{2A}R$ 124

4.1 INTRODUCTION 125

4.2 MATERIALS AND METHODS 127

4.2.1 MATERIALS 127

4.2.2 SITE-DIRECTED MUTAGENESIS 127

4.2.3 EXPRESSION 128

4.2.4 YEAST CELL GROWTH ASSAY 128

4.3 RESULTS 129

4.3.1 EXPRESSION LEVELS 129

4.3.2 F79A ENHANCES CONSTITUTIVE ACTIVITY AND POTENCY 130

4.3.3 R199A REDUCES CONSTITUTIVE ACTIVITY AND POTENCY 134

4.3.4 L208A MUTATION REDUCES CONSTITUTIVE ACTIVITY AND EFFICACY 136

4.3.5 THE EFFECTS OF A184L AND L272A ARE OVERCOME BY THE OTHER MUTATIONS 138

4.4 DISCUSSION 141

4.4.1 STRUCTURAL BASIS OF THE EFFECTS OF THE F79A MUTATION 141

4.4.2 STRUCTURAL BASIS OF THE EFFECTS OF THE R199A AND L208A MUTATIONS 144

4.4.3 STRUCTURAL BASIS FOR THE EFFECTS OF THE A184L AND L272A MUTATIONS 146

5 DISCUSSION AND FUTURE OUTLOOK 148

5.1 AGONIST-INDUCED AND CONSTITUTIVE ACTIVE CONFORMATIONS ARE DISTINCT 150

5.2 ROLE OF INDIVIDUAL RESIDUES IN RECEPTOR FUNCTION AND STABILISATION 151

5.2.1 T88 PLAYS A CRUCIAL ROLE FOR AGONIST-INDUCED ACTIVITY 151

5.2.2 ROLE OF INDIVIDUAL RESIDUES ON CONSTITUTIVE ACTIVITY 152

5.3 THE YEAST FUNCTIONAL ASSAY AS A SCREENING TOOL 154

5.4 FUTURE OUTLOOK 155

6 APPENDIX 174

6.1 GRAPHICAL DATA FOR ALL THE RAG23 INTERMEDIATE MUTANTS 174

6.2 PERMISSION TO REPUBLISH THIRD PARTY COPYRIGHTED WORK FROM CHAPTER 3 178

6.3 YEAST TRANSFORMATION PROTOCOL 179

List of figures

Figure 1-1 Different types of ligands and their efficacies. 19
Figure 1-2 The ternary complex model. 20
Figure 1-3 The extended ternary complex model. 21
Figure 1-4 The cubic ternary complex model. 22
Figure 1-5 Schematic of the activation steps of a GPCR. 24
Figure 1-6 Structure of the $G\alpha_i$ 25
Figure 1-7 Crystal structure of a $G\alpha$ subunit 26
Figure 1-8 Structure of the $\beta\gamma$ subunit of the G_i 27
Figure 1-9 Crystal structure of the β_2AR in complex with G_S 29
Figure 1-10 GPCR desensitization, degradation and resensitization mechanisms. ... 32
Figure 1-11 Superimposition of the β_2AR structure fused to T4L with the β_2R structure in complex with a Fab 43
Figure 1-12 Structure of the β_2R, the Nociceptin/orphanin FQ receptor and the corticotropin-releasing factor receptor 45
Figure 1-13 Comparison of the active and inactive-state structures of the β_2AR 47
Figure 1-14 High resolution structure of the β_2AR 48
Figure 1-15 High resolution structures of thermostable mutants 51
Figure 1-16 Comparison of the structures of the A_{2A}R bound to ZM241385 54
Figure 1-17 Superposition of the "bent" and "straight" conformations of the β_1AR bound to the antagonist carazolol 55
Figure 1-18 Comparison of the structures of the A_{2A}R bound to ZM241385 and UK-432097 56
Figure 1-19 Ligand binding cradle of the human κ-opioid receptor 57
Figure 1-20 Interactions between different ligands and the β_1AR 59
Figure 1-21 Extra interactions between bucindolol and the β_1AR 61
Figure 1-22 Superimposition of the structures of the A_{2A}R bound to the agonist NECA and bound to the inverse agonist ZM241385. 62
Figure 1-23 Superposition of the opsin and rhodopsin structures 64

Figure 1-24 Superposition of the opsin and rhodopsin (cyan) 65
Figure 1-25 Superimposition of the structures of β_2AR in an inactive conformation and in an active conformation 66
Figure 1-26 Snake plot showing the position of the mutations for the thermostable mutants 71
Figure 2-1 Structure of the A_{2A}R as a fusion protein with the T4L (A) and in complex with a Fab (B). 73
Figure 2-2 Yeast growth functional assay. 76
Figure 2-3 Schematic representation of the adenosine A_{2A}R constructs. 79
Figure 2-4 SDS-PAGE In-gel fluorescence analysis of Rant5 and Rag23. 84
Figure 2-5 Confocal imaging for Rag23. 85
Figure 2-6 Confocal imaging for Rant5 (B). 86
Figure 2-7 Incubation time optimization using the Rag23 mutant. 87
Figure 2-8 3AT concentration optimization. 88
Figure 2-9 Effect of ADA. 89
Figure 3-1 Dose-response curve illustrating the concepts of efficacy, potency and constitutive activity. 95
Figure 3-2 Functional data for the thermostabilised A_{2A} mutants Rag23, Rant5 and Rant21 compared to WT. 105
Figure 3-3 Pharmacological profiles of four different ligands. 106
Figure 3-4 Saturation binding of [^{3}H]ZM241385. 107
Figure 3-5 Competition binding assy using NECA. 108
Figure 3-6 Saturation binding assay using [^{3}H]NECA. 110
Figure 3-7 Functional data for the thermostabilised A_{2A} intermediate mutants. 111
Figure 3-8 Activity of the T88A mutant compared to wild-type A_{2A}R. 113
Figure 3-9 Effect of high concentrations of adenosine. 114
Figure 3-10 Functional characterization of the A54L+V239I mutant. 115
Figure 3-11 An extended cubic ternary complex model. 119
Figure 3-12 Interaction between the Thr88 of the A_{2A}R and NECA. 121
Figure 3-13 Superposition of helices III and VI of the inactive thermostabilized A_{2A}R mutant. 122
Figure 4-1 Functional profiles of constructs illustrating the major effects of the F79A mutation. 131

Figure 4-2 Functional profiles of constructs illustrating the major effects of the R199A mutation. 135
Figure 4-3 Functional profiles of constructs illustrating the major effects of the L208A mutation..... 137
Figure 4-4 Functional profiles of constructs illustrating the major effects of the A184L mutation..... 139
Figure 4-5 Functional profiles of constructs illustrating the major effects of the L272A mutation..... 140
Figure 4-6 Position of the F79, R199A, L208, A184 and L272 residues in the high-resolution crystal structure of the $A_{2A}R$. 143
Figure 4-7 Structure of the β_2AR in complex with G_S protein..... 145
Figure 5-1 Position of the R199 residue of the $A_{2A}R$ or its equivalent R221 of the β_2AR in an inactive conformation (A), in a partially active conformation (B) and in a fully active conformation (C). 153

List of tables

Table 1-1 Point mutations contained in the different thermostable constructs studied *70*
Table 2-1 Primers used to clone the $A_{2A}R$ mutant genes in the pDDGFP vector by homologous recombination. The primer contains a gene specific sequence and an overhang region used for the homologous recombination into 2 μ S. cerevisiae GFP-fusion vector. *78*
Table 2-2 Mutagenic primers used to generate the intermediate mutant $A_{2A}R$ constructs. *78*
Table 3-1 Mutagenic primers used to generate the intermediate mutant and wild-type $A_{2A}R$ constructs. *97*
Table 3-2 Expression levels of the different $A_{2A}R$ + eGFP constructs in the MMY24 strain. *103*
Table 3-3 Pharmacological characteristics of the wild-type and mutants A_{2A} forms. *106*
Table 3-4 K_d and K_i values for the different $A_{2A}R$ forms obtained from saturation and competition binding assay using [^{3}H] ZM235481 and [^{3}H]NECA as hot ligand and NECA and Adenosine as cold ligand. *110*
Table 3-5 Pharmacological characteristics of the intermediate mutants. Data are presented as mean ± standard error means of at least two independent experiments performed in triplicate. *112*
Table 3-6 Comparison of the NECA and adenosine binding and activation profile of T88A *113*
Table 4-1 Mutagenic primers used to generate the Rag intermediate mutant $A_{2A}R$ constructs. *127*
Table 4-2 Expression levels of the thirty mutants and the wild-type calculated using the eGFP fluorescence as described by Drew et al. *129*
Table 4-3 Constitutive activities, potencies and efficacies of the Rag intermediate mutants. *133*

List of abbreviations

Abbreviation	Definition
3AT	3-Amino Triazole
β_1AR	β_1 Adrenergic Receptor
β_2AR	β_2 Adrenergic Receptor
A_{2A}R	Adenosine A_{2A} Receptor
A_{2B}R	Adenosine A_{2B} Receptor
ADA	Adenosine Deaminase
AMP	Adenosine MonoPhosphate
AOX	Alcohol Oxidase
$AT1_AR$	Angiotensin 1_A receptor
ATP	Adeonsine Triphosphate
BSA	Bovine Serum Albumin
cAMP	Cyclic Adenosine MonoPhosphate
CCD	Charge Couple Device
DDM	n-Dodecyl-β-D-Maltoside
DM	n-Decyl-β-D-Maltoside
DMSO	Dimethyl Sulphoxide
DPM	Disintegration Per Minute
ECL	Extracellular loop
EDTA	Ethylenediaminetetraacetic Acid
EGFR	Epidermal Growth Factor
EGTA	Ethylene Glycol Tetraacetic Acid
EP4	Prostaglandin E receptor type 4
ERK	Extracellular signal-Regulated Kinase
FDGlu	Fluorescein-Di-β-glucopyranoside
GEF	Guanine nucleotide Exchange Factor
GDP	Guanine Diphosphate
GFP	Enhanced Green Fluorescent Protein
GPCR	G Protein Coupled Receptor
GRK	G protein coupled Receptor Kinase
GTP	Guanine Triphosphate
HEK293	Human Embryonic Kidney 293 cells
ICL	Intracellular Loop
IP3	Inositol Trisphosphate
JNK3	c-Jun N-terminal Kinase 3
K_D	Dissociation Constant
Ki	Inhibition Constant
MAPK	Mitogen Activated Protein Kinase
NECA	5'-N-Ethylcarboxamidoadenosine
NMR	Nuclear Magnetic Resonance
NTS1	Neurotensin receptor 1

OD_{600}	Optical Density at 600nm
PAR2	Protease-Activated Receptor 2
PBS	Phosphate Buffered Saline
PCR	Polymerase Chain Reaction
PDB	Protein Data Bank
PI	Protease Inhibitor
PIP2	Phosphatidylinositol 4,5 bisphosphate
PKA	Protein Kinase A
PKC	Protein Kinase C
PP2A	Protein Phosphatase 2
RFU	Relative Fluorescence Unit
RGS	Regulators of G protein Signalling
SAR	Structure Activity Relationship
SDS	Sodium Dodecyl Sulfate
SDS PAGE	SDS Polyacrylamide Gel Electrophoresis
T4L	T4 Lysozyme
TCA	TriChloro Acetic Acid
TM	TransMembrane
WT	Wild Type
YNB	Yeast Nitrogen Base
YSB	Yeast Suspension Buffer
ZM241385	4-(2-[7-Amino-2-(2-furyl)[1,2,4]triazolo[2,3-a][1,3,5]triazin-5-ylamino]ethyl)phenol

1 Introduction

1.1 Overview

The plasma membrane plays a major role in maintaining cell integrity by separating the inside of the cell from its external environment. However, it is essential for the cell to be able to respond to changes in the extracellular environment. This is done through the action of integral membrane proteins, which span the phospholipid bilayer composing the plasma membrane. These receptors mediate the cellular responses to a range of bioactive molecules such as hormones, neurotransmitters and a large number of drugs.

1.1.1 G-protein coupled receptors

G-protein coupled receptors (GPCRs) form the largest family of integral membrane protein with ~800 members (Gloriam *et al.*, 2007). Various external stimuli such as light, odorants, amino acids, nucleotides, nucleosides, neurotransmitters, hormones or peptides can interact with the extracellular side of the GPCRs and this triggers a conformational change of the receptor, allowing binding and activation of an intracellular heterotrimeric G protein. Once activated by the receptor, this G protein is able to interact with secondary effectors to induce a cellular response (Howard *et al.*, 2001). It is estimated that between 30 and 50 % of all modern drugs and 25 % of the top 100 best selling drugs target GPCRs (Hopkins & Groom, 2002; Klabunde & Hessler, 2002). Their importance in terms of cellular function and as potential drug targets means that they have been subject to intense study.

GPCRs have previously been classified into five families based on their sequence homology and structural similarities. The first one is the rhodopsin family or

family A and is by far the largest family with a total of 701 members including 241 non-olfactory receptors. The second one is the secretin family or family B, which comprises 15 receptors. The glutamate family also known as family C is composed of 15 receptors. Finally, the adhesion and Frizzled/Taste2 families comprise 24 receptors each (Fredriksson *et al.*, 2003).

1.1.2 Structural characteristics of GPCRs

All GPCRs share a very similar basic structure comprising seven transmembrane α-helices (7TM) separated by alternating intracellular and extracellular loop regions, an extracellular N-terminus and an intracellular C-terminus (Fredriksson, 2005). In addition to these common transmembrane domains, each family has its own characteristics. The receptors belonging to the rhodopsin subfamily share several features; a single conserved cysteine residue in the first two extracellular loops, three conserved residues known as the E/DRY motif located on helix III (Howard *et al.*, 2001), the CWxPFF motif in the top region of helix VI (Shi & Javitch, 2002) and the NPxxY motif on helix VII (van Rhee & Jacobson, 1996). All these conserved features are believed to be involved in receptor stability or activation.

The receptors from the family B bind large peptides and their large N termini (~150-180 amino-acids) contain three conserved cysteine bridges (Wheatley *et al.*, 2012). Furthermore, the structures of N termini of several Family B receptors in complex with their cognates ligand from different family B receptors allowed the identification of a common fold known as “the secretin family recognition fold” (Parthier *et al.*, 2009) believed to be crucial for ligand recognition and binding.

The metabotropic glutamate receptors of family C also have large N termini (280 to 580 amino acids), containing the ligand recognition site. The N termini of the

receptors of the adhesion family can vary between 200 to 2800 amino acids in length and are usually rich in glycosylation sites and contain motifs believed to be involved in cell adhesion (McKnight & Gordon, 1998; Stacey *et al.*, 2000).

The Frizzled/Taste2 family comprises two different groups of receptors. The main difference between the two groups is their N terminus, which is small and unlikely to contain a ligand recognition domain in the Taste2 receptor while it is much longer in the frizzled receptors. However, these two groups share several features such as an IFL motif in helix II, an SFLL motif in helix V and an SxKTL motif in helix VII (Fredriksson *et al.*, 2003).

However, the overall sequence homology between GPCRs is low particularly in the extracellular loop regions, most likely as a result of the requirement for recognition and binding of a wide range of ligands (Peeters *et al.*, 2010). GPCRs exhibit significant conformational flexibility reflecting a number of functional states (Kobilka & Deupi, 2007). Agonists cause full activation of the receptor whereas partial agonists induce submaximal activation of the G protein even at saturating concentrations. In addition, it is well documented that many GPCRs exhibit constitutive, agonist-independent activity, activating their cognate G proteins in the absence of agonist (Milligan *et al.*, 1995; Strange, 2002). Antagonists inhibit ligand binding but do not affect constitutive activity, while inverse agonists decrease constitutive activity (Fig 1-1). This range of efficacies shows the complexity of the activation mechanism of GPCRs. These receptors were usually considered as switching between two states, active and inactive but now there is growing evidence to suggest multiple active and inactive states (Kahsai *et al.*, 2011; Riitano *et al.*, 1997; Rosenbaum *et al.*, 2009; Scaramellini & Leff, 1998). The wide range of conformations adopted by the GPCRs make them particularly flexible and unstable

proteins (Fredriksson *et al.*, 2003).

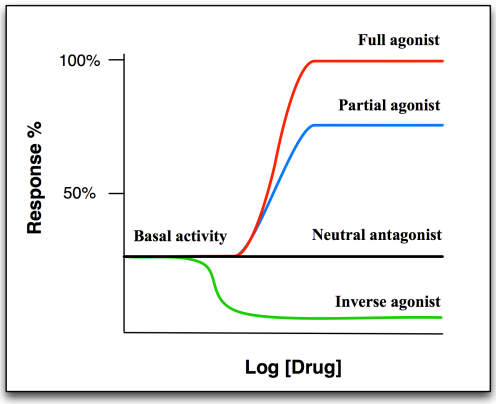


Figure 1-1 The level of GPCR activation in the presence of different ligands. Many GPCRs have been reported to be constitutively active and hence show a basal level of activation (black line) even in the absence of ligands. Full activation of the receptor is achieved with full agonists (red line), whereas partial agonists are only able to partially activate the receptor (blue line). Inverse agonists (green line) are able to inhibit the basal level of activation of receptor. An antagonist (black line) binds to the receptor and inhibits an agonist from activating the receptor however it has no effect on the constitutive activity of the GPCR.

1.2 GPCR activation and signalling pathways

1.2.1 Ligand binding models

The interactions between the receptor, a G protein and an agonist have been described by the "Ternary complex model" (De Lean *et al.*, 1980). Historically, this model was developed to account for the unique properties of agonist binding to the frog erythrocyte β-adrenergic receptor, which included low affinity and high affinity states. De Lean and co-workers explained these experimental data by the intervention of a third component: a G protein (Fig 1-2). The binding of the G protein to the receptor increases the affinity of the agonist for the receptor accounting for the high affinity state observed, while the low affinity state is when the agonist binds to the receptor unbound to the G protein.

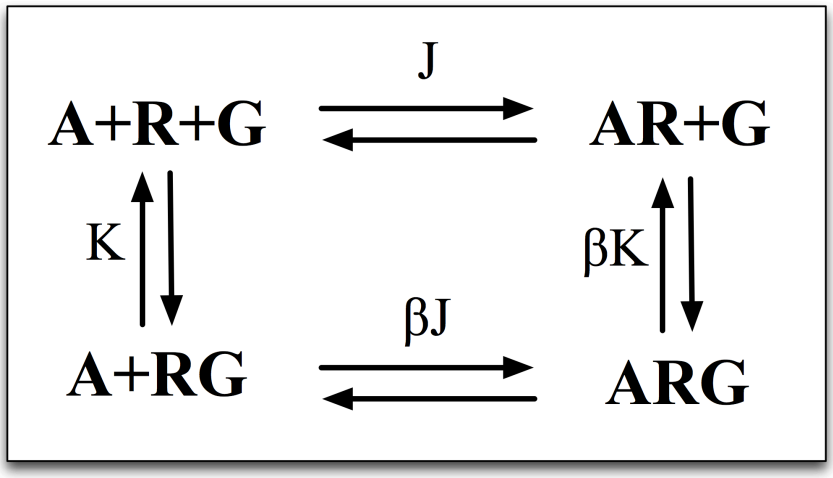


Figure 1-2 The ternary complex model described the high and low affinity states of the receptor by introducing a third component: the G protein. The high affinity state corresponds to the receptor bound to the G protein while the low affinity state corresponds to the unbound receptor. The equilibrium constant J defines binding of agonist to the receptor while the constant K defines the binding of GPCR to G-protein. The β constant defines the differential affinity of the compound to bind to the active versus the inactive form of the GPCR (De Lean *et al.*, 1980).

This model was later expanded to the so-called "extended ternary complex

model" (Samama *et al.*, 1993). In this model (Fig 1-3), there is an equilibrium between an inactive R state and an active R* state. An agonist would stabilize the receptor in its active R* state, an antagonist has no influence on the equilibrium while an inverse agonist stabilizes the receptor in its inactive R conformation. According to this model only the R* state of the receptor is able to bind to the G protein and triggers the physiological response. This model explains the constitutive activity observed for some GPCRs by assuming the transition between the inactive R to active state R* carries a sufficiently low energetic cost that it is possible for some receptors to be in the R* state even in the absence of ligand.

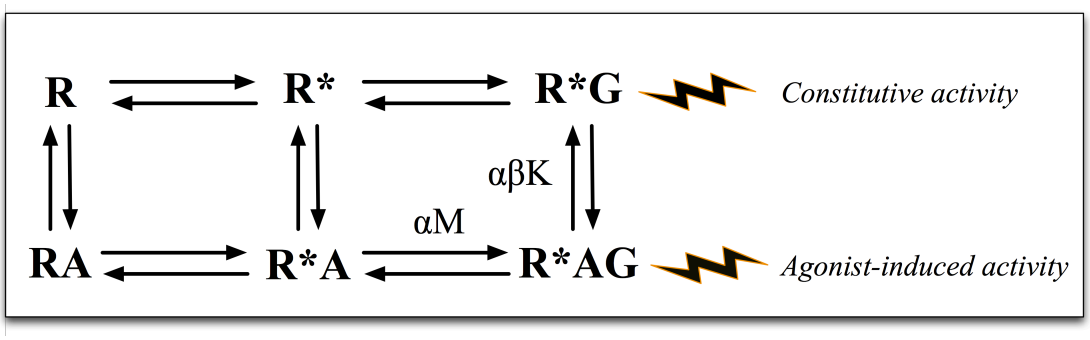


Figure 1-3 The extended ternary complex model describes the different states of the receptor and its interaction with an agonist (A) and a G protein (G). The receptor undergoes a conformational change from R to R* defined by the constant J. The effect of agonist binding is defined by the constant α and the effect of G protein binding is defined by the constant M. (Samama *et al.*, 1993)

The extended ternary complex model also suggests that the G protein is only able to bind the active R* state of the receptor. However recent evidence shows that the M_3 muscarinic acetycholine receptor forms an inactive-state complex with G_q protein in intact cells (Qin *et al.*, 2011). This inactive-state complex is thought to increase the rate of G protein activation and differs from the active-state complex. However, there is also evidence for a "collision coupling" model for the α_2-adrenergic receptor (Hein *et al.*, 2005). Using FRET experiments, the authors showed that the receptor and the G protein interact only upon agonist binding and that there is no pre-assembly of the α_2-adrenergic receptor with its G protein. This means that the

pre-assembly of a G protein with its GPCR could be a receptor specific event. These results strengthen the idea of a more complete model, the so-called cubic ternary complex (Fig 1-4). In this model the G protein can bind both the inactive and active states of the receptor (Weiss *et al.*, 1996).

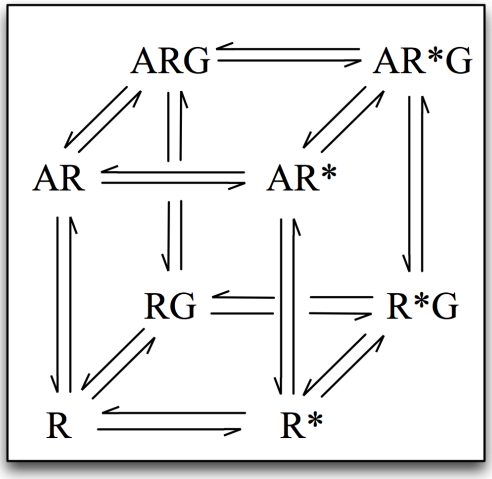


Figure 1-4 The cubic ternary complex model describes the different states (active R* state and inactive R state) of the receptor and its interaction with the agonist (A) and the G protein (G). In this model the inactive R state of the receptor is able to interact with the G protein forming an inactive complex. (Weiss *et al.*, 1996)

1.2.2 G protein activation and signalling pathways

1.2.2.1 G protein overview

Heterotrimeric G proteins are the molecular intermediates within the cells that switch on specific signalling cascades upon GPCR activation. Heterotrimeric G proteins are part of the large family of GTPases and they comprise three subunits: α, β and γ. There are 16 genes encoding for Gα subunits, 5 genes encoding for Gβ subunits and 12 genes encoding for Gγ subunits, forming over 20 different G proteins (Downes & Gautam, 1999). They are divided into four subfamilies according to their α subunits: $G\alpha_s$, $G\alpha_i$, $G\alpha_q$ and $G\alpha_{12}$ (Hepler & Gilman, 1992). In their inactive form, G proteins bind GDP tightly through their α subunits. Once a GPCR has been

activated, a conformational change within its transmembrane domains allows it to interact with its G protein; binding to the receptor triggers a conformational change within the G protein resulting in the exchange of GDP for GTP. In turn, this exchange causes the dissociation of the α subunit from the βγ dimer. Both the α subunit and the βγ complex are then free to interact with effector proteins to propagate the signal and trigger a physiological response within the cell. The type of effector protein and the response are dependent on the G protein activated. The specific roles of the different Gα subunits are unclear but as a rule of thumb, $G\alpha_s$ activates adenylate cyclase while $G\alpha_i$ inhibits adenylate cyclase. Therefore $G\alpha_s$ and $G\alpha_i$ regulate the level of cyclic AMP (cAMP) within the cell. $G\alpha_q$ activates phospholipase Cβ, which hydrolyses phosphatidylinositol 4,5 bisphosphate (PIP2). Hydrolysis of PIP2 results in the formation of two important second messengers namely inositol trisphosphate (IP3) and diacylglycerol. IP3 activates calcium channels leading to release of Ca^{2+} from intracellular stores into the cytosol (Bockaert & Pin, 1999) while diacylglycerol activates protein kinase C. $G\alpha_{12}$ activates Rho guanine nucleotide exchange factors (GEFs) (Simon *et al.*, 1991). The βγ subunit has been shown to interact with Phospholipase A and C, ion channels and kinases (Milligan & Kostenis, 2006).

The autocatalytic activity of the α subunit then hydrolyses the GTP back to GDP allowing the heterotrimer to reform and end the signalling cascade (Fig 1-5). The duration of the signal depends on the rate of GTP hydrolysis by the autocatalytic α subunit (Cabrera-Vera *et al.*, 2003).

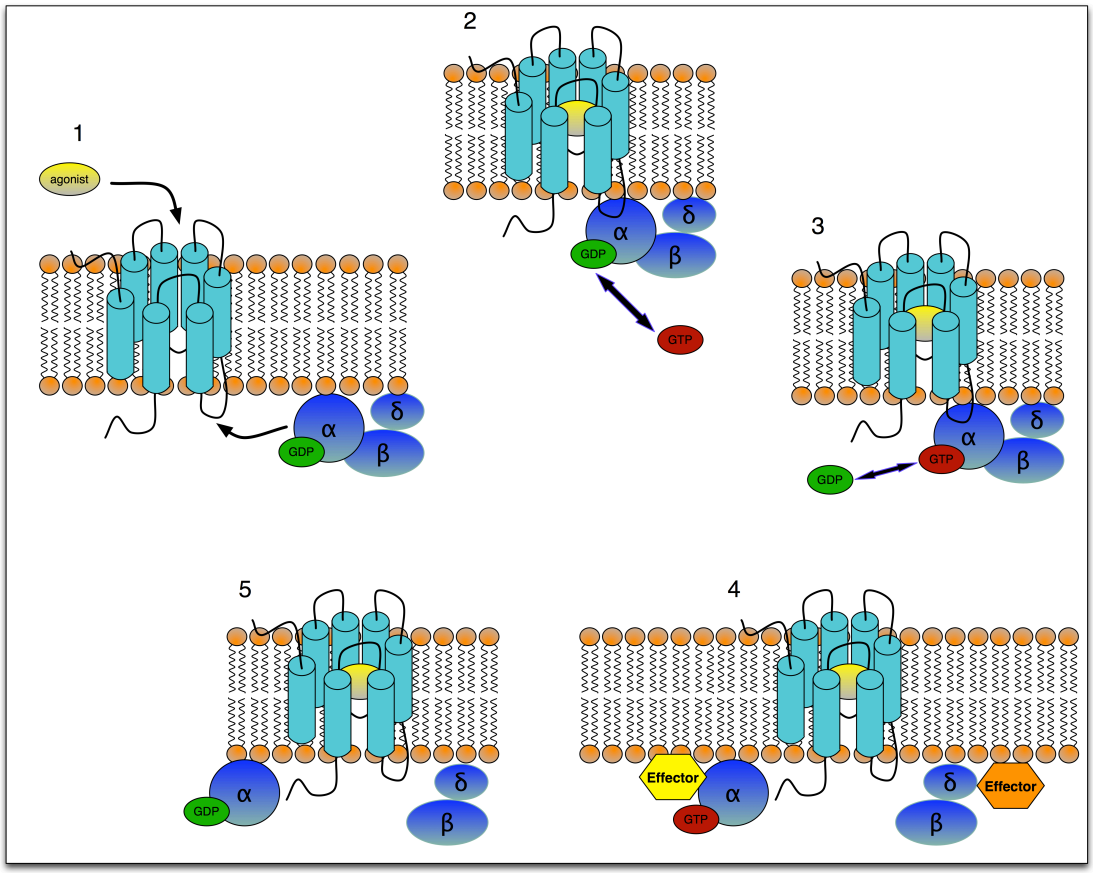


Figure 1-5 Schematic of the activation steps of a GPCR: 1 Agonist binds to the receptor. 2 Recruitment of the G protein on the intracellular side of the GPCR. 3 GDP/GTP exchange. 4. G protein dissociation and activation of effector proteins. 5 Hydrolysis of GTP to GDP.

1.2.2.2 The Gα subunit structure

The Gα subunit comprises two domains: a GTPase domain involved in binding and hydrolysing GTP and a helical domain, which binds the GTP to a site within the core of the G protein. The GTPase domain comprises a six-stranded β-sheet surrounded by five α-helices (Fig 1-6). The most conserved regions of this domain are the five loops containing the diphosphate-binding (P^-) loop (GxGESGKS), the Mg^{2+}-binding domain (RxxTxGI and DxxG) and the guanine ring binding motifs (NKxD and TCAT). All α-subunits contain a post-translational lipid modification at the N terminus responsible for the membrane localisation of the α subunit (Chen & Manning, 2001; Smotrys & Linder, 2004).

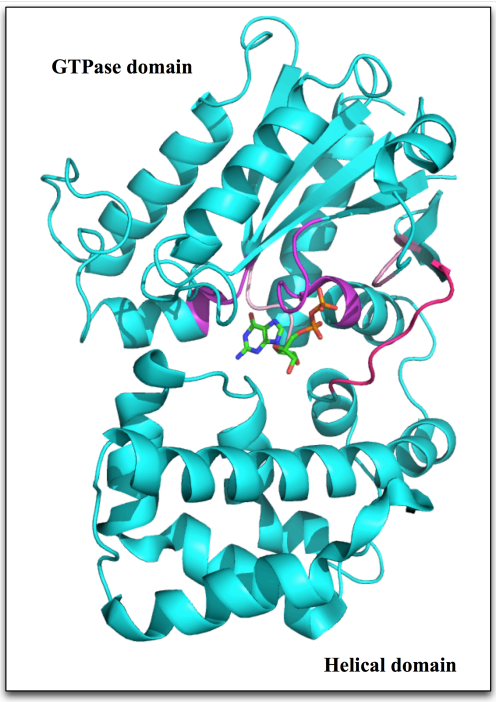


Figure 1-6 Structure of the $G\alpha_i$ subunit bound to GDP, showing the GTPase domain containing the conserved regions within the loops in magentas and the helical domain burying the GDP within the core of the protein (pdb access code: 1GG2)

The GTPase domain also contains three flexible loops near the c-phosphate binding site, named Switches I, II and III (Oldham & Hamm, 2006). Switch II is of particular interest as it plays a crucial role in the binding of effector proteins. When the GDP bound α subunit is in complex with the βγ dimer, the switch II forms a loop that is buried within the heterotrimer (Fig 1-7A). In contrast, in the active GTP bound state, the γ-phosphate stabilizes the α-helix formed by switch II, which then becomes available for interaction upon dissociation of the α subunit from the βγ complex (Fig 1-7B). The importance of this switch II α-helix for interaction with effector protein has been confirmed by the high-resolution structure of the $G\alpha_S$ domain in complex with the catalytic domain of the mammalian adenylate cyclase (Tesmer *et al.*, 1997) (Fig 1-7C). Upon hydrolysis of GTP to GDP, the helix formed by the switch II is no longer stabilised and becomes disordered (Fig 1-7D).

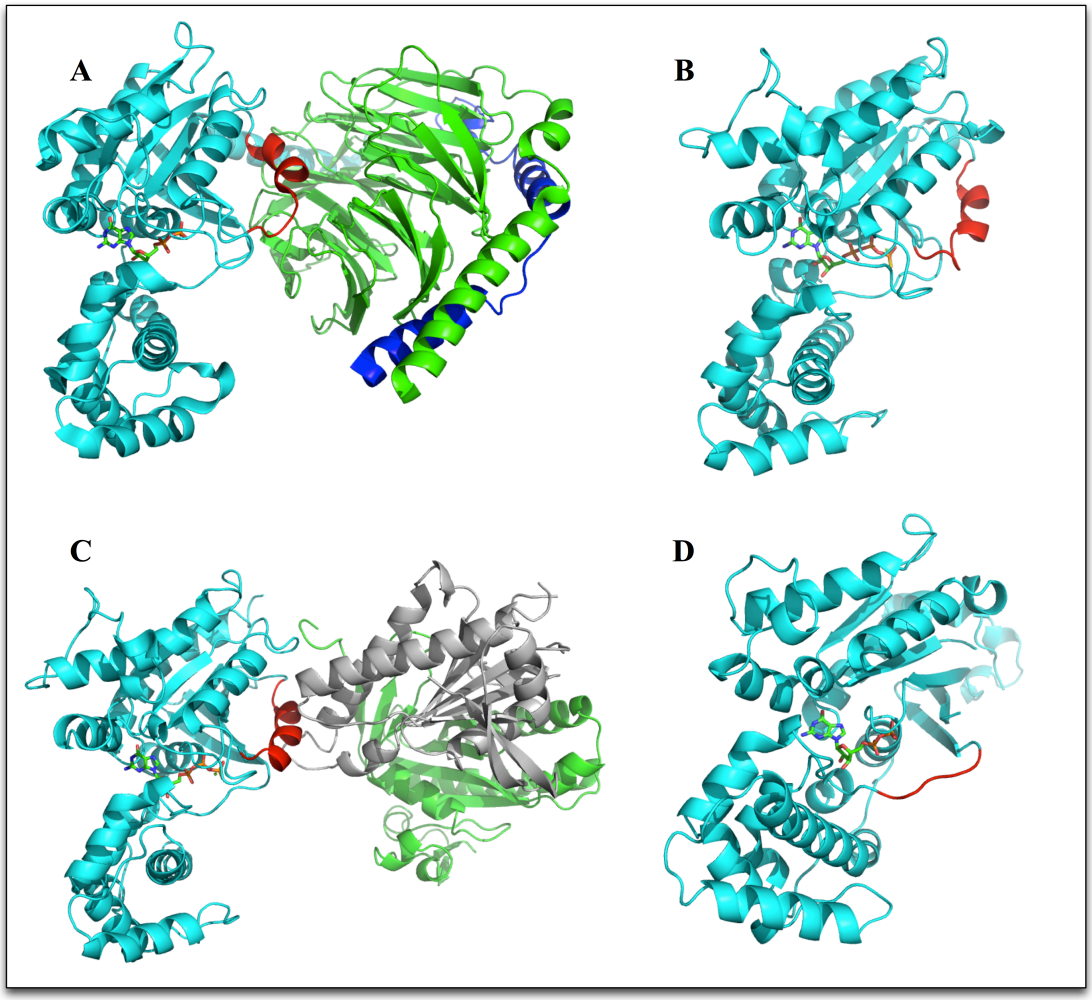


Figure 1-7 Crystal structure of a Gα subunit bound to (A) GDP and in complex the βγ subunits (pdb access code: 1GG2), (B) bound to GTPγS (pdb access code: 1AZT), (C) bound GTP and interacting with the catalytic domain of the adenylate cyclase (pdb access code: 1AZS) and (D) bound to GDP in its deactivated form (pdb access code: 1GDD). In each case, the switch II is shown in red.

1.2.2.3 The Gβγ subunit structure

The β subunit structure is a seven-bladed β-propeller structure with seven WD-40 repeats. Each blade comprises four anti-parallel β-strands and the N terminus forms an α-helix that interacts with the N terminus of the γ subunit through a coiled coil interaction, while the C terminus of the γ subunit interacts with the core of the β subunit (Garritsen *et al.*, 1993) (Fig 1-8). The γ subunit is composed of two helices connected by a loop. Together with the β subunit they form a complex that does not dissociate except by denaturation. The γ subunit undergoes post-translational lipid

modifications, which allow the protein to associate with the membrane (Fukada & Kokame, 1994).

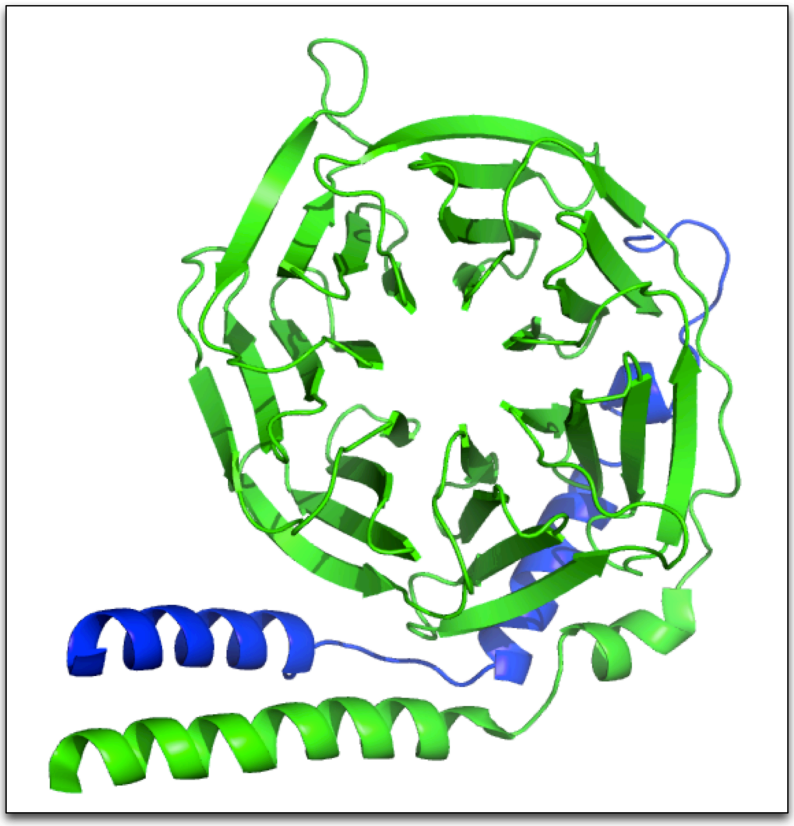


Figure 1-8 Structure of the βγ subunit of the G_i (pdb access code: 1GG2). The β subunit in green forms a seven-bladed β-propeller structure. The γ subunit in blue comprises two helices connected by a loop

1.2.2.4 Receptor/G protein interaction

The recent structure of the β_2 adrenergic receptor (β_2AR) in complex with the G_s protein has provided unprecedented details of G protein/GPCR interaction (Rasmussen *et al.*, 2011a). However, prior to that a number of different studies had highlighted a number of key regions of the G protein important for receptor/G protein interaction and specificity. The C terminus of the α subunit has been shown to play a crucial role in receptor/G protein interaction (Bourne, 1997; Conklin & Bourne, 1993; Martin *et al.*, 1996; Wess, 1997). For example, an 11-amino acid peptide corresponding to the C terminus of the α_t subunit is able to bind the activated

rhodopsin receptor and to compete with the G_t heterotrimer (Aris *et al.*, 2001; Hamm *et al.*, 1988). In addition, *pertussis* toxin uncouples the G_i protein from its GPCR by catalyzing the ADP ribosylation of a Cys residue located on the C-terminus of the $G\alpha_i$ subunit (Van Dop *et al.*, 1984; West *et al.*, 1985). Moreover, several reports of mutations in this region of the G protein affecting the receptor-G protein specificity have been published (Conklin *et al.*, 1996; Osawa & Weiss, 1995; Sullivan *et al.*, 1987). Although, the last 11 amino acids of the C terminus of the α subunit play a critical role, there are other regions of the G protein involved in receptor-G protein interactions. Indeed, within the last 11 amino acids of the C terminus of α_t and α_i, only one is different, yet the $5HT_{1B}$ serotonin receptor selectively activates G_i. Other critical regions for receptor coupling specificity have been identified within the N terminus region of the α subunit (Kostenis *et al.*, 1997) as well as several loops (Bae *et al.*, 1999; Cai *et al.*, 2001; Onrust *et al.*, 1997). There is also evidence that the βγ subunits play a role in receptor binding either directly or indirectly through stabilization of the α subunit (Ford *et al.*, 1998).

As mentioned earlier, a crystal structure of the β_2AR in complex with a G_s protein has now been solved. This high-resolution structure shows details of the interaction between the receptor and the C terminus of the α subunit. The large movement of helices V and VI away from the core of the receptor allows the α subunit C terminus to penetrate within the transmembrane domain of the receptor where it forms primarily non-polar interactions except for the packing of Tyr391 of the G protein against Arg131 of the highly conserved DRY motif (Rasmussen *et al.*, 2011a). There is also an extensive polar interaction network between the C terminus of the α subunit and the intracellular ends of helices III and V (Fig 1-9). The crystal structure also shows interaction between the N terminus of the α subunit and the ICL2

of the receptor. Interestingly, when comparing the structure of the α subunit in complex with the β_2AR (pdb access code: 3SN6) with the structure of the α subunit bound to GTPγS (pdb access code: 1AZT), the main difference is a large rotation of the helical domain relative to the GTPase domain leaving the nucleotide-binding site open (Rasmussen *et al.*, 2011a).

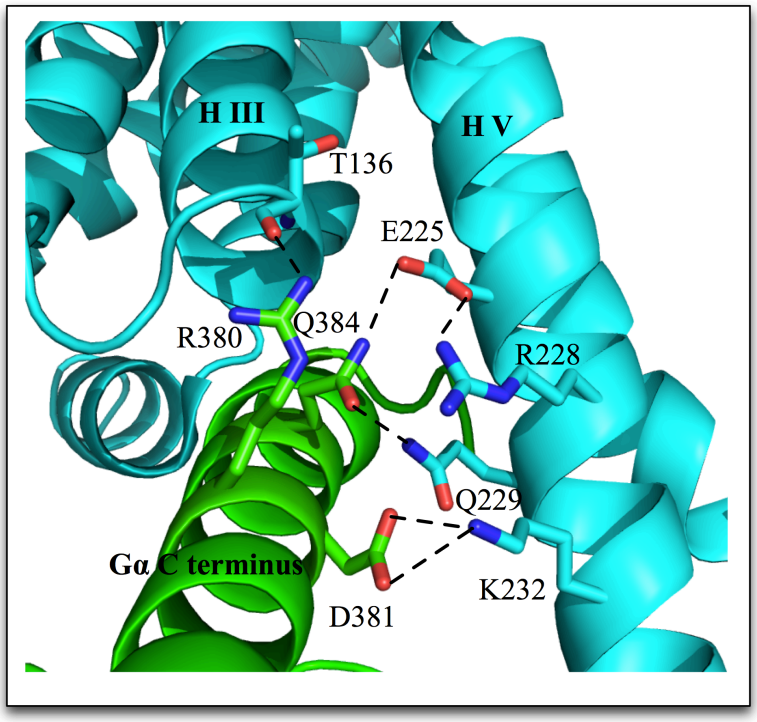


Figure 1-9 Crystal structure of the β_2AR (cyan) in complex with G_S (green) showing the polar interaction network between the C terminal tail of the $G\alpha_s$ subunit and the intracellular ends of helices H III and H V (pdb access code: 3SN6) (Adapted from Rasmussen *et al*, 2011)

1.2.3 Other processes in the GPCR activation cycle

In addition to G protein activation, there are other essential processes in the GPCR activation cycle such as desensitization, internalization, degradation and resensitization. The desensitization of the receptor is essential to protect the cell from over-stimulation of the receptor and is achieved at different levels of the activation pathway (Luttrell & Gesty-Palmer, 2010). For instance, G protein signalling is terminated through the GTPase activity of the regulators of G protein signalling

(RGS) family of proteins (Ross & Wilkie, 2000). These proteins enhance the intrinsic GTPase activity of the Gα subunit and therefore accelerate the reformation of the inactive G protein heterotrimeric complex. The most important desensitization mechanisms happen through receptor phophorylation, either by second-messenger dependent kinases (cAMP-dependent protein kinase (PKA) and protein kinase C (PKC)) or by G protein-coupled receptor kinases (GRK). PKA and PKC are activated by increasing concentrations of second messengers such as cAMP, Ca^{2+} and diacyglycerol, due to GPCR activation (Ferguson, 2001). Phophorylation of the receptor at the ICL3 or at the C-terminal tail by PKA and PKC decreases receptor/G protein coupling. This desensitization is called "heterologous" desensitization because it is independent of ligand binding. In contrast, "homologous" desensitization only occurs on activated receptors. GRKs only phophorylate activated receptors on serine and threonine residues within ICL3 and the C-terminal tail of the receptor. Phophorylation by GRKs of the receptor triggers translocation of arrestins from the cytosol to the plasma membrane where they bind to the intracellular part of the receptor, preventing G protein binding (Stoffel *et al.*, 1997). The recent high resolution structure of active β-arrestin 1 in complex with a V2 vasopressin-receptor-derived phosphopeptide shows detailed interactions between the phosphates of the peptide and arginine and lysine residues on the β-arrestin, highlighting the role of phosphorylation in β-arrestin binding (Shukla *et al.*, 2013).

Binding of arrestin to the receptor upon phophorylation by GRKs triggers another key event in GPCR regulation: internalization via clathrin-coated vesicles (Fig 1-10). There are seven GRKs and four arrestins. Two GRKs and two arrestins (arrestin 1 and 4) are expressed exclusively in the retina. The other GRKs and arrestins (arrestin 2 or β-arrestin 1 and arrestin 3 or β-arrestin 2) are ubiquitously

expressed. Upon binding to a phophorylated receptor, the β-arrestins are able to bind to the heavy chain of clathrin and to the β2 adaptin subunit of the AP-2 complex (Goodman *et al.*, 1996; Krupnick *et al.*, 1997; Laporte *et al.*, 2000; Laporte *et al.*, 1999). Upon formation of this complex, the receptor is then clustered in clathrin-coated pits, which are pinched of the cell surface by the motor protein, dynamin (Pierce *et al.*, 2002) (Fig 1-10). Once a receptor has been internalized, it is either rapidly recycled, targeted to endosomes and then slowly recycled or targeted to lysosomes for degradation. The rate of receptor recycling, or resensitization, is dependent on receptor subtypes. One class of GPCR, class A, forms transient complexes with arrestins that dissociate shortly after internalization at or near the cellular surface (Anborgh *et al.*, 2000; Oakley *et al.*, 2000). These receptors, including the β_2AR, tend to resensitize rapidly. In contrast, members of family B, form tighter complexes with arrestins and are targeted to larger endosomes enriched in a GPCR-specific phosphatase activity (Ferguson, 2001; Oakley *et al.*, 2000). These receptors are slowly recycled back to the plasma membrane. Finally, some GPCRs are not resensitized at all, but exclusively targeted to lysosomes where they are degraded (Bremnes *et al.*, 2000; Trejo & Coughlin, 1999). Several studies have shown that the C-terminal tail of the receptor plays a key role in the intracellular sorting of GPCRs (Anborgh *et al.*, 2000; Trejo & Coughlin, 1999; Zhang *et al.*, 1999).

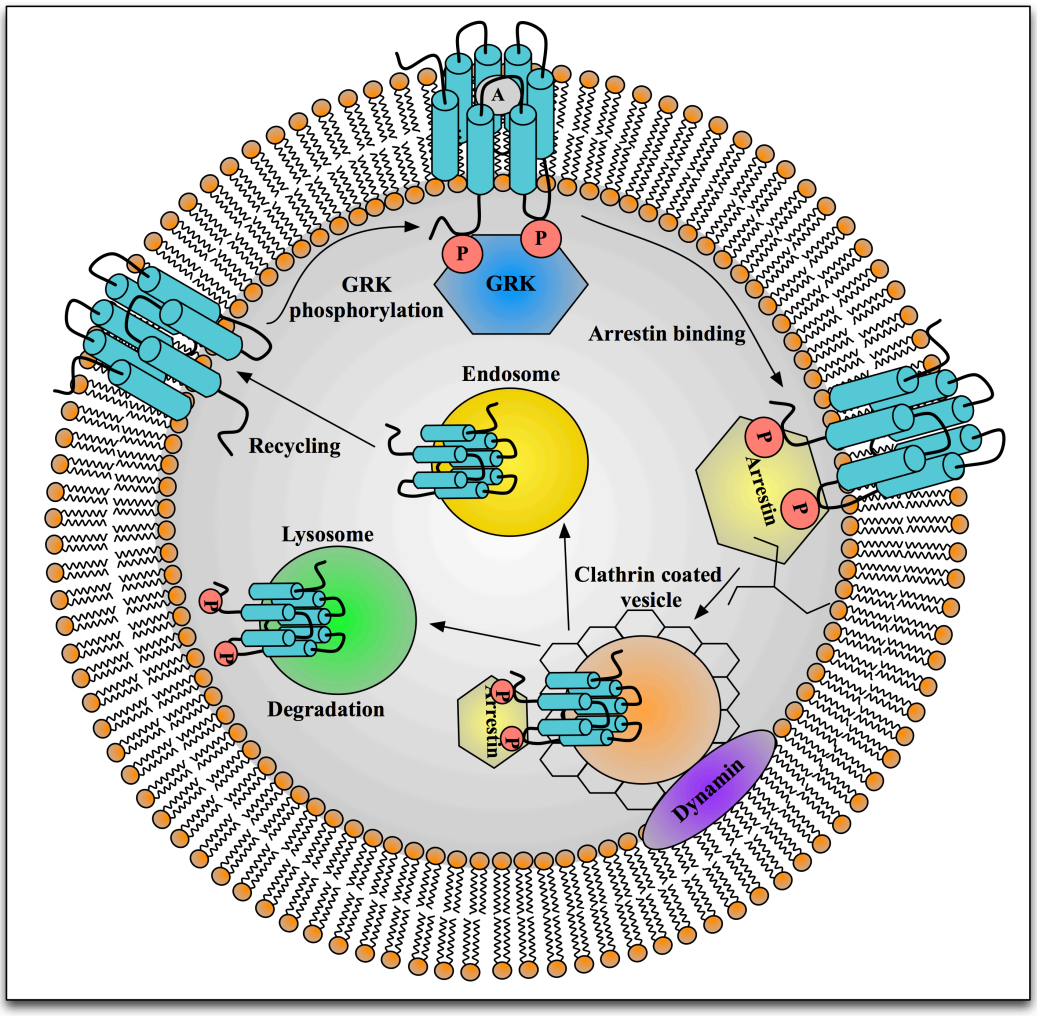


Figure 1-10 GPCR desensitization, degradation and resensitization mechanisms. Upon activation by an agonist, the receptor is phosphorylated on its ICL3 and C-terminal tail. Once phophorylated, the receptor forms a complex with β-arrestin, which triggers internalization via clathrin coated vesicles. Once internalized, the receptor is either recycled back to the plasma membrane or targeted to lysosomes for degradation.

In addition to preventing G protein coupling and triggering receptor internalization, arrestins are also able to attenuate G-protein-dependent signalling by recruiting enzymes that degrade second messenger (Luttrell & Gesty-Palmer, 2010). For instance, the β_2AR forms a complex with β-arrestin 2 and with a cAMP phosphodiesterase, increasing the rate of cAMP degradation (Perry *et al.*, 2002). Similarly, the diacylglycerol produced upon activation of the muscarinic M1 receptor is degraded to phosphatidic acid by diacylglycerol kinase recruited by arrestin (Nelson *et al.*, 2007)

1.3 Biased agonism and multiple active conformations

1.3.1 G protein independent signalling

It was originally thought that GPCRs signalled exclusively through G proteins and that β-arrestins were only responsible for receptor desensitization and internalization. However, it has now become evident that GPCRs are also able to signal in a G-protein-independent manner through β-arrestins. Several reports have shown that β-arrestins are involved in kinase activation (DeWire *et al.*, 2007), transcriptional control (Ma & Pei, 2007) and transactivation (Buchanan *et al.*, 2006).

The first example of GPCR signalling through a β-arrestin-dependent pathway was the recruitment of activated SRC, a tyrosine kinase, that led to the activation of extracellular signal-regulated kinase (ERK) (DeFea *et al.*, 2000a; Luttrell *et al.*, 1999). It was demonstrated that β-arrestins are able to scaffold specific components of the mitogen-activated protein kinase (MAPK) cascade. For instance, an agonist-induced β-arrestin 2, Raf-1, MEK1, and ERK1/2 signaling complex was described upon activation of the Angiotensin 1_A receptor ($AT1_AR$) (Luttrell *et al.*, 2001). Furthermore, stimulation of the protease-activated receptor 2 (PAR2) resulted in the formation of a complex involving the activated receptor, β-arrestin 1, Raf-1 and phosphorylated ERK (DeFea *et al.*, 2000b). Interestingly, ERK activation by β-arrestins seems to have different physiological consequences compared to ERK activation by G protein. Indeed, ERK activated by G protein triggers stimulation of transcription factors such as ELK1 in the nucleus (Tohgo *et al.*, 2002) while ERK activated by β-arrestins are retained in endocytic vesicles (Luttrell *et al.*, 2001) and

seems to have effects on chemotaxis and cytoskeletal rearrangements (Barnes *et al.*, 2005; Ge *et al.*, 2003). Not only are the effects of the two ERK pathways spatially distinct but they are also temporally distinct. Indeed, G-protein-activation of phosphorylated ERK reaches its maximum after 2 minutes while β-arrestin-activation of phosphorylated ERK is maximal after 30 minutes (Ahn *et al.*, 2004; Rajagopal *et al.*, 2010). In addition to ERK, β-arrestins have been involved with other MAPKs such as c-Jun N-terminal kinase 3 (JNK3) (McDonald *et al.*, 2000; Miller *et al.*, 2001) and p38 (Bruchas *et al.*, 2006; Sun *et al.*, 2002) as well as non-MAPK members including PI3K (Povsic *et al.*, 2003) and Akt (Beaulieu *et al.*, 2005).

Furthermore, β-arrestins have also been shown to interact with transcription factors such as NFκB. Both β-arrestin 1 and 2 form complexes with IκBα, a protein that binds NFκB preventing its nuclear translocation and therefore regulating its activity (Gao *et al.*, 2004; Witherow *et al.*, 2004). In addition, β-arrestin 1 has been shown to directly interact in the nucleus with the promoter region of several genes such as *FOS* and *p27* following activation of δ-opioid receptor (Kang *et al.*, 2005).

Finally, β-arrestins have been implicated in transactivation of the epidermal growth factor receptor (EGFR). This transactivation of EGFR via β-arrestin occurs upon activation of the prostaglandine E4 (EP_4) receptor (Buchanan *et al.*, 2006). In a similar way, β-arrestins can activate the EGFR upon activation of the β_1 adrenergic receptor, resulting in the activation of cardioprotective pathways (Noma *et al.*, 2007).

1.3.2 Biased agonism

It is clear that GPCRs are able to bind and signal through β-arrestins. In addition, there is also evidence that specific GPCR is able to couple to different G proteins and activate multiple signalling pathways (Hermans, 2003). For instance, the α_2-adrenergic receptor has been shown to interact with both $G\alpha_s$ and $G\alpha_i$ (Eason *et al.*, 1992). The ability of a ligand to favour one pathway over the others compared with the endogenous ligand, is called "biased agonism". The muscarinic acetylcholine M1 receptor provided one of the first examples of biased agonism. Indeed, binding of the agonist carbachol resulted in activation of both $G\alpha_s$ and $G\alpha_q$, whereas only PLC activity mediated through $G\alpha_q$ was observed when the agonist pilocarpine was used (Fisher *et al.*, 1993; Gurwitz *et al.*, 1994). The physiological consequences of biased agonism are not yet fully understood but might have important implications for clinical therapies. For instance, although morphine biases the activity of the μ-opioid receptor towards G protein activation compared with endogenous enkephalin peptides, it still triggers some β-arrestin-dependent pathways (Bohn *et al.*, 1999). β-arrestin 2 knockout mice do not exhibit the side effects associated with morphine such as respiratory depression and constipation (Raehal *et al.*, 2005) whereas the analgesic effects are still observed. Therefore, a purely G protein biased agonist should exhibit the desired analgesic effects without the side effects. The importance of understanding biased agonism is also demonstrated by the D_2 dopamine receptor, which is involved in mental illness. Effects of antipsychotic drugs were believed to be mediated through inhibition of adenylyl cyclase upon activation of $G\alpha_i$ and $G\alpha_o$ (Enjalbert & Bockaert, 1983). However, recent studies have demonstrated the formation of a protein complex comprising the β-arrestin 2, AKT and protein

phosphatase 2 (PP2A) in response to dopamine. This complex is the target of Lithium, used to treat mental illness such as bipolar disorder (Beaulieu *et al.*, 2005). Therefore, it is crucial to better understand the physiological relevance of each specific pathway in order to design drugs with retained efficacy but reduced side effects.

The ability of a receptor to signal through either the G protein or β-arrestin pathways appears to be dependent on receptor conformation induced upon binding "biased ligands", which cause receptors to adopt active conformations preferentially signalling through one or the other pathway (Kenakin, 2007). However, more intriguingly it seems that receptors can adopt alternative active conformations even when binding different ligands with the same downstream effects (Kahsai *et al.*, 2011). It is becoming increasingly clear that the number of active conformations of receptors is far greater than originally thought.

1.4 Structure determination of GPCRs

The numerous high-resolution structure determinations of rhodopsin, a non-typical GPCR with a covalently bound ligand (Li *et al.*, 2004; Nakamichi & Okada, 2006; Okada *et al.*, 2004; Palczewski, 2000; Salom *et al.*, 2006; Standfuss *et al.*, 2007) have been use as models for other GPCRs. However, these models have limitations and it was therefore necessary to obtain high-resolution structures of other GPCRs to further understand the precise molecular basis of receptor-ligand interaction and the basis of receptor and G protein activation. The high-resolution structure determination of bovine rhodopsin was facilitated by its natural abundance in bovine eye and by its intrinsic stability. It took another seven years for researchers to determine the structure of another GPCR that of the β_2AR expressed in a recombinant system (Cherezov *et al.*, 2007). This highlights the difficulties of obtaining high-resolution structures of GPCRs due to their highly dynamic nature and the challenges associated with overexpression of these proteins. However, in the last few years, there have been an astonishing 22 further independent X ray high-resolution GPCR structures excluding Rhodopsin (overall total of 58 structures in different conformations or bound to different ligands). This has been made possible by the development of expression systems that produce sufficient quantities of functional protein for structural studies and a range of new methodological approaches, which stabilize the receptors sufficiently to allow purification and crystallization.

1.4.1 Expression of GPCRs

1.4.1.1 Escherichia coli

The use of *E. coli* as expression system offers several advantages such as rapid and inexpensive production of proteins. *E. coli* was used successfully for expression and purification of several GPCRs such as the cannabinoid CB_2 receptor ((Yeliseev *et al.*, 2005), the adenosine A_{2A} receptor ($A_{2A}R$) (Weiss & Grisshammer, 2002) and the serotonin 5-HT_{1A} receptor (Bertin *et al.*, 1992). Although the lack of post-translational modification of *E. coli* allows the production of a homogenous population of protein, it can also lead to the misfolding and impaired trafficking of the GPCR. For instance, it has been shown that glycosylation is required for proper folding and therefore function of rhodopsin (Kaushal & Khorana, 1994). In addition, the lipid composition of *E. coli* membranes differs from that of eukaryotic cells. Lipid compositions of membranes have been shown to be crucial for proper folding and function of GPCRs such as the oxytocin and the μ-opioid receptors (Gimpl *et al.*, 1995; Hasegawa *et al.*, 1987; Lagane *et al.*, 2000).

However, expression of GPCRs in *E. coli* can be used for rapid expression of a large number of constructs for expression and stability screening (Grisshammer *et al.*, 1993). This method was used to develop thermostable mutants of the neurotensin receptor 1 (NTS1) (Shibata *et al.*, 2009), the $A_{2A}R$ (Magnani *et al.*, 2008) and the turkey β_1 adrenergic receptor (β_1AR) (Serrano-Vega *et al.*, 2008). Furthermore, *E. coli* has been used to express the CXCR1 chemokine receptor as inclusion bodies. The protein was subsequently refolded and its structure determined by solid state NMR (Park *et al.*, 2012).

1.4.1.2 Yeast systems

In contrast to *E. coli*, yeasts are able to perform post-translational modifications, which makes them a more attractive system for GPCR overexpression. In addition, yeasts possess endogenous GPCR and G proteins, which means they possess the processing machinery needed for functional expression of GPCRs. Furthermore, yeasts have a short generation time and the ability to grow on simple media making them easy and inexpensive systems to work with. Expression plasmids, which can be maintained in episomal form or integrated into the host genome are readily available. These incorporate strong promoters such as GAL1 for *S.cerevisiae* and AOX1 for *P.pastoris* that drive overexpression where up to 80% of protein content can be the target protein (Sarramegna *et al.*, 2003).

However, the lipid composition of yeast membranes is different from mammalian membranes. Indeed, yeast produces ergosterol instead of cholesterol, which has been reported to be problematic for the proper folding of the target receptor (Lagane *et al.*, 2000).

The methylotrophic yeast *Pichia pastoris* was used to produce sufficient amount of $A_{2A}R$ and histamine H1 receptor for purification and crystallization. The high-resolution structures of both receptors were determined subsequently (Hino *et al.*, 2012; Shimamura *et al.*, 2011). To date no GPCR structures have been reported using protein from the other popular yeast expression system, *Saccharomyces cerevisiae,* although there are a number of reports of high-level functional expression of receptors in this system (O'Malley *et al.*, 2007).

1.4.1.3 Baculovirus/insect cell system

Most of the recent GPCRs structures were determined with protein expressed in insect cells using the Baculovirus system. The *Autographa californica* baculovirus is able to selectively infect insect cells. The gene of interest is cloned into a plasmid between sequences of high homology with the Baculovirus genome. When cotransfected with the virus in insect cells, the gene of interest is integrated to the virus genome by homologous recombination. The most frequently insect cells used are those of *Spodoptera frugiperda* (*Sf9* cell line). Due to their eukaryotic nature, they are able to perform post-translational modifications, which can be necessary for proper folding of the protein (Kaushal & Khorana, 1994) but can also lead to a heterogeneous population of receptor (Reilander *et al.*, 1991). The relatively long generation time (up to 24 hours) and the complex media needed for the culture of *Sf9* cells make this system both more expensive and time-consuming than yeast or *E. coli*. However, the strong track record of high-resolution structures obtained from protein expressed in insect cells make it the standard expression system for structural studies of GPCRs.

1.4.1.4 Mammalian cells

Mammalians cell lines offer the closest environment to the GPCR native tissue and therefore present several advantages. Firstly, they can perform very complex post-translational modifications. Secondly, the lipid composition of their membranes is similar to that of the native environment of the receptor, which as discussed earlier can be critical for membrane protein folding (Lagane *et al.*, 2000). Finally, they contain G proteins and secondary effectors, which mean they are suitable for functional studies. However, the low yield of protein typically obtained

from mammalian cells, though GPCR-dependent, make them less suitable for structural work (Sarramegna *et al.*, 2003). Furthermore, generation of a stable cell line overexpressing recombinant GPCR is extremely time-consuming. To date, no high-resolution structure of GPCR has been reported using protein expressed in mammalian cells. However they have been extremely useful for biochemical and pharmacological characterisation of GPCRs.

1.4.2 Stabilisation of GPCRs for structural studies

1.4.2.1 Fusion protein approach

Researchers have made remarkable progress in structural studies through the development of GPCR fusion proteins, where a T4 lysozyme (T4L) replaces the conformationally dynamic third intracellular loop (ICL3). Although the ICL3 is necessary for GPCR function and interaction with G protein, it has been observed that proteolytic cleavage of this domain does not lead to the dissociation of the receptor. The two domains linked by ICL3 can even be expressed separately and assembled later to form a functional receptor (Kobilka *et al.*, 1988). The dynamic nature of ICL3 was thought to play a key role in the problems associated with crystallisation and structure determination of GPCRs. Replacing ICL3 with a well-ordered and stable protein removed a dynamic domain, reduced the movement of the transmembrane domains and facilitated the formation of crystal contacts essential for growth of well diffracting crystals (Rosenbaum *et al.*, 2007). The T4L fulfilled these criteria. In addition, the distance between the N and C termini of T4L is similar to the predicted distance between the two helices linked by ICL3, and thus can be introduced without

distorting the protein structure. Therefore ICL3 was replaced by the T4L. This approach has been successfully used to obtain high-resolution structures of a range of different GPCRs in complex with antagonists: β_2AR (Cherezov *et al.*, 2007; Rosenbaum *et al.*, 2007); human A_{2A}R (Jaakola *et al.*, 2008); human dopamine D3 receptor (Chien *et al.*, 2010); CXCR4 chemokine receptor (Wu *et al.*, 2010); human histamine H_1 receptor (Shimamura *et al.*, 2011); δ-opioid receptor (Granier *et al.*, 2012); human κ-opioid receptor (Wu *et al.*, 2012); μ-opioid receptor (Manglik *et al.*, 2012); the muscarinic M2 (Haga *et al.*, 2012) and M3 (Kruse *et al.*, 2012) receptors; the sphingosine-1-phosphate receptor (Hanson *et al.*, 2012); the protease-activated receptor 1 (Zhang *et al.*, 2012) and the corticotropin-releasing factor receptor (Hollenstein *et al.*, 2013). In addition, this approach has also been successfully applied to the structure determination of two agonist-bound state GPCRs: A_{2A}R (Xu *et al.*, 2011) and neurotensin receptor (NTSR1) (White *et al.*, 2012). In each case the insertion was essential for obtaining well-diffracting crystals, with the T4L mediating the crystal contacts.

In the case of the β_2AR, the presence of the T4L was shown to have little effect on the ligand binding properties of the receptor (Rosenbaum *et al.*, 2007). In addition, comparison of the structures of the β_2AR in complex with an antibody or fused to the T4L revealed that the two structures were very similar (Rasmussen *et al.*, 2007) (Fig 1-11) indicating that the presence of the T4L had not greatly altered the structure of the receptor and demonstrating the validity of this approach.

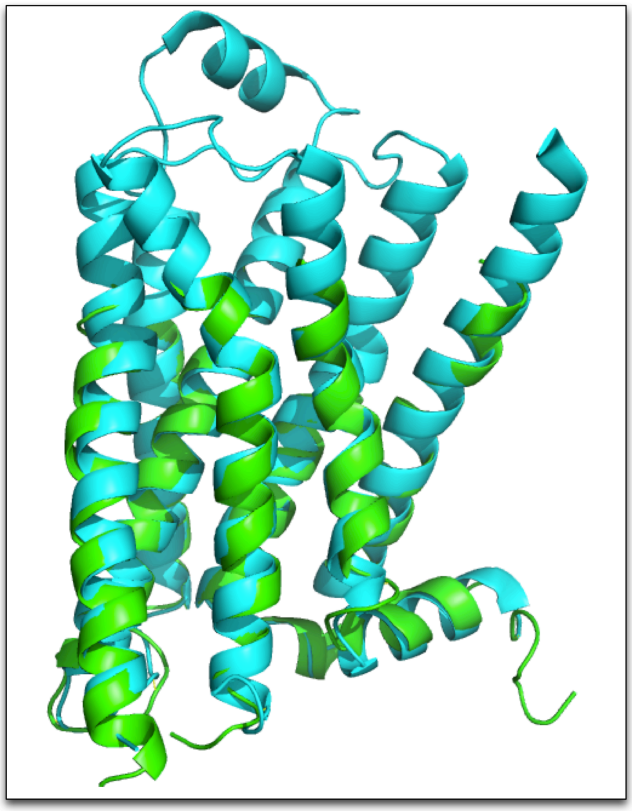


Figure 1-11 Superimposition of the β_2AR structure fused to T4L (cyan; pdb access code: 2RH1) with the β_2R structure in complex with a Fab (green; pdb access code: 2R4R) reveals that the two structure are very similar.

Although the insertion of the T4L has proven highly successful for the high-resolution structure determination of a number of GPCRs, it has been shown that this approach is not suitable for every GPCR since some receptors exhibit decrease in expression or stability when fused to T4L (Chun *et al.*, 2012). Five other potential fusion partners were identified by Ray Stevens' group (Chun *et al.*, 2012). The five proteins, a C-terminal fragment of T4L, flavodoxin, xylanase, rubredoxin and a thermostabilized cytochrome b_{562} (named cytochrome b_{562}RIL), were selected based on the key criteria of appropriate distance between the N and C-termini (between 6-14 Å) to allow accommodation between helices V and VI of the fusion partner and propensity to crystallise. Fusion proteins of both the β_2AR and the A_{2A}R were screened for expression, yield of isolated protein, thermostability and their propensity

to crystallise. The b_{562}RIL-receptor chimeric proteins were selected for further study based on their increased thermostability and their improved ability to diffuse through the lipidic cubic phase compared with the other chimeric receptors. Both the β_2AR-b_{562}RIL and A_{2A}R-b_{562}RIL produced crystals that diffracted to a resolution of 2.8 and 1.7 Å respectively. The A_{2A}R-b_{562}RIL structure was subsequently solved to a resolution of 1.8 Å, which revealed the presence of a number of water and lipid molecules in the structure and provided insights into the allosteric regulation of the receptor by sodium ions (Liu *et al.*, 2012). The b_{562}RIL fusion partner was subsequently used to obtain the high-resolution structure of the nociceptin/orphanin receptor FQ (Thompson *et al.*, 2012), the 5-HT_{1B} and 5-HT_{2B} serotonin receptors (Wacker *et al.*, 2013; Wang *et al.*, 2013a), a member of the Frizzled family, the smoothed receptor (Wang *et al.*, 2013b), and a member of the secretin family, the glucagon receptor (Siu *et al.*, 2013).

Although b_{562}RIL gave the best results for the β_2AR and the A_{2A}R when compared with the other fusion partners and allowed the high-resolution structure determination of several GPCRs, Rubredoxin gave better results in term of thermostability for the CCR5 chemokine receptor. This allowed the subsequent high-resolution structure determination of the CCR5 chemokine receptor to a 2.7 Å resolution (Tan *et al.*, 2013).

Whilst most of the fusion proteins have involved replacement of the flexible ICL3, it is possible to attach the fusion partner to the N-terminus of the receptor (Zou *et al.*, 2012) or to replace the ICL2 {Congreve, 2012 #289} (Fig 1-12C). This approach was used for the β_2 adrenergic receptor + G protein complex (Rasmussen *et al.*, 2011a), the nociceptin/orphanin receptor FQ (Thompson *et al.*, 2012) (Fig 1-12B),

the smoothed receptor (Wang *et al.*, 2013b) and the glucagon receptor (Siu *et al.*, 2013). Thus there is flexibility with the fusions with respect to the attachment point as well as the fusion partner that can be used (Fig 1-12).

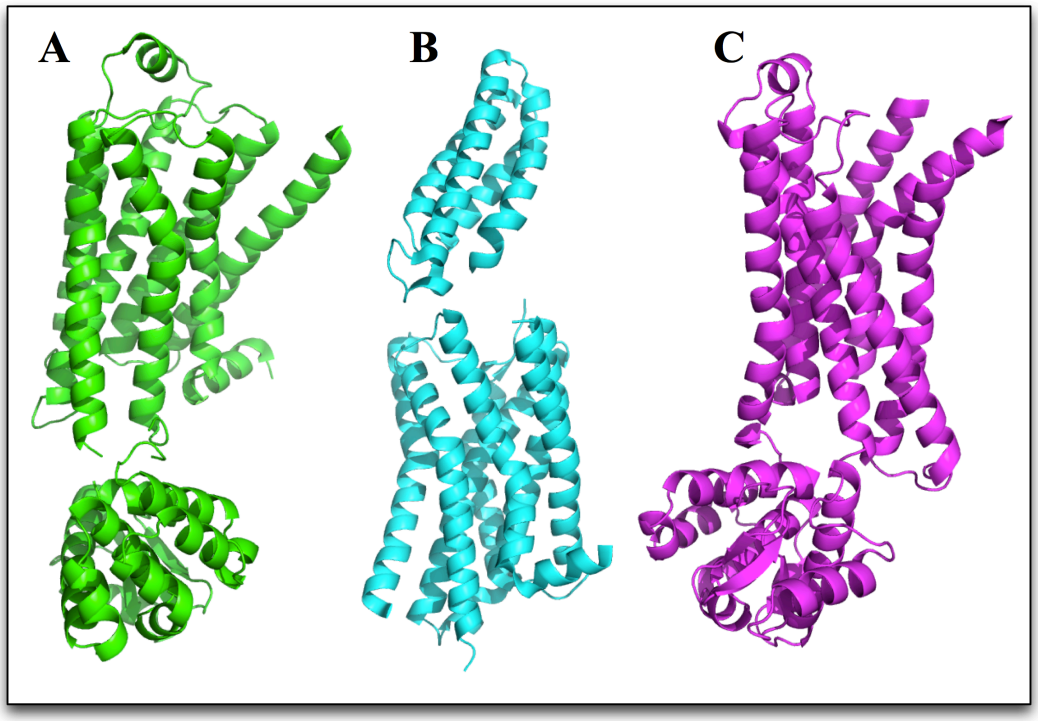


Figure 1-12 (A) Structure of the β_2R with the T4L inserted between helices V and VI (pdb access code 2RH1, (B) Structure of the Nociceptin/orphanin FQ receptor with b_{562}RIL attached at the N-terminus (pdb access code: 4EA3, (C) Structure of the corticotropin-releasing factor receptor with the T4L inserted between helices III and IV (pdb access code: 4K5Y)

1.4.2.2 Complex formation with antibody fragments

Although agonist-bound structures have been solved using the fusion partner approach, the receptors were either in an inactive state (Warne *et al.*, 2011) or only partially active state (Lebon *et al.*, 2011a; Lebon *et al.*, 2011b; Xu *et al.*, 2011). In order to obtain a crystal structure of a fully activated receptor a different approach was needed. This was achieved using antibody fragments. Protein specific antibody fragments bind to the receptor of interest and increase the size of the soluble part of the molecule, facilitating crystal formation. In addition, the antibody fragment is not only protein specific but also conformation specific. This means that the formation of

the protein-antibody complex stabilises the receptor in a specific conformation and therefore reduces the conformational flexibility of the protein. The first high-resolution structure of a non-rhodopsin GPCR, the β_2AR was determined in an inactive conformation using a Fab (Rasmussen *et al.*, 2007) . The structure was solved to approximately 3.4 Å and revealed the first insights into the precise structure of a receptor ligand binding site as well as providing some information on the overall architecture of the helices and loops.

Subsequently, Rasmussen and co-workers developed a camelid antibody fragment, called a nanobody. The nanobody is a single domain protein engineered from heavy chain only camelid antibodies and was raised by injecting the β_2AR bound to the high affinity, slow off-rate agonist (BI71067) into a llama. The nanobody exhibits G-protein-like behaviour and stabilises the active-state of the β_2AR. The β_2AR was subsequently crystallised with the nanobody with and without the T4L inserted between helices V and VI. However, only the receptor containing the T4L produced a high-resolution structure at 3.5 Å (Rasmussen *et al.*, 2011b). Comparison of the active-state structure of the β_2AR with the inactive-state structure provides details on the conformational change undergone by the receptor upon activation (Fig 1-13).

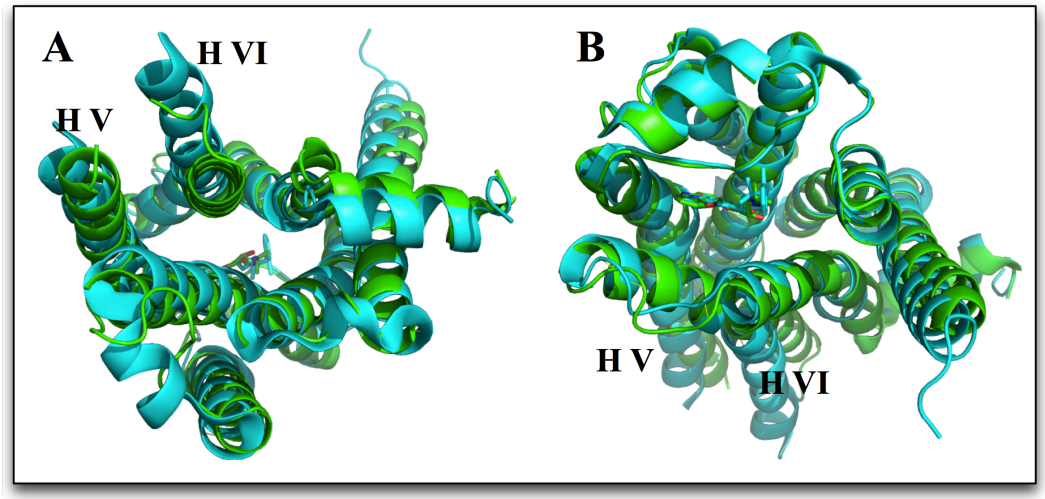


Figure 1-13 Comparison of the active-state (cyan, pdb access code: 3POG) and inactive-state structures of the β_2AR (A) intracellular view of the protein showing the large movement of helix VI (H VI) upon activation of the receptor (B) extracellular view of the protein showing that both structures are very similar**.**

A nanobody also contributed to the structure determination of the β_2AR-G_s protein complex (Rasmussen *et al.*, 2011a). The high affinity agonist, BI71067, was used to allow the formation of the β_2AR-G_s protein complex. Crystallogenesis was improved by replacement of the unstructured N-terminus of the receptor with T4L. The α-helical component of the $G\alpha_s$ protein was shown to have a variable position relative to the rest of the complex. The addition of the pyrophosphate mimic, foscarnet, stabilized the α-helical component of the $G\alpha_s$ subunit without disturbing the β_2AR-G_s complex. Finally, in order to further stabilise the β_2AR-$G\alpha_s$ complex, a nanobody, Nb35, which bound to both the $G\alpha_s$ and $G\beta_s$ subunits was also used. Both the nanobody and the T4L were involved in the formation of crystal contacts essential for crystal lattice formation. This was the first and so far only structure revealing details of the precise molecular interactions between a receptor and a heterotrimeric G protein (Fig 1-13).

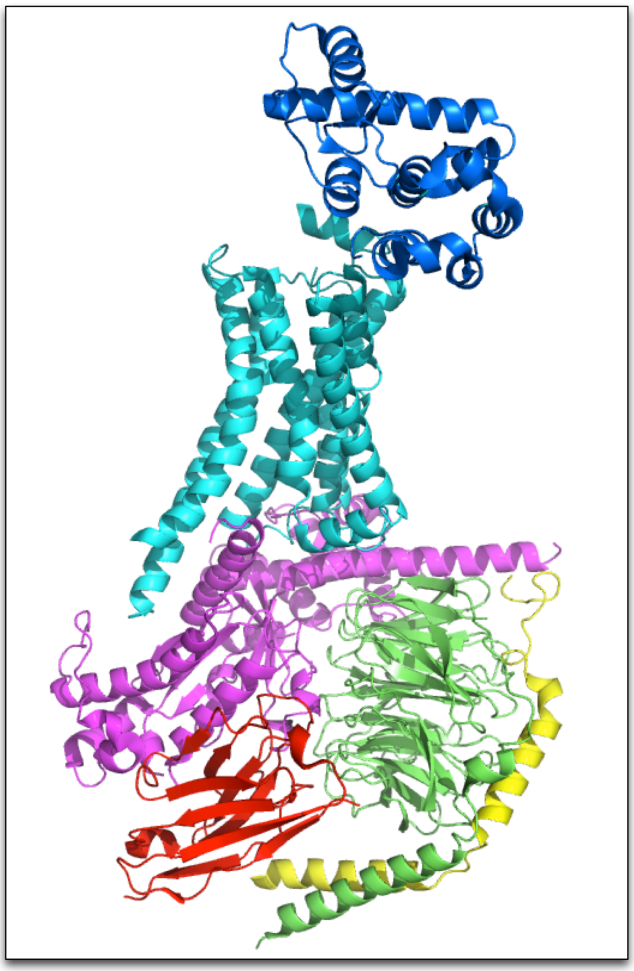


Figure 1-14 High resolution structure of the β_2AR (cyan) in complex the Gs protein. The T4L fused to the N terminus of the receptor is shown in blue, the α subunit is shown is magenta, the β subunit is shown in green, the γ subunit is shown in yellow and the Nb35 nanobody is shown in red. (pdb access code 3SN6)

Furthermore, the use of a mouse monoclonal antibody has allowed the resolution of the A_{2A}R crystal structure (Hino *et al.*, 2012). The protein, expressed in *Pichia pastoris* with its full length ICL3, is bound to an antagonist and therefore locked in an inactive conformation.

1.4.2.3 Mutagenesis approach

Finally, another technique, developed by Chris Tate and co-workers, involves alanine-scanning mutagenesis coupled with radioligand binding analysis following heat treatment of the receptor in order to identify mutants with retained functional expression but increased thermostability. The stability of the mutants is tested using an agonist and/or an antagonist. This strategy produces mutants stabilized in either an agonist conformation or an antagonist conformation, hence reducing the conformational instability inherent to GPCRs. This in turn facilitates the formation of well-diffracting crystals. This approach has been applied to four receptors to date, the turkey β_1 adrenergic receptor (β_1AR) (Serrano-Vega *et al.*, 2008), the $A_{2A}R$ (Magnani *et al.*, 2008), the NTSR1 (Shibata *et al.*, 2009) and the human corticotropin-releasing factor receptor type 1 (Hollenstein *et al.*, 2013). In each case combinations of a small number of point mutations resulted in a dramatic increase in the T_m of the receptor. Mutants obtained are much more stable in small chain detergents than the wild-type form.

More specifically, for the $A_{2A}R$, each residue of the $A_{2A}R$-A316 truncated receptor, between Pro2 and Ala316 were mutated to an alanine or to a leucine if the original residue was an alanine. Each mutant is then expressed in *E. coli* and solubilised in *n*-Dodecyl-β-D-maltopyranoside (DDM). Thermostable mutants were determined by heating the receptors at 30°C for 30 min in the absence of ligand, and then a ligand binding assay was performed using either the agonist [^{3}H]NECA or the inverse agonist [^{3}H]ZM241385. In these conditions, the WT $A_{2A}R$ had a residual activity of 50%. Thermostable mutations were selected on the basis of a residual activity greater than 70% and 65% and expression levels greater than 30% and 40%

of the WT for agonist and antagonist screening respectively. Iterative rounds of mutagenesis combining different thermostabilizing mutants resulted in two receptor constructs, Rag23, in an agonist conformation, containing five point mutations and a T_m 9°C higher than the WT and Rant21, in an antagonist conformation, containing four point mutations and a T_m 17°C higher than the WT. Despite these increases in T_m, Rag23 and Rant21 were not considered stable enough for crystallisation and a slightly different technique was used to further improve the stability of the receptor. Instead of heating the partially purified receptor in the ligand free state, it was heated in the presence of either the agonist [^{3}H]NECA or the inverse agonist [^{3}H]ZM241385. In the case of the agonist conformation, this process resulted in the identification of GL26, which has a T_m of 45°C in *n*-Decyl-β-D-maltopyranoside (DM) and contains four point mutations different from those contained in Rag23 (Lebon *et al.*, 2011a). In the case of the antagonist conformation, it resulted in the identification of four additional point mutations to form A_{2A}R-Star2, which has a T_m of 47°C in DM. For both mutants, an extra mutation (N154A) was added to remove a glycosylation site.

Using this approach, the thermostabilised turkey β_1AR was successfully crystallised and a number of high-resolution structures of the receptor in complex with a range of ligands or without ligand were solved (Huang *et al.*, 2013; Moukhametzianov *et al.*, 2011; Warne *et al.*, 2012; Warne *et al.*, 2011; Warne *et al.*, 2008). The adenosine A_{2A}R was also crystallised resulting in a range of agonist-bound and antagonist-bound structures (Dore *et al.*, 2011; Lebon *et al.*, 2011b). The NTSR1 was also recently crystallised resulting in an agonist-bound structure (White *et al.*, 2012). However, in that case, the mutant not only contained six thermostabilising mutations but also the T4L inserted between helices V and VI.

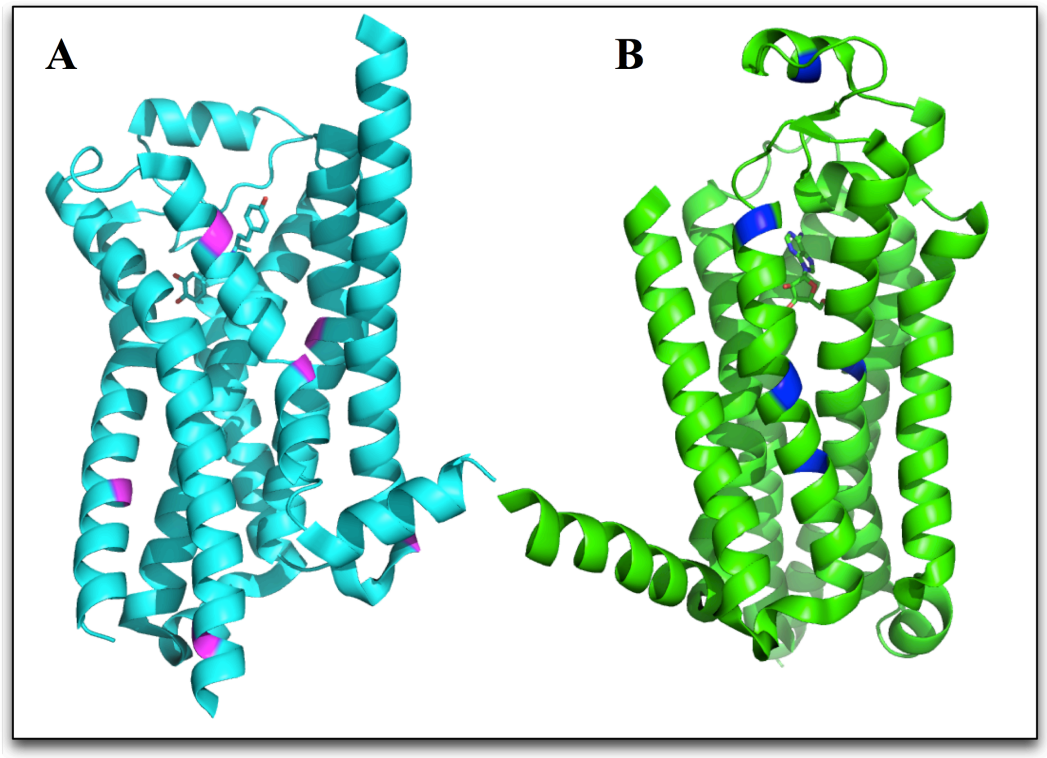


Figure 1-15 High resolution structures of thermostable mutants (A) the β_1AR containing six point mutations (magenta) in complex with the partial agonist dobutamine (pdb access code: 2YO1) (B) the A_{2A}R in an agonist conformation containing five mutations (blue) and bound to the agonist adenosine (pdb access code: 2YDO)

One issue with this method is that while the thermostabilising mutations are transferable between highly homologous receptors, eg the β_1AR and the β_2AR (Serrano-Vega & Tate, 2009) it has so far not been possible to transfer mutations between more distantly related receptors and thus a complete alanine scan must be completed for each receptor. One other issue with this approach is the need for a reliable ligand-binding assay.

However, this method has several advantages over the insertion of the T4L between helices V and VI or the use of an antibody fragment. Firstly, the ICL3 is intact which means the receptor is still able to interact with its G protein. Since the protein is still capable of binding to its G protein, it is therefore possible to use a signalling assay to investigate the functional profiles of the engineered protein.

Consequently, it is possible to determine the physiological relevance of such constructs. That is not the case when the T4L fusion technique is used. Secondly, as described earlier, the stabilization of the protein occurs through the insertion of several point mutations while when using the T4L technique, stabilization mainly occurs by the use of high affinity binding and slow off-rate ligands as demonstrated by the structure of the $A_{2A}R$ fused to the T4L (Jaakola *et al.*, 2008; Xu *et al.*, 2011). This means that the thermostabilising mutation strategy is more relevant to help drug design than the T4L fusion strategy. Indeed, in order to be a useful tool for drug design, high-resolution structures need to be obtained with different ligands to fully explore the structure/activity relationship (SAR) of a family of small molecules (Congreve *et al.*, 2012). That includes ligands with low affinity and fast off-rate. By definition this would not be possible with the T4L fusion strategy.

1.5 Structural insight

1.5.1 Comparison of crystals structures obtained using different approaches

As described in the previous section, in the last few years, technical advances have allowed the determination of the high-resolution structures of a number of GPCRs bound to a number of ligands. However, all of the high-resolution structures obtained were of highly engineered receptors. It is therefore crucial to understand what impact these modifications have on the crystal structures. The $A_{2A}R$ provides useful information in that regard since its structure bound to the inverse agonist ZM241385 has been determined using the three different techniques: the T4-lysozyme fusion strategy (Jaakola *et al.*, 2008), the thermostabilisation approach (Dore *et al.*, 2011) and in complex with a mouse antibody (Hino *et al.*, 2012). Comparison of these three structures shows interesting features. Although all the critical interactions between the ligand and the receptor seem conserved, the position of the phenol group of the antagonist differs according to the structures (Fig 1-16C). The overall architecture is maintained across the three structures especially within transmembrane domains 1, 2, 3, 4 and 7. The main differences lies in TM5 and 6. These transmembrane domains are more ordered and extended in the mutant and antibody structures compared with the T4L structure, which is certainly due to the replacement of the ICL3 by the T4L (Fig 1-16A). In addition, the fusion of the T4L and the antibody seem to have disturbed the ionic lock present in the thermostable mutant structure and also present in the inactive state of Rhodopsin (Fig 1-16B). This is in accordance with the increased affinity for agonist relative to the WT displayed by the T4L receptor fusion protein (Rosenbaum *et al.*, 2007).

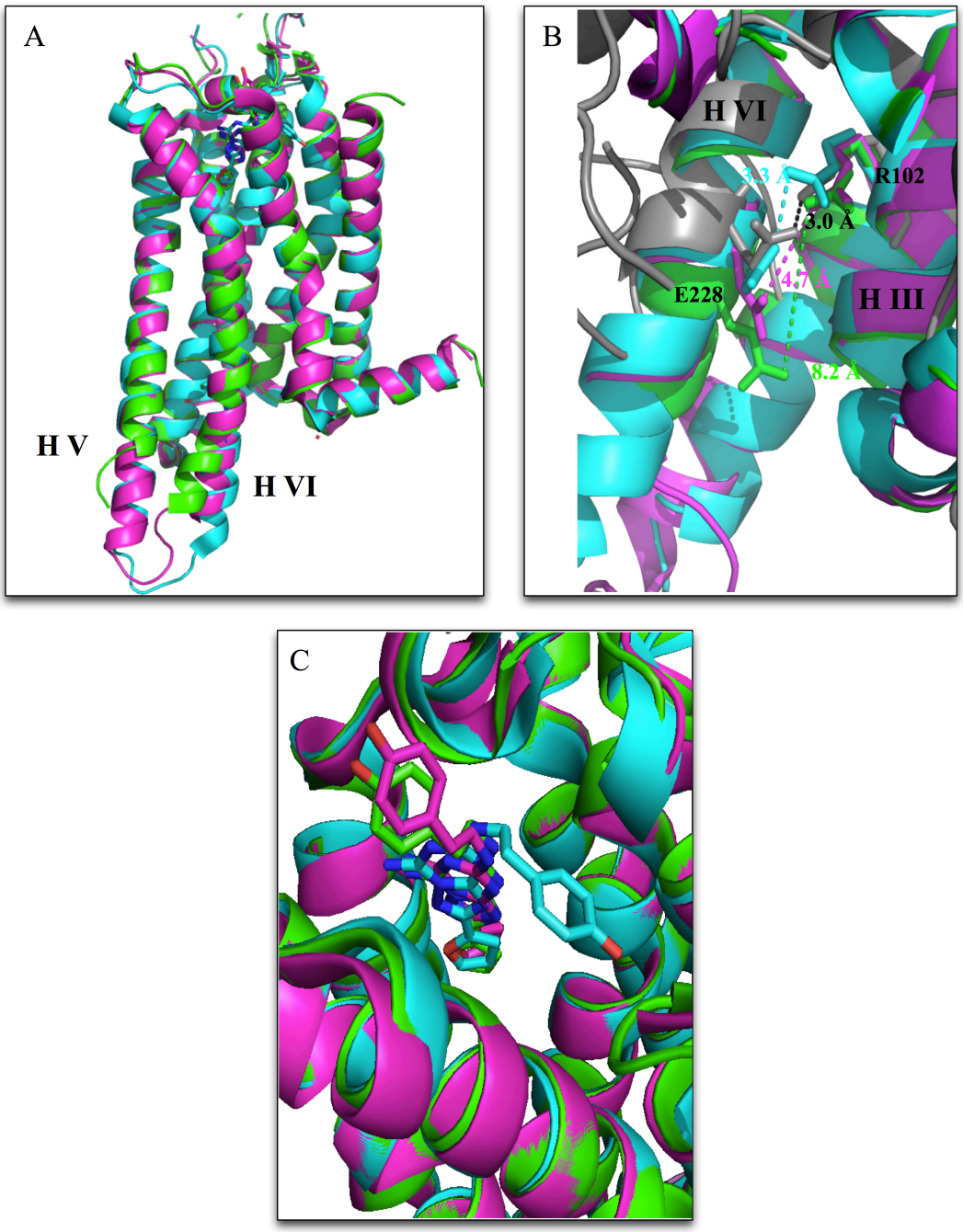


Figure 1-16 Comparison between the three independent high-resolution structures of the $A_{2A}R$ bound to the antagonist ZM241385 (sticks): $A_{2A}R$ fused to the T4-lysozyme (green, PDB 3EML), the thermostable $A_{2A}R$ mutant (cyan, PDB 3PWH) and the $A_{2A}R$ in complex with a mouse antibody (magenta, PDB 3VG9). (A) Differences between TM5 and TM6. (B) The ionic lock in the Rhodopsin structure (grey, PDB access code: 1F88) and in the three independent high-resolution structures of the $A_{2A}R$. The distances shown are between are between R102 from the DRY motif on H III and E228 on H VI. (C) Differences in the position of the phenol group of the antagonist in the structures.

However, the mechanism underlying the formation of the ionic lock seems to be more complicated than originally thought. For instance, the ionic lock is present in the high-resolution structure of the human dopamine D3 receptor despite the insertion

of the T4L between helices V and VI. Furthermore, the recent structure of the β_1AR bound to the antagonist carazolol, showed that the receptor can adopt two inactive conformations (Moukhametzianov *et al.*, 2011). In the "bent conformation", the ionic lock is present and in the "straight conformation", helices III and VI are too far apart to allow the formation of the ionic lock (Fig 1-17). Surprisingly, the two structures are monomers obtained from a single crystal. A similar observation was made with cyanopindolol from two different crystals.

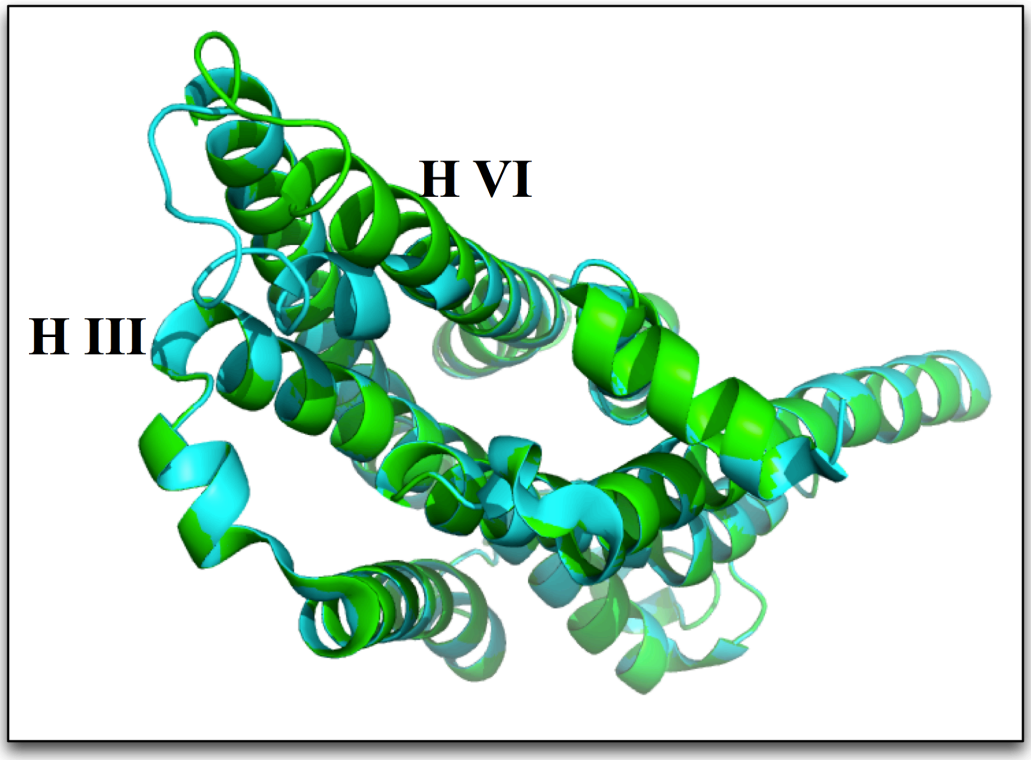


Figure 1-17 Superposition of the "bent" (Cyan) and "straight" (green) conformations of the β_1AR bound to the antagonist carazolol (pdb access code: 2YCW. In the bent conformation, the cytoplasmic end of HVI is bent towards HIII allowing the formation of the ionic lock. In the case of the straight conformation, HVI and HIII are too far apart to allow the formation of the ionic lock.

The high-resolution structure of the A_{2A}R was also obtained bound to the agonist UK-432097 with the T4L inserted between helices V and VI (Xu *et al.*, 2011) and bound to the agonists NECA and adenosine as a thermostable mutant (Lebon *et al.*, 2011b). Although, the structures were obtained with an agonist bound, it is proposed that the receptor is in an intermediate active conformation rather than the

fully active conformation. Again, this allows comparison of the influence of the two different techniques on the overall structure of the receptor. Although, the agonist-bound structures were co-crystallised with different ligands, they are very similar especially in the transmembrane regions. However, they show small differences in the extracellular region, probably due to the difference in the ligands and the absence of density for residues 149-157 (Fig 1-18).

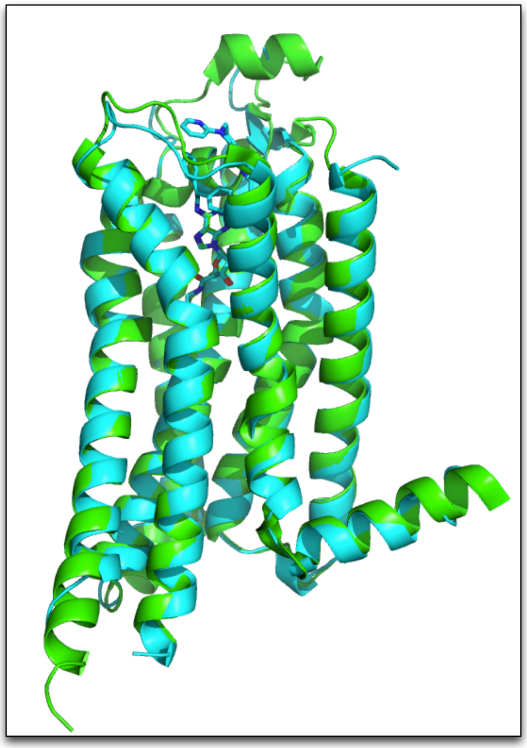


Figure 1-18 Structural alignment of the thermostabilised $A_{2A}R$ mutant bound to the agonist NECA (green, PDB 2YDV) with the $A_{2A}R$-T4-lysozyme fusion protein bound to the agonist UK-432097 (cyan, PDB 3QAK).

1.5.2 The ligand-binding pocket of GPCRs

Crystal structures obtained owing to the technological advances made in the recent years have provided unprecedented details on GPCRs. The ligand-binding pocket is of particular interest in regard to drug design. A systematic comparison of residues involved in ligand binding of all the GPCR structures revealed some common features in the binding pockets of the different receptors (Venkatakrishnan *et al.*, 2013). The following "topologically equivalent residues" located in helices III, VI and VII are involved in ligand binding in almost all the receptors: 3.32, 3.33, 3.36, 6.48, 6.51, 7.39. Of these residues, two pairs (3.36-6.48 and 6.51-7.39) are in contact in most receptors and seem to form "a ligand binding cradle" (Fig 1-19) (Venkatakrishnan *et al.*, 2013). Residues from other helices form contacts with specific ligands in specific receptors. Interestingly, helix I does not seem to be directly involved in ligand binding.

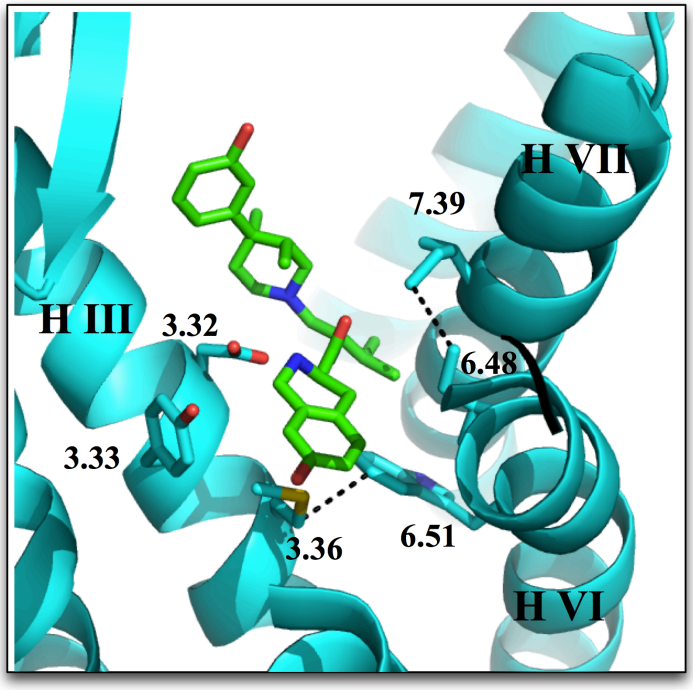


Figure 1-19 Ligand binding cradle of the human κ-opioid receptor (pdB access code: 4DJH). The ligand is represented as green sticks and the residues forming the ligand binding cradle as cyan sticks. The dashed lines show the interactions between the residues.

The work done by Chris Tate's group on the turkey β_1AR provides valuable details on the ligand-binding pocket and insight into how small changes into the ligand-binding pocket can induce a much larger conformational modification in the receptor. In addition, their work provides the platform to compare the different binding modes of pharmacologically different ligands since they published the high-resolution crystal structure of the turkey β_1AR in complex with antagonists (Moukhametzianov *et al.*, 2011; Warne *et al.*, 2008), full agonists, partial agonists (Warne *et al.*, 2011) and biased agonists (Warne *et al.*, 2012).

Although all the different ligands bind in a similar way, a detailed comparison of the structure of the receptor in complex with the full agonist carmoterol, the antagonist cyanopindolol, the partial agonist salbutamol and the biased agonist bucindolol reveals three significant differences which are the rotamer conformation changes of S212 and S215 and the contraction of the binding pocket by ~1 Å (Warne *et al.*, 2011). It is proposed that the rotamer conformation change of S215 upon binding of full agonists disrupts interactions between Helices IV and V and thus facilitates the formation of the active state of the receptor (Warne *et al.*, 2011). Furthermore, the rotamer conformation change of S215 observed upon full agonist binding, allows formation of a hydrogen bond between the ligand and the receptor (Fig 1-20A), whereas when the receptor is bound to the antagonist cyanopindolol, S215 forms a hydrogen bond with T126 (Fig 1-20B). This interaction between helices III and V is also present in the structures of the receptor bound to partial agonists and to biased agonists (Fig 1-20C and D). The disruption of this interaction between helices III and V is probably another factor facilitating the formation of the active state of the receptor. In contrast, the rotamer conformation change of S212 results in the strengthening of interactions between helices V and VI

as demonstrated by the formation of a hydrogen bond between S212 and N310. This interaction is formed upon binding of full, partial and biased agonists but not in the case of antagonists (Fig 1-20).

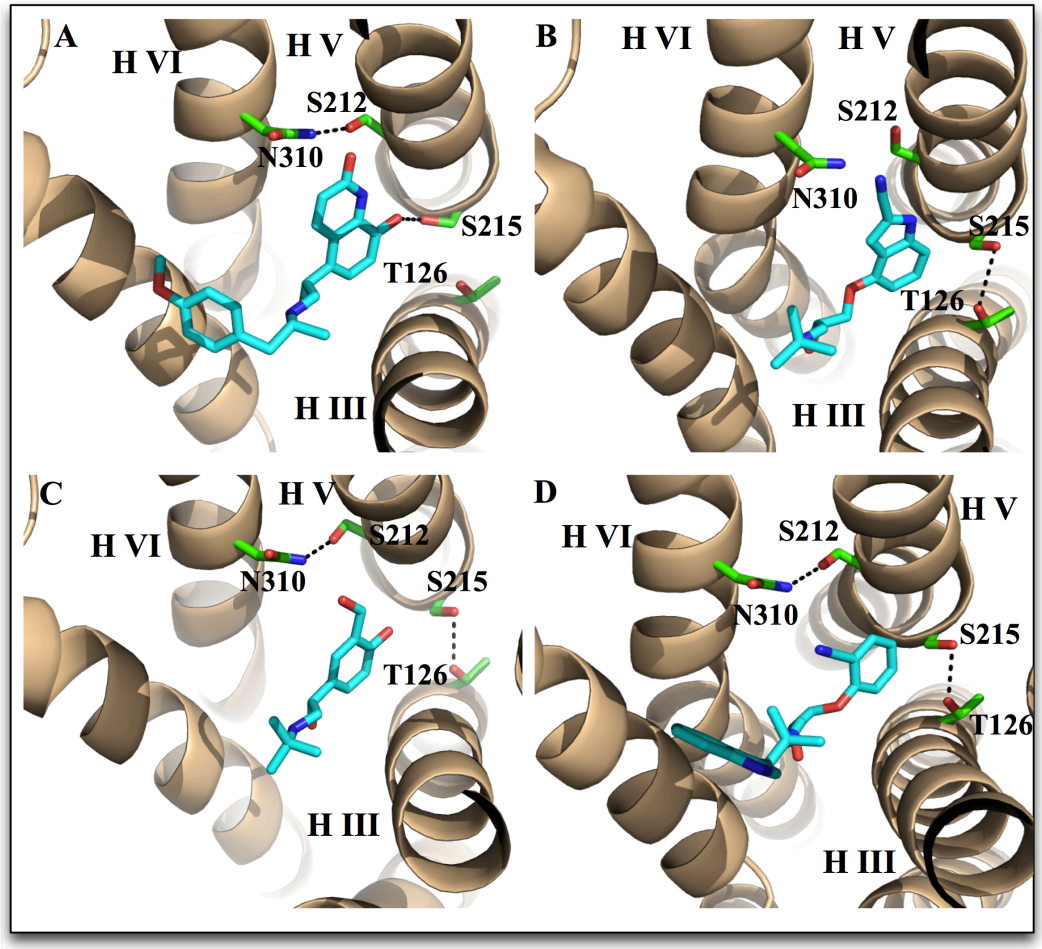


Figure 1-20 Interactions between different ligands and the β_1AR. (A) The full agonist carmoterol interacts with S215 and induces the rotamer conformation change of S212 leading to the interaction between S212 and N310 (pdb access code: 2YO2). (B) The antagonist cyanopindolol does not disrupt the interaction between helices III and V and does not induce the rotamer conformation change of S212 (pdb access code: 2VT4). (C) The partial agonist salbutamol does not disrupt the interaction between helices III and V but induces the rotamer conformation change of S212 leading to the interaction between S212 and N310 (pdb access code: 2YO4). (D) The biased agonist bucindolol does not disrupt the interaction between helices III and V but induces the rotamer conformation change of S212 leading to the interaction between S212 and N310 (pdb access code: 4AMI).

In addition, the contraction of the ligand binding pocket observed is specific to full and partial agonists. It is proposed that this contraction relies on strong hydrogen bonds between the catechol (or equivalent) moiety and helices V and VI on one hand and between the secondary amine and the β-hydroxyl group in the agonist

and the amino acid side chains in helices III and VII on the other hand (Warne *et al.*, 2011). While this is the case for the full agonists, it is also true, though weaker for the partial agonists, which is probably due to a reduced number of hydrogen bonds compared with the full agonist. However, this contraction is not observed in the cases of the antagonists and biased agonists. This is certainly due to the increased distance between the catechol (or equivalent) moiety and the secondary amine within the ligands. The two biased agonists co-crystallised with the β_1AR have previously been shown to be β_1AR antagonists but they are able to activate G-protein-independent pathways (Warne *et al.*, 2012). It is therefore not surprising that they exhibit at least partially similar binding characteristics to the antagonist cyanopindolol. However, both biased agonists have aromatic substituents on the secondary amine. These substituents are able to make additional interactions with helices 2, 3 and 7 of the receptor as well as with extra-cellular loop 2 (Fig 1-21). It is therefore only logical to propose that the G-protein-independent signalling properties of these compounds are due to these extra interactions since they are unique to the biased agonists (Warne *et al.*, 2012).

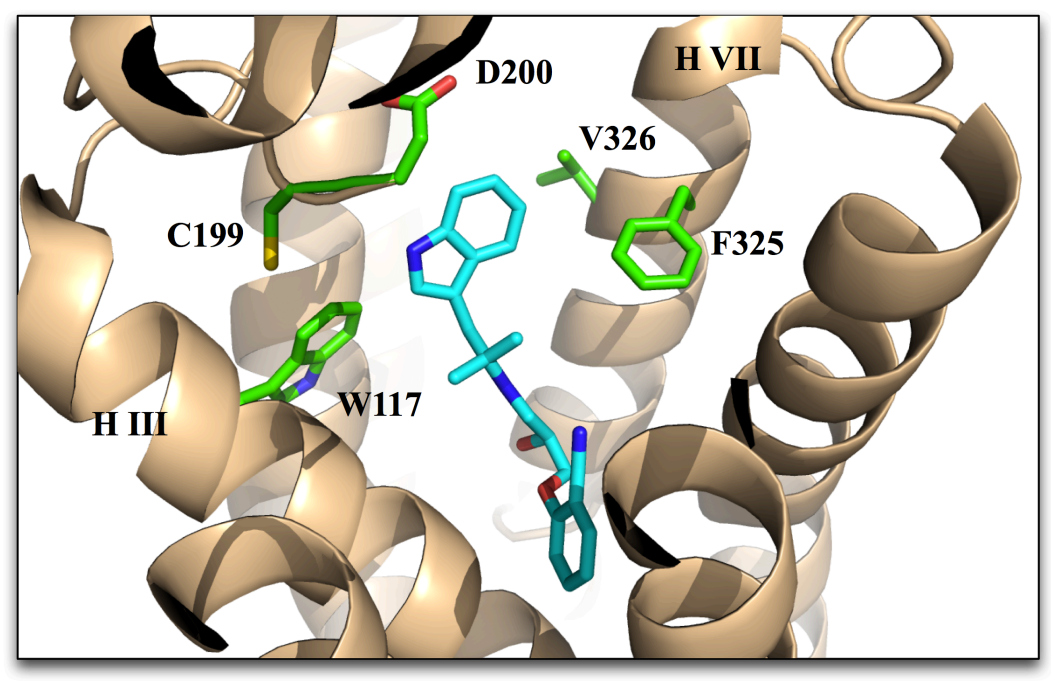


Figure 1-21 Extra interactions between the aromatic substituent of the biased agonist bucindolol and the β_1AR (pdb access code: 4AMI). The protein is shown in wheat, the ligand in cyan and the residues in green.

1.5.3 Structural changes in GPCRs upon activation

Although some of the crystal structures of the β_1AR described in the previous section were obtained in complex with agonists, the receptor was in an inactive, non-signalling conformation formed on initial agonist binding. Despite the valuable details these structures provided on the ligand-binding pocket and the ligand binding mechanisms, they did not provide any information on the conformational changes undergone by the receptor upon activation. However, the high-resolution structures of the A_{2A}R bound to agonists, the bovine ligand-free opsin receptor in an active conformation and the β_2AR in complex with G_s or a nanobody, have provided some of the missing information.

1.5.3.1 The $A_{2A}R$ structures

Three different structures of the $A_{2A}R$ bound to agonists were obtained. The first one was solved in complex with the high affinity slow off-rate agonist UK-432097 with the T4L inserted between helices V and VI (Xu *et al.*, 2011), the other two were obtained from a thermostabilised mutant in an agonist binding conformation and in complex with either adenosine or NECA (Lebon *et al.*, 2011b). All three structures are very similar and the structure of the $A_{2A}R$ in complex with NECA will be used for further discussion in this paragraph. Comparison of the active conformation with the structure of the $A_{2A}R$ thermostabilised in an antagonist conformation bound to ZM241385 (Dore *et al.*, 2011), reveals three major differences in the overall architecture of the receptor. Firstly, the interaction between Thr88 and the ribose ring of the agonist, as well as non polar interactions with Val84 and Leu85 result in a ~2 Å upward movement of helix III along the helical axis (Fig 1-22A).

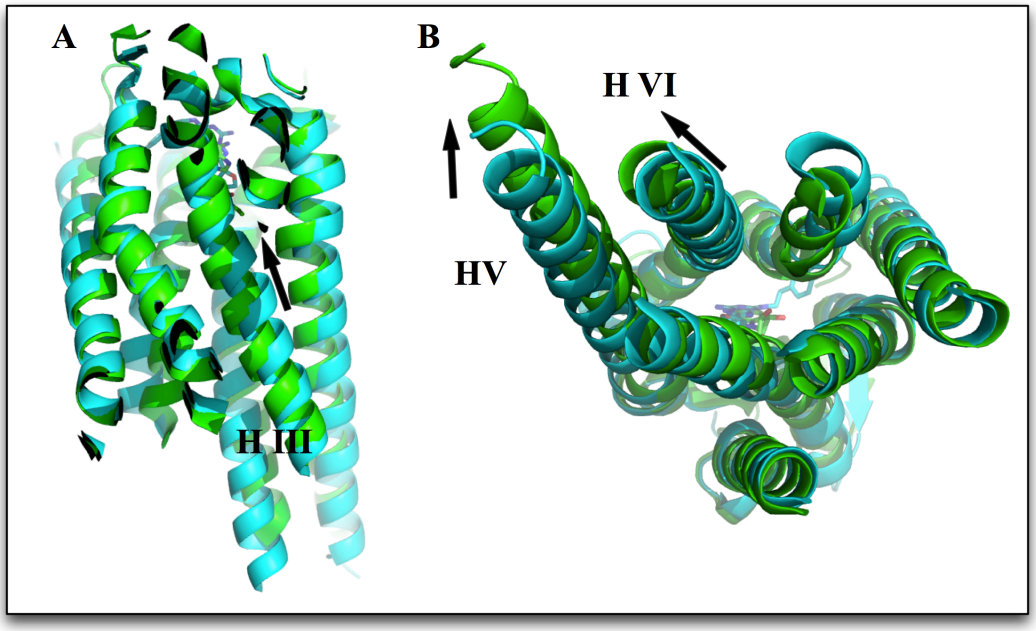


Figure 1-22 Superimposition of the structures of the $A_{2A}R$ bound to the agonist NECA (green, pdb access code: 2YDV) and bound to the inverse agonist ZM241385 (cyan, pdb access code: 3PWH). (A) 2 Å upward movement of helix III upon binding of the agonist NECA. (B) Movements of helices V and VI upon binding of the agonist NECA viewed from cytoplasmic side.

Secondly, the interaction of the agonist with helices III and VII, thought to be involved in receptor activation, leads to the inward shift of helix VII and the upward movement of helix III resulting in the formation of a bulge in helix V (Lebon *et al.*, 2011b). The formation of the bulge is prevented by the binding of the inverse agonist ZM241385, demonstrating its importance in the activation mechanism. Finally, there is also a modification in the conformation of the intracellular ends of helices V, VI and VII (Fig 1-22B). Indeed, there is a 40° rotation and a 3 to 4 Å outward tilt of helix VI. As a result, helices V and VI are closer to each other by about 2 Å in the active conformation. However, it is believed that the receptor bound to NECA is not in the fully active conformation. Indeed, the outward movement of helix VI observed is not enough to open up the G protein-binding cleft.

1.5.3.2 The rhodopsin structures

In this regard, the crystal structures of the bovine opsin receptor both alone or in complex with a synthetic peptide corresponding to the C-terminus of the Gα, in the fully active Ops* conformation provide useful information (Park *et al.*, 2008; Scheerer *et al.*, 2008). Comparison of the rhodopsin and the opsin structures reveals several key conformational changes upon receptor activation (Hofmann *et al.*, 2009). It is worth noting that very few changes are observed in the extracellular end of the receptor. Furthermore, helices I to IV form a stable helical bundle that is unchanged in the Ops* structure (Fig 1-23).

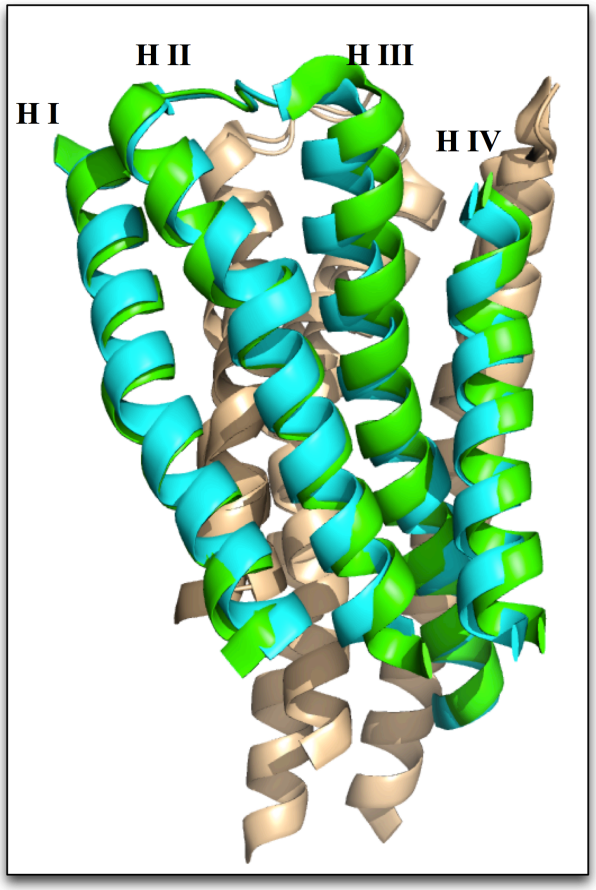


Figure 1-23 Superposition of the opsin (green) and rhodopsin (cyan) structures (pdb access code: 3CAP and 1F88 respectively) showing the similarity in helices I to IV that form a stable helical bundle. Helices V, VI and VII are shown in wheat.

The main conformational modifications are observed in helices V, VI and VII. Indeed, the intracellular part of helix VI undergoes an outward movement of 5 to 6 Å. In addition, helix 5 is extended by 1.5 to 2.5 turns and moves towards helix VI by 2 to 3 Å. Consequently, helices V and VI move closer to each other and away from the helix bundle, resulting in opening of the G protein-binding cleft as observed in the structure of opsin in complex with the G_{α} peptide (Park *et al.*, 2008). In the Ops^{*} structure, the highly conserved DRY and NPxxY motifs form new interactions. Helices III and V interact through the formation of a hydrogen bond between Arg135 and Tyr223 and similarly, helices V and VI interact through the formation of a hydrogen bond between Lys231 and Glu247. This means that in this conformation,

the “ionic lock” is broken and the new position of helix VI is stabilised through this new interaction with helix V. In addition, the conformational change of the intracellular end of helix VII results in the rotation of Tyr306, which prevents helix VI to move back towards helix III (Fig 1-24).

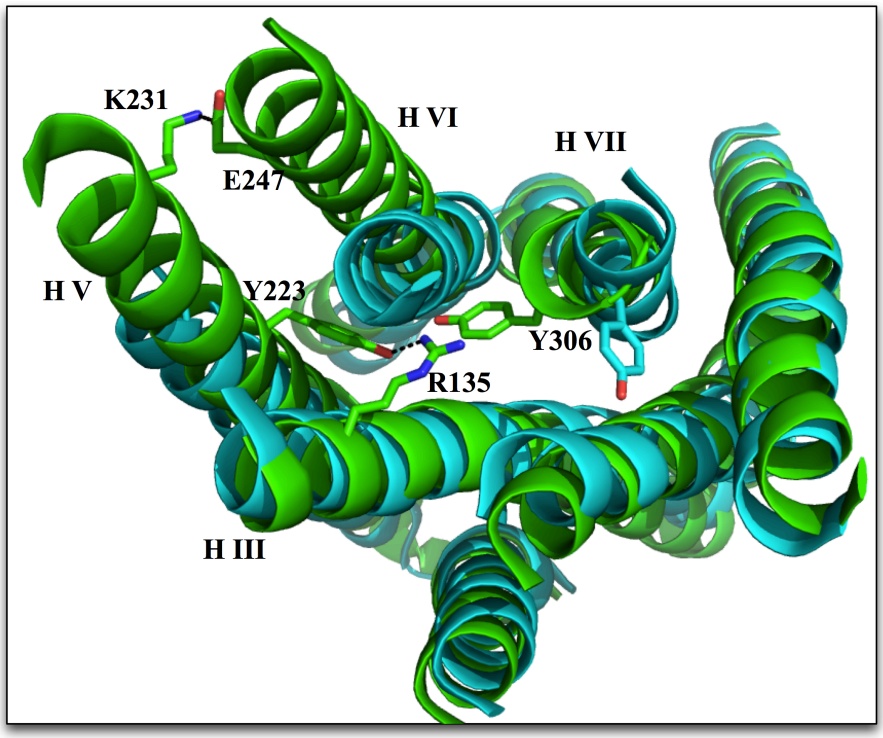


Figure 1-24 Superposition of the opsin (green) and rhodopsin (cyan) (pdb access code: 3CAP and 1F88 respectively) showing the large conformational changes of helices V, VI and VII viewed from cytoplasmic side. Helix V moves towards helix VI, which moves outward, allowing a hydrogen bond formation between K231 and E247. Movement of helix V also allows interaction between Y223 and R135, while rotation of Y306 prevents helix VI from moving back towards helix III.

1.5.3.3 The β_2AR structures

The most exciting addition to the growing collection of high-resolution structures of GPCRs is most certainly the structure obtained by Brian Kobilka’s group of the β_2AR in the active state in complex with the G_s protein (Rasmussen *et al.*, 2011a). Although prior to this one, an other structure of the β_2AR in an active conformation in complex with a nanobody was solved (Rasmussen *et al.*, 2011b), the β_2AR-G_s complex structure will be used for further discussion in this paragraph. The

changes observed in the structure of the β_2AR receptor in the active conformation compared with the receptor in an inactive conformation bound to the antagonist carazolol are very similar to that observed between the Ops* and rhodopsin structures. Indeed, the major modification in the β_2AR-G_s structure is an outward movement of helix VI of 14 Å compared with the β_2AR in complex with carazolol (Fig 1-25). In addition, as previously observed, the rotation of Tyr326 on the intracellular end of helix VII, stops helix VI from moving back towards helix III (Fig 1-25) and the ionic lock is broken. However, while the arginine of the DRY motif in the opsin structure interacts with helix V, in the case of the β_2AR, the arginine interacts with the G protein.

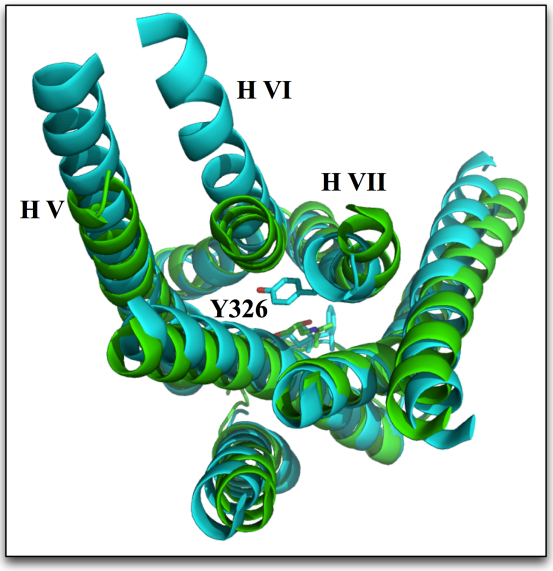


Figure 1-25 Superimposition of the structures of β_2AR in an inactive conformation bound to the inverse agonist carazolol (green, pdb access code: 2RH1) and in an active conformation bound to an agonist and in complex with G_S (cyan, pdb access code: 3SN6) viewed from cytoplasmic side.

As seen in the A_{2A}R, helix V forms a bulge centred on Ser207, which moves towards the binding pocket by 2.1 Å. This leads to the rotation and subsequently to the tilt of helix VI. Finally, one key observation is that the active conformation is stabilised by extensive interactions with GαRas while there are no direct interactions between the receptor and the Gβ or Gγ subunits.

1.5.3.4 Molecular signatures

Ventakakrishnan and colleagues performed a systematic comparison of all GPCRs structures regardless of their conformation. They identified “a consensus network of 24 inter-TM contacts mediated by 36 topologically equivalent amino acids” (Venkatakrishnan *et al.*, 2013). Interestingly, helix III seems to play a central role in maintaining the helical bundle scaffold as it does in the ligand-binding pocket. This is indeed confirmed by mutagenesis studies that demonstrated that in general mutation in helix III causes either constitutive activity or receptor inactivation (Han *et al.*, 2012; Jiang *et al.*, 1997; Jiang *et al.*, 1996).

1.6 The adenosine receptors family

The adenosine receptor family is part of the class A GPCR family and is comprised of four proteins, the A_1, A_{2A}, A_{2B} and A_3 receptors, which all bind the endogenous ligand adenosine (Fredholm *et al.*, 2001). These receptors are classified based on their affinities for adenosine analogues and their mechanism of signal transduction (Klinger *et al.*, 2002a). Both $A_{2A}R$ and $A_{2B}R$ activate adenylyl cyclase via G_s resulting in an increase of cyclic AMP levels (Hide *et al.*, 1992). The A_1 and A_3 receptors interact with G_i and G_o proteins, leading to inhibition of cAMP production (Klinger *et al.*, 2002a).

The $A_{2A}R$ is highly expressed in the spleen, thymus, leukocytes, blood platelets, striatopallidal GABAergic neurons and the olfactory bulb. It is also expressed at lower levels in the heart, lung and blood vessels (Fredholm *et al.*, 2001). It is therefore not surprising that the $A_{2A}R$ has been linked to a number of various diseases such as neurodegeneration (Stevens *et al.*, 2002), Parkinson's disease (Hauser & Schwarzschild, 2005; Volpini *et al.*, 2009; Xu *et al.*, 2005), sleep disorder (Satoh *et al.*, 1998), respiratory disorder (Fozard *et al.*, 2002), hypertension (Fredholm *et al.*, 2001) and ischaemia (Chen *et al.*, 1999; Gui *et al.*, 2009) among others. In addition, the role and function of the $A_{2A}R$ is further complicated by its propensity to form heterodimers with other GPCRs. The $A_{2A}R$ has been shown to form dimers with the cannabinoid CB1 receptor (Ferre *et al.*, 2009), the glutamate mGluR5 receptor (Ferre *et al.*, 2002) and finally the dopamine receptors D2 (Fuxe *et al.*, 2005) and D3 (Torvinen *et al.*, 2005), which have important implications in the treatment of Parkinson's disease. This underlines the importance of the adenosine receptors as therapeutic targets and the need to obtain selective agonists and

antagonists. A large number of pharmaceutical companies have developed or are developing $A_{2A}R$ selective agonists or antagonists with various successes. Of these, Regadenoson is an FDA approved $A_{2A}R$ selective agonist used in cardiac stress tests, Preladenant is a selective $A_{2A}R$ antagonist that showed great results in Parkinson's disease animal model but failed to show efficacy over placebo in phase III clinical trials and Tozadenant is a selective $A_{2A}R$ antagonist for the treatment of Parkinson's disease that was discontinued due to toxicology issues (de Lera Ruiz *et al.*, 2013). The abundance of publications and patents is proof that the $A_{2A}R$ is still actively investigated by pharmaceutical companies. This is one of the reasons why so much effort has been invested in the structure determination of $A_{2A}R$. Five independent structures of this GPCR have now been solved: a thermostabilised $A_{2A}R$ mutant bound to two different agonists (Lebon *et al.*, 2011b), a thermostabilised $A_{2A}R$ mutant bound to a range of antagonists (Dore *et al.*, 2011), the $A_{2A}R$-T4-lysozyme fusion protein bound to an agonist (Xu *et al.*, 2011) and an antagonist (Jaakola *et al.*, 2008) and finally the full length $A_{2A}R$ in an inactive complex with a mouse antibody (Hino *et al.*, 2012).

1.7 Aim of the study

Despite the significant progress made towards structure elucidation of GPCRs in the last few years, the mechanisms of ligand recognition and receptor activation are still unclear. Although the high-resolution structures of the non-rhodopsin GPCRs published so far show surprising similarities, it is still necessary to obtain further structures. In addition, it is important to understand at a molecular level the specificity of each receptor as well as the difference of efficacies of the ligands as it becomes clearer that the GPCRs adopt a much greater range of conformations than originally described by the classical models of GPCR activation.

As discussed previously, one way of stabilising a given GPCR is to generate thermostable mutants through alanine-scanning mutagenesis coupled with radioligand binding analysis. This technique has been used to produce thermostable mutants of the $A_{2A}R$ (Magnani *et al.*, 2008). In the present study, three of the most stable mutants, at that time, were selected for further functional characterisation, namely Rag23, Rant5 and Rant21 (fig 1-26, Table 1-1). Two of these mutants are in a preferentially antagonist conformation (Rant5 and Rant21) and the other one in an agonist conformation (Rag23). All these receptors contain several point mutations. The intermediate mutants between Rant5 and WT as well as between Rag23 and WT have also been characterised.

Table 1-1 Point mutations contained in the different thermostable constructs studied

Constructs	**Mutations**
Rag23	F79A, A184L, R199A, L208A, L272A
Rant5	A54L, T88A, V239A
Rant21	A54L, T88A, K122A, V239A

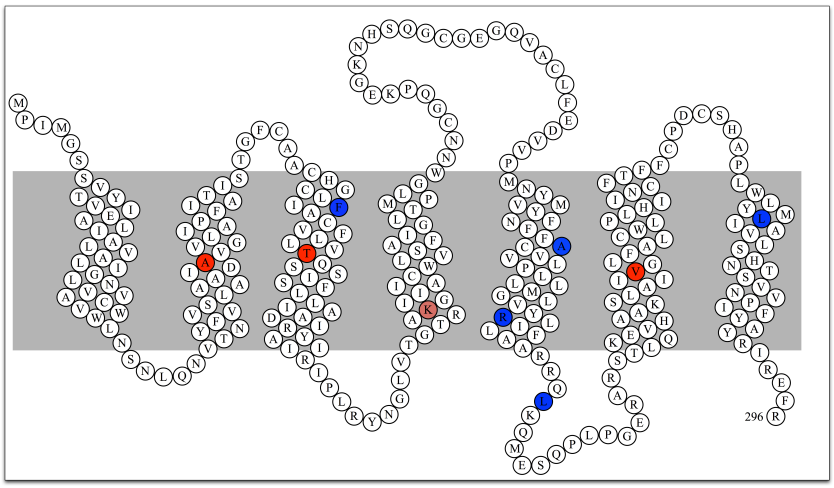


Figure 1-26 Snake plot of the $A_{2A}R$ showing the position of the mutations for the thermostable mutants (Blue: agonist mutations, Red: antagonists mutations) (adapted from Magnami *et al.* 2008)

The aim of this study was to functionally characterise these mutants using a yeast whole cell growth assay in order to further understand how these mutations stabilise the receptor and affect its function and also to develop a high throughput and inexpensive tool to screen for thermostable mutants for other GPCRs. Indeed the functional assay is virtually applicable to any GPCR that can be expressed in yeast and has been used successfully with the cannabinoid CB_1 and CB_2 receptors (Dowell & Brown, 2009), GPR41 and GPR43 (Brown *et al.*, 2003), the adenosine A_{2B} receptor (Beukers, 2004) and the sphingosine S1P1 receptor. Therefore, if the stabilizing effects of the mutant receptors can be linked to function in the yeast growth assay, it may be that this method used in combination with either alanine-scanning mutagenesis or random mutagenesis methods (Dodevski & Pluckthun, 2011) would provide a powerful screening tool for the production of thermostable mutants.

The results presented here reveal that inhibition of constitutive activity is correlated with receptor thermostabilisation. The data also strongly suggest that the agonist-induced and constitutive active conformations are distinct. In addition, the data highlight the role of individual amino acids residues in receptor function.

2 Development of the Yeast Functional Assay

2.1 Introduction

As described previously, most of the crystal structures of GPCRs obtained so far are of highly engineered proteins. Although most of these engineered receptors have been well characterized in terms of ligand binding, far less is known about their signalling profiles. Indeed, replacement of ICL3 by T4L or the presence of an antibody at the G protein-binding site has prevented characterization of signalling function (Fig 2-1).

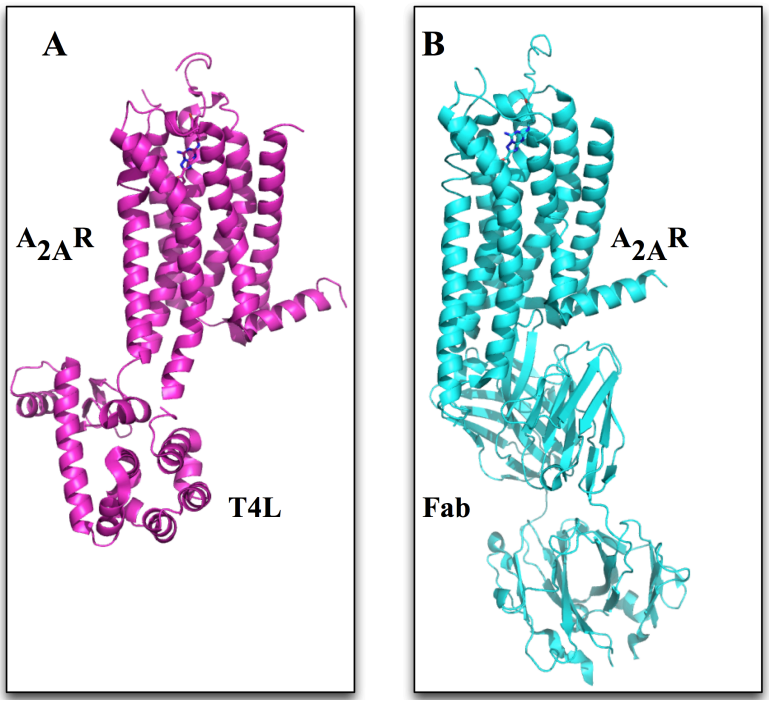


Figure 2-1 Structure of the $A_{2A}R$ as a fusion protein with the T4L (A) and in complex with a Fab (B). In both cases the presence of partner protein prevents the G protein from interacting with the receptor.

In addition, many of the thermostabilised mutant structures have been obtained of receptor preferentially in an antagonist conformation, with reduced affinity for agonists, making meaningful functional characterization difficult. However, one of the thermostabilised mutants of the $A_{2A}R$ ($A_{2A}R$-GL31), expressed in HEK293 cells (Lebon *et al.*, 2011b) and preferentially in an agonist conformation, has been functionally characterized using a cAMP assay. The construct used to

determine the crystal structure of the neurotensin receptor (NTSR1-GW5), expressed in insect cells, has also been functionally characterized using a GTPγS assay (White *et al.*, 2012). However, in both cases, the thermostable mutants were unable to activate their cognate G protein upon agonist binding (Lebon *et al.*, 2011b; White *et al.*, 2012). The deletion of the C-terminal tail of the receptor may partly explain the absence of agonist-induced activity in the case of the A_{2A}R-GL31. Klinger and colleagues showed that a truncated version of the A_{2A}R (1-311) exhibited no constitutive activity at all in a cAMP assay compared with the wild-type (Klinger *et al.*, 2002b). However, the A_{2A}R-GL31 construct shows similar levels of constitutive activity in the cAMP assay compared with the wild-type (Lebon *et al.*, 2011b) despite the truncation of the C-terminal tail (1-316).

Although, the GTPγS and the cAMP assays have the advantage of assessing the receptor in a mammalian system or in insect cells, they also have their limitations. For instance, the GTPγS assay requires the handling of radioactive material, which has inherent disadvantages including cost and safety considerations. The cAMP assay requires expression of the mutants in mammalian cells, which is labour intensive and expensive. Furthermore, mammalian expression systems are complex and expression levels are often difficult to control and vary according to the type of cell used (Atwood *et al.*, 2011). In addition, recombinant host cells may express more than one G protein, which may affect the pharmacological profile of the receptor studied. Indeed, the receptor of interest might interact with more than one G protein, which could make the data more difficult to interpret.

For these reasons a simple, inexpensive and high-throughput signalling assay is required in order to functionally characterize the thermostable A_{2A}R mutants. The

aim of the research in this chapter was to explore the suitability of a yeast GPCR signalling system for assessment of the function of the thermostabilised mutants.

The yeast functional assay used for this study utilizes a modified *S. cerevisiae* strain, MMY24 (Brown *et al.*, 2003), which has been genetically engineered to allow functional characterization of heterologous GPCRs. In this strain, the gene encoding Ste2p, the only yeast GPCR capable of coupling to the yeast pheromone pathway in a haploid cell, was deleted and a chimeric Gα subunit was introduced in which the five C-terminal amino acids of the yeast Gα protein Gpa1p were replaced with the corresponding residues from mammalian Gαi3 (Brown *et al.*, 2003). Therefore, the GPCR is isolated from its native environment and can be studied in combination with a single G protein species in a completely defined system. Receptor activation induces a reporter gene (FUS1-HIS3) in which HIS3, encoding the biosynthetic enzyme imidazoleglycerol-phosphate dehydratase, is under control of the pheromone-responsive FUS1 promoter. Stimulation of the pathway by GPCR activation allows the yeast to grow in media lacking histidine. Hence, growth of the cells in the absence of histidine but the presence of receptor specific agonist provides a measure of receptor activation and signalling. Growth of the cells is measured by changes in the levels of fluorescein, the product of the reaction between Fluorescein-Di-β-D-glucopyranoside (FDGlu) and exoglucanase, an endogenous yeast enzyme secreted from dividing cells (Fig 2-2) (Dowell & Brown, 2009). The output can be manipulated easily to obtain the required sensitivity by varying components such as 3-Amino Triazole (3AT) that is used to regulate both the background and also the reporter capacity. Since 3AT is an inhibitor of imidazoleglycerol-phosphate dehydratase, an essential enzyme for the biosynthesis of

histidine, 3AT is able to reduce any histidine production due to endogenous activity of this enzyme. Therefore only cells expressing functional receptors are able to grow in a media lacking histidine.

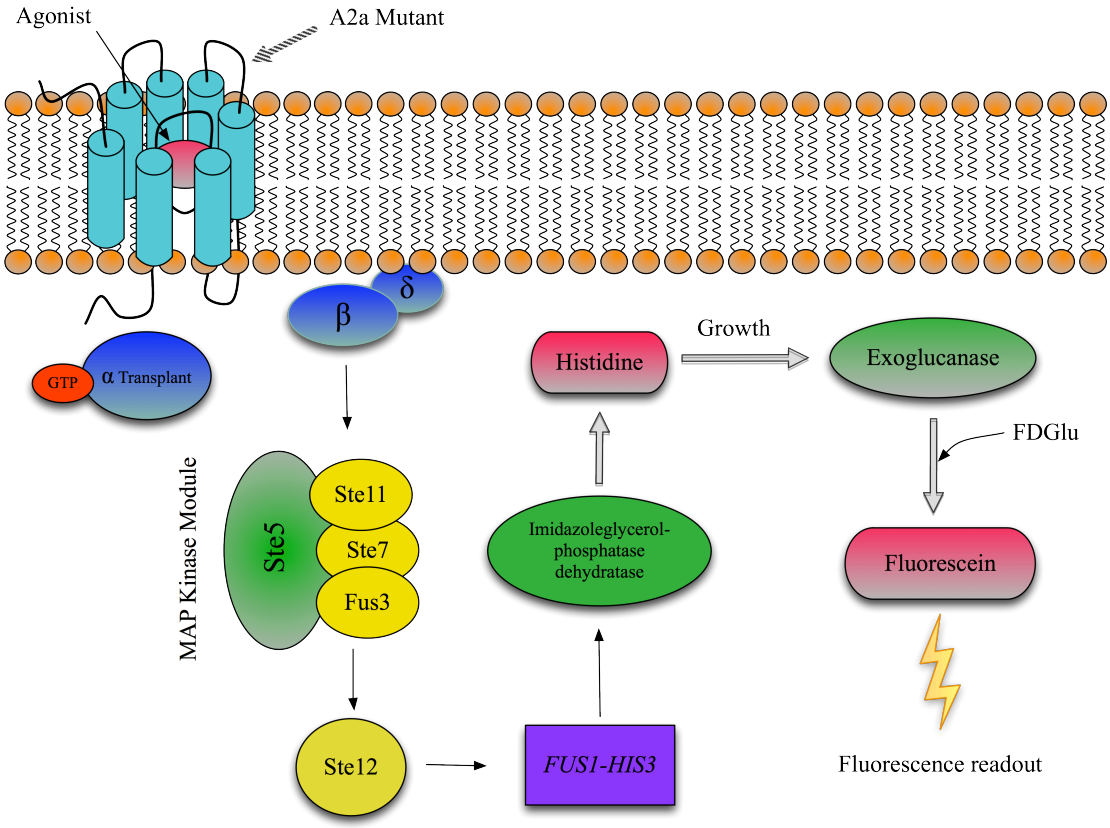


Figure 2-2 Yeast growth functional assay. Activation of the receptor after binding of an agonist induces expression of the *FUS1-HIS3* reporter gene through the yeast pheromone pathway. The product of the *HIS3* gene triggers production of Histidine allowing the yeast to grow in media lacking Histidine. Dividing cells produce exoglucanase which reduces FDGlu to Fluorescein producing fluorescence.

The results presented in this chapter demonstrate that the optimum conditions to assess the pharmacological profiles of the $A_{2A}R$ mutants are when the genes are chromosomally integrated using the p306GPD vector, with an incubation time of 23 hours and a concentration of 3AT of 5 mM.

2.2 Materials and Methods

2.2.1 Materials

StuI, *BamHI* and *HindIII* restriction enzymes were purchased from New England Biolabs (Ipswich, MA, USA). The T4 DNA ligase kit and the QuickChange Lightning Site-Directed Mutagenesis kit were obtained from Agilent technology (Wokingham, UK) while Fluorescein Di-β-D-Glucopyranoside was obtained from Invitrogen (Paisley, UK). The amino acids, as well as the Yeast Nitrogen Base (YNB), the adenosine deaminase and the 3AT were purchased from Sigma (Haverhill, UK). The glucose was obtained from Merck (Nottingham, UK) and the protease inhibitor tablets from Roche (Burgess Hill, UK). The Tris-HCl and the glycerol were purchased from AnalaR NORMAPUR.

2.2.2 Construct generation

Rant5, Rant21 and Rag23 $A_{2A}R$ mutants were obtained from GeneArt (Regensburg, Germany). All synthetic genes encoded the full-length $A_{2A}R$ gene, contained a FLAG tag at the N terminus and were codon optimized for *S. cerevisiae*. The genes were cloned into the pDDGFP *S. cerevisiae* expression plasmid (Newstead *et al.*, 2007) by homologous recombination exactly as described by Drew and colleagues (Drew *et al.*, 2008) using the primers detailed in table 2-1. This places the gene encoding the $A_{2A}R$ upstream of the gene coding for GFP-His8. The pDDGFP plasmids were then digested using *BamHI* and *HindIII* which excised the complete gene coding for the $A_{2A}R$ + GFP-His8 fusion proteins (Fig 2-3). These genes were then ligated into three different expression vectors, p306GPD, p426GPD and

p426GPD-L3, using T4 DNA ligase. p426GPD is an episomal vector with 2μ replication origin and has been fully described previously (Mumberg *et al.*, 1995). p426GPD-L3 is similar to p426GPD but contains the α-factor signalling sequence and p306GPD is an integrating vector based on the pRS306 vector (Sikorski & Hieter, 1989) with a modified promoter. The wild-type $A_{2A}R$ was generated from the Rant5 synthetic gene by site-directed mutagenesis using the QuickChange Lightning Site-Directed Mutagenesis kit and the primers detailed in Table 2.2.

Table 2-1 Primers used to clone the $A_{2A}R$ mutant genes in the pDDGFP vector by homologous recombination. The primer contains a gene specific sequence and an overhang region used for the homologous recombination into 2 μ *S. cerevisiae* GFP-fusion vector.

Primer	Sequence
A_{2A} forward	tcgacggattctagaactagtggatcccccatggattacaaggatgatgatgatgc
A_{2A} A316_reverse	Aaattgaccttgaaaatataaattttccccggcctttgaatggttcttgttg

Table 2-2 Mutagenic primers used to generate the intermediate mutant $A_{2A}R$ constructs.

Primer	**Sequence (5' to 3')**
L54A_forward	cgttgtttctttggctgctgctgatattgcggttggtgttttagc
L54A_reverse	gctaaaacaccaaccgcaatatcagcagcagccaaagaaacaacg
A88T_forward	cttgcttcgttttggttttgactcaatcttctatcttctcc
A88T_reverse	ggagaagatagaagattgagtcaaaaccaaaacgaagcaag
A239V_forward	ctaagtccttggctattatagttggtttgttcgctttgtgttg
A239V_reverse	caacacaaagcgaacaaaccaactataatagccaaggacttag

2.2.3 Expression vector optimization

In order to determine the best expression vector for the yeast functional assay, the Rag23, Rant5 and Rant21 mutants, containing the GFP-His8 tag, were cloned into the three different expression vectors: p426GPD, p426GPD-L3,

containing the α factor signalling sequence and p306GPD (Dowell & Brown, 2009). All three vectors contain the strong GPD constitutive promoter. While the p306GPD is an integrating vector, both p426GPD are episomal vectors.

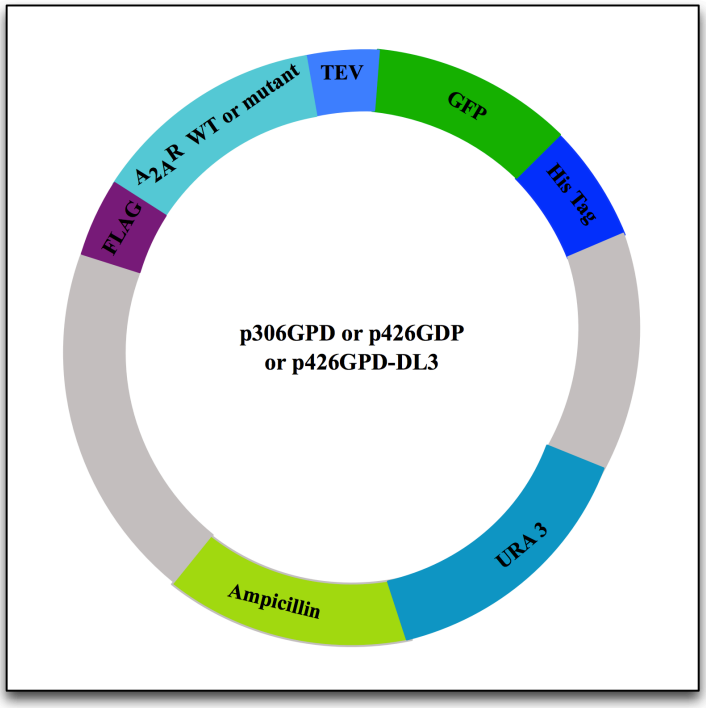


Figure 2-3 Schematic representation of the adenosine $A_{2A}R$ constructs used for the functional assay: The FLAG tag precedes the $A_{2A}R$ gene, which is then followed by a Tobacco etch virus (TEV) cleavage site present to remove the GFP and the 8 His TAG after purification**.**

The three different $A_{2A}R$ vector constructs were transformed using the lithium-acetate procedure (Gietz and Schiestl, 2007) (see appendix 6.3). Prior to transformation, the p306GPD plasmids containing the genes of interest were digested for one hour at 37°C with StuI and subsequently chromosomally integrated at the *ura3* locus in the MMY24 (*MAT*a *fus1*::*FUS1-HIS3 LEU2*::*FUS1-lacZ far1 sst2 ste2 gpa1*::*ADE2 his3 ura3 trp1* Gpa1p/Ga_{i3}) yeast strain (Dowell and Brown, 2009).

2.2.4 In-gel fluorescence

The presence of the GFP tag was used to monitor the expression and quality of the protein produced. The -URA agar transformation plates were first screened after three days incubation at 30°C, using a mercury lamp coupled to a microscope to detect green colonies. Then for each mutant, three green colonies were inoculated in 10 ml of –URA media (6.7g YNB, 2% D-glucose, 1.92g/L amino acid supplement (23.53 mg of L-arginine (HCl), 117.6 mg of L-aspartic acid, 117.6 mg of glutamic acid (monosodium), 35.29 mg of L-lysine, 23.53 mg of L-methionine, 58.82 mg of L-phenylalanine, 441.2 mg of L-serine, 235.3 mg of L-threonine, 35.29 mg of L-tyrosine and 176.5 mg of L-valine) supplemented with 2% glucose and histidine to a final concentration of 20 mg/L, in 50 ml aerated capped tubes. Cultures were incubated at 30°C overnight with shaking at 300 rpm. Cells were harvested by centrifugation at 4 000 g for 10 mins. The supernatants were removed and the cell pellets resuspended in 500 µl of ice cold Yeast Suspension Buffer (YSB) (50 mM Tris-HCl (pH7.6), 5 mM EDTA, 10% glycerol, 1 complete protease inhibitor cocktail tablet (Roche) per 20ml buffer) and transferred into 1.5 ml Eppendorf tubes. 200 mls of acid washed glass beads were added and the tubes were shaken at a frequency of 20 sec^{-1} for 10 mins, using a Tissue Lyser to break the cells. The tubes were then centrifuged at 2 000 g for 15 sec and the supernatants harvested in clean Eppendorf tubes and 500 µl of ice cold YSB added to the cell debris. The operation was repeated, the supernatants collected again and combined with the previous supernatants. The combined supernatants were then centrifuged at 13 000 g for 1 hr. The supernatants were removed and discarded and the membrane pellets resuspended in 100 µl of ice-cold YSB. A 10 µl aliquot of membrane suspension was mixed with

an equal volume of 2X Novex® Tris-Gly SDS-PAGE sample buffer (Invitrogen) for each preparation and the proteins separated on a Novex® 12% Tris-Gly gel (Invitrogen). The Benchmark Fluorescent protein markers (Invitrogen) were used as protein standards. The fluorescent protein bands were detected using a LAS-1000-3000 charged-coupled device (CCD) imaging system (Fujifilm) with an excitation wavelength of 460 nm.

In-gel fluorescence analysis of Rant21 was performed in both the presence and absence of protease inhibitors (PI). One complete protease inhibitor cocktail tablet (Roche) was dissolved in 50 ml of YSB. Cell pellets were then resuspended either in YSB or in YSB+PI.

2.2.5 Confocal microscopy

For each mutant, the same three colonies used for the in-gel fluorescence were inoculated in 10 ml of -URA media supplemented with 2% glucose and histidine to a final concentration of 20 mg/L, in three different 50 ml aerated capped tubes. Cultures were incubated at 30°C overnight with shaking at 300 rpm. Cells were harvested by centrifugation at 4 000 g for 10 mins and the supernatant removed and discarded. A 6 µl of each cell pellet was mixed individually with 24 µl of PBS (137 mM NaCl, 2.7 mM KCl, 10 mM Na_2HPO_4, 1.8 mM KH_2PO_4) and 100 µl of parafix. Each sample mixture was dispensed into individual well of a black 96 well plate (Costar). After 30 mins to allow cells to settle, the supernatants were carefully removed and 50 µl of PBS added to each well. Localization of the properly folded mutants containing the GFP tag was detected using a TCS SP5 II confocal microscope from Leica.

2.2.6 Yeast cell growth assay

The mutants expressed in MMY24 were inoculated in –URA media supplemented with histidine to a final concentration of 20 mg/L, overnight at 30°C. The cultures obtained were diluted into –URA media supplemented with 26.1 mM $Na_2HPO_4.7H_2O$, 21.1 mM NaH_2PO_4 pH 7.0 to an OD_{600} of 0.02. The assay mix was supplemented with 3-aminotriazole (3AT), to a range of final concentrations (see below for details). Fluorescein Di-β-D-Glucopyranoside (FDGlu) was also added to the media to a final concentration of 20 μM. 100 μl of this mix was dispensed across 20 wells of a 96-well plate. 20 different concentrations of NECA, ranging from 0.20 mM to 0.17 pM, were then dispensed across the 20 wells and the plate incubated at 30°C. Yeast growth was assessed by fluorescence measurement using a micro-plate reader (TECAN Ultra Evolution) 23 hours or 44 hours following incubation at 30°C. Log_{10} [NECA] against fluorescence curves were plotted and fitted to non-linear regression, providing EC_{50} values. Data were analyzed using GraphPad Prism 5.0 (GraphPad Software, San Diego, CA, USA).

2.2.7 Optimisation of assay conditions

Different aspects of the assay can be modified to optimize the signal window and to increase the signal to noise ratio. The first parameter examined was the incubation time at 30°C. The fluorescence readings were therefore performed after 23 hours and after 44 hours, in order to monitor the importance of incubation time for the assay. While optimizing the incubation time, a concentration of 2 mM 3AT was used.

As mentioned earlier, the 3AT plays a crucial role in knocking out the endogenous activity of the imidazoleglycerol-phosphate dehydratase. However, it is important to optimize the concentration of 3AT in the assay, to make sure that it does not interfere with the response triggered by the activation of the receptor and to get a good signal window which is defined as the ratio of maximum response : lower response being greater than two. Seven different concentrations were used to determine the most suitable one for this assay. Different volumes of a 1 M stock solution were added to the assay mixture to obtain the final following concentrations: 0 mM, 0.5 mM, 1 mM, 2 mM, 5mM, 10 mM and 20 mM.

Finally, the influence of endogenous adenosine on the assay results was investigated by addition of adenosine deaminase (ADA) to the assay mixture to a final concentration of 100 μM and results were compared with the assay run in the absence of adenosine deaminase both for Rag23 and the wild-type $A_{2A}R$. For this analysis, 5 mM of 3AT were used.

2.3 Results

2.3.1 p306GPD vector is the most suitable vector for the yeast functional assay

The three mutants, namely Rag23, Rant5 and Rant21, were expressed using three different expression vectors: p426GPD, p426GPD-L3 (containing a signalling sequence allowing proper trafficking of the receptor) and p306GPD. In each case protein expression is under control of the GPD constitutive promoter. p426GPD and p426GPD-L3 are episomal vectors while p306GPD vector is an integrating vector.

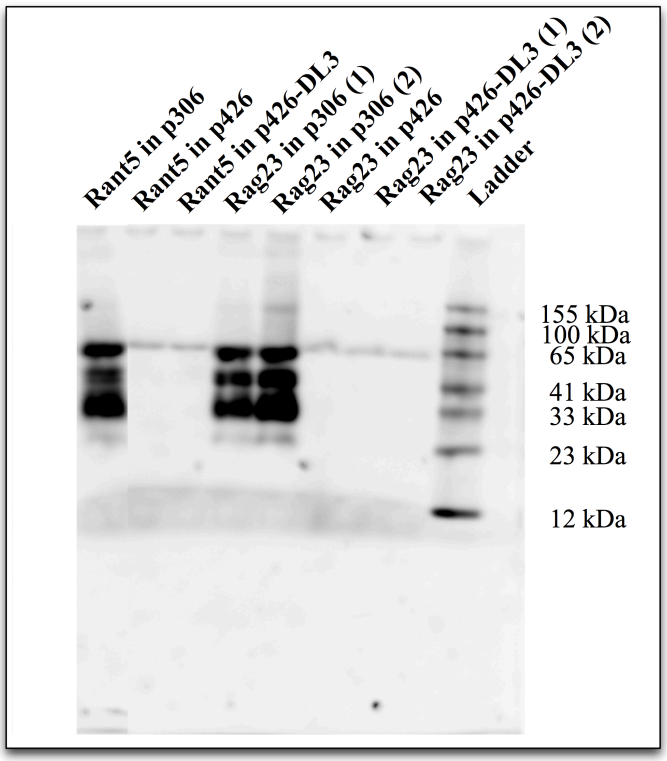


Figure 2-4 SDS-PAGE In-gel fluorescence analysis of Rant5 and Rag23 cloned in p306GPD, p426GPD and p426GPD-L3.expressed in the MMY24 yeast strain

The in-gel fluorescence shows a faint band of approximately 65 kDa for all the lanes. This band is commonly seen when running in-gel fluorescence on membranes obtained from *S. cervisiae* and corresponds to a nonspecific autofluorescent protein (Newstead *et al.*, 2007). For Rag23 and Rant5 in p306GPD, three strong bands can be

seen on the gel, one of which corresponds to the $A_{2A}R$ fused to the GFP (Fig 2-4). The other two bands are likely to be degradation products. No other band than the faint band at 65 kDa is observed when the constructs are cloned in the p426GPD or the p426GPD-L3 vectors. Addition of protease inhibitors did not improve the profiles observed. This could mean that either the protease inhibitors used are not efficient against the proteases degrading the protein or that the degradation observed is not due to protease activity but might be due to modification of the plasmid.

To further assess which one of the expression vectors was the most suitable for the assay, localization of the receptor fused to the GFP was monitored using confocal microscopy. Only the Rag23 and the Rant5 mutants were examined in this case. For Rag23, the images show a high number of cells expressing the receptor, with most of the cells showing green fluorescence and localization to the membrane when the mutant was cloned into the p306GPD vector (Fig 2-5A). However, when cloned into the p426GPD or into the p426GPD-L3 vectors, only a very small number of cells were green and the amount of receptor trafficking to the plasma membrane was much lower than observed for the p306 vector (Fig 2-5B and C).

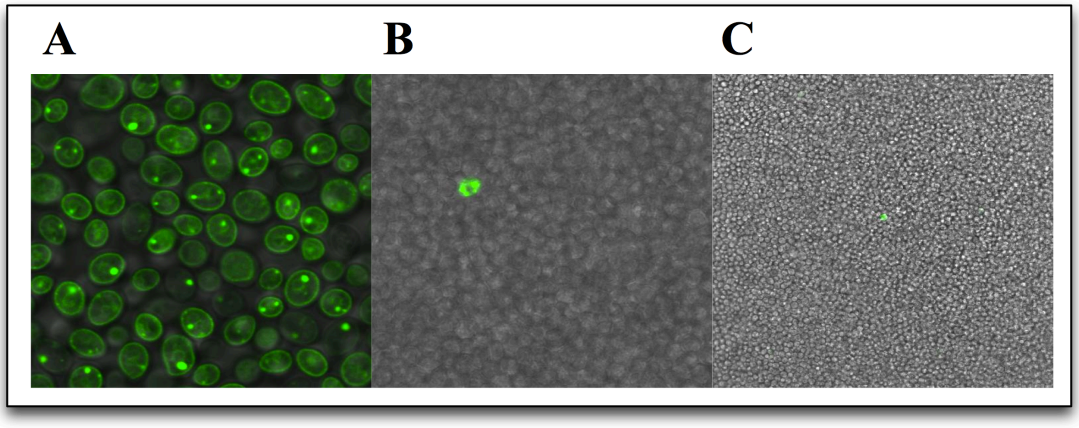


Figure 2-5 Confocal imaging for Rag23 cloned into the p306GPD vector (picture showing only fluorescent cells obtained with the x63 lens) (A), the p426GPD vector (picture showing both fluorescent and non fluorescent cells obtained with x40 lens) (B) and the p426GPD-L3 vector (picture showing both fluorescent and non fluorescent cells, obtained with the x25 lens) (C).

Similarly, the expression of the Rant5 in p306GPD is high, as shown by the number of green cells (Fig 2-6A). Based on GFP fluorescence, the mutant seems to be trafficked properly into the cellular membrane. However, when cloned into the p426GPD or the p426GPD-L3, the number of cells expressing the receptor is low (Fig 2-6B and C) and only receptor produced by the p426GPD-L3 construct is correctly trafficked to the membrane.

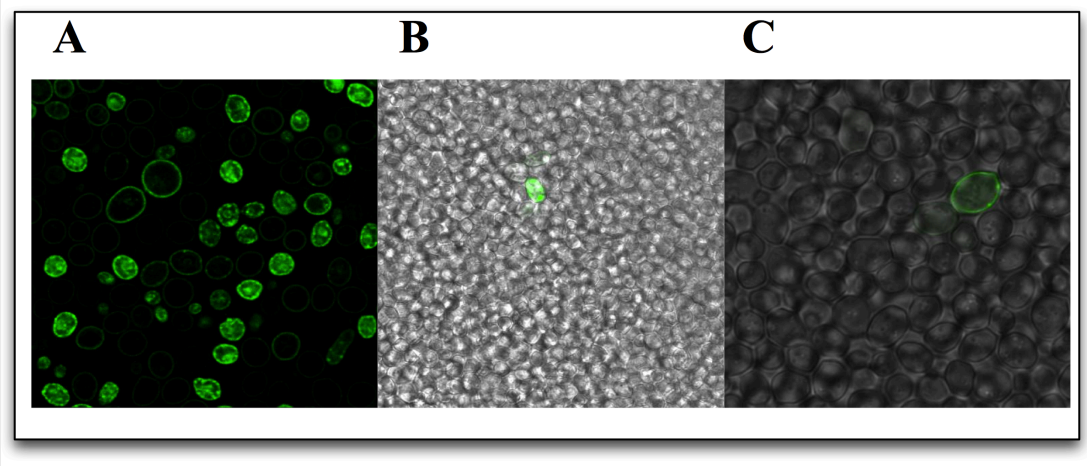


Figure 2-6 Confocal imaging for Rant5 cloned into the p306GPD **vector** (picture showing only fluorescent cells obtained with the x63 lens) (A), the p426GPD vector (picture showing both fluorescent and non fluorescent cells obtained with x40 lens) (B) and the p426GPD-L3 vector (picture showing both fluorescent and non-fluorescent cells, obtained with the x63 lens) (C).

2.3.2 Incubation time and 3AT concentration are critical

As the read out of this assay is a measure of the growth of the yeast, the incubation time before taking the readings is a crucial parameter of this assay. Two different incubation times were investigated using the Rag23 mutant: 23 hours and 44 hours. In both cases the three previously used expression vectors were investigated. The Rag23 mutant, cloned into the p306GPD expression vector yielded a dose-response curve with a positive signal window after 23 hours of induction at 30°C (Fig 2-8A), as demonstrated by the difference between the maximum and the minimum

responses. After 44 hours, although there was still a dose-response curve, the noise has increased significantly compared to the 23 hours incubation time (Fig 2-7B).

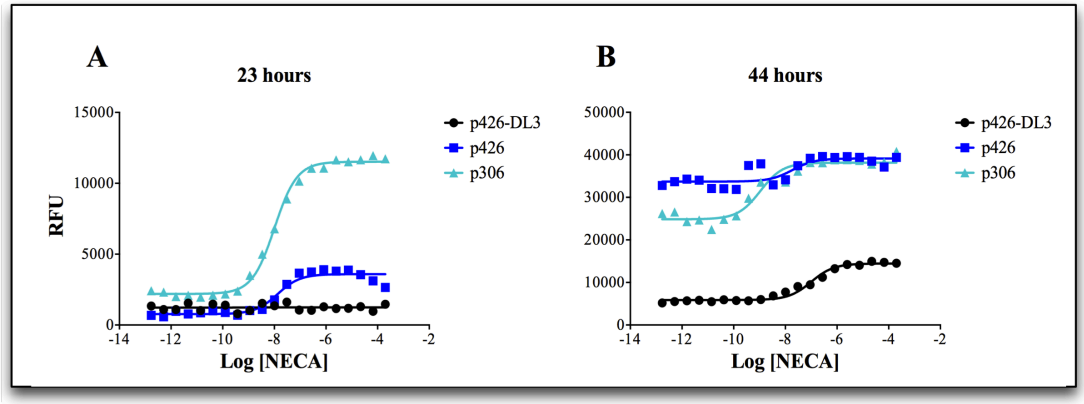


Figure 2-7 Incubation time optimization using the Rag23 mutant cloned into the p306GPD, p426GPD and the p426GPD-L3 expression vectors. Cells were incubated for 23 hours (A) and 44 hours (B) prior to readings being taken. Data points are the average of one experiment performed in triplicate.

When cloned into the p426GPD expression vector, the Rag23 gave a dose-response curve with a very small signal window after 23 hours (Fig 2-7A). After 44 hours cells expressing this construct showed very high levels of growth regardless of the concentration of agonist applied (Fig 2-7B).

After 23 hours, the Rag23 mutant cloned in p426GPD-L3 displayed no growth at all regardless of the concentration of agonist used (Fig 2-8A). However, after 44 hours of incubation, a dose-response curve can be observed (Fig 2-7B). All further work was carried out using the p306GPD vector with a 23 hours incubation time.

As mentioned earlier, another critical parameter of this yeast growth assay is the concentration of 3AT, an inhibitor of the imidazoleglycerol-phosphate dehydratase. Seven different concentrations of 3AT were investigated using the wild-type $A_{2A}R$ cloned into the p306GPD expression vector. Readings were taken following 23 hours incubation at 30°C. When 0 mM, 0.5 mM and 1 mM final concentration of 3AT were used there is no dose-response curve observed, due to very high background (Fig 2-8). When the 3AT concentration was increased to 2 mM, a dose-response curve can be

seen but the signal window is very small due to a very high background. When 5 mM, 10 mM and 20 mM of 3AT were used, dose-response curves were obtained with good signal windows. However, only at 5 mM 3AT was the maximum response not affected, thus this concentration was used for further experiments.

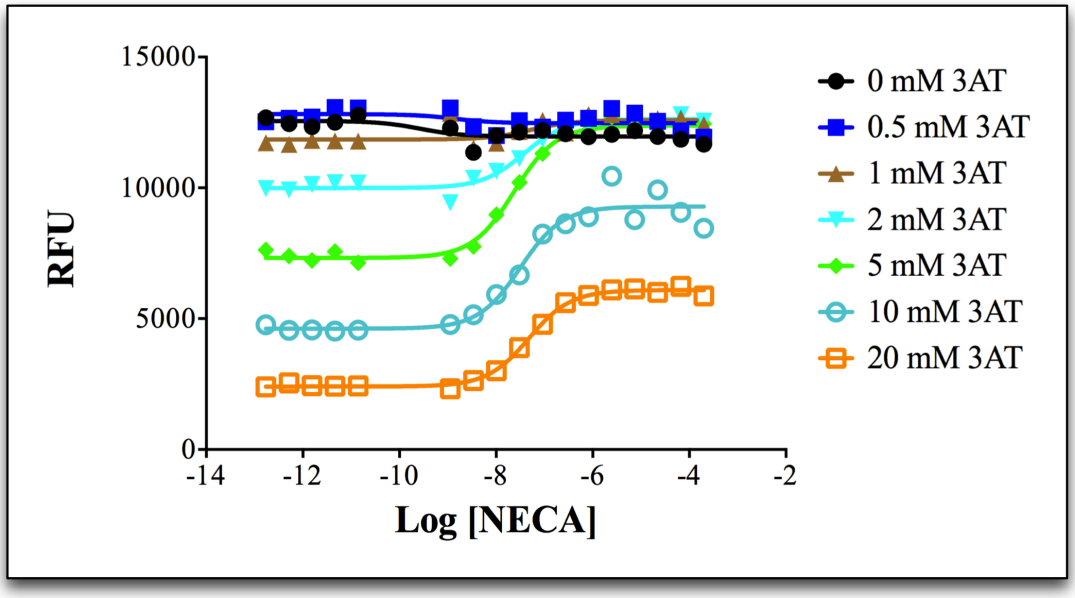


Figure 2-8 3AT concentration optimization: 7 different concentrations of 3AT were investigated using the wild-type $A_{2A}R$ cloned in the p306GPD vector. Data points are the average of one experiment performed in triplicate.

The effect of any potential endogenous adenosine on the output of the assay was investigated by the addition of Adenosine deaminase. Fig 2-9 clearly shows that the addition of ADA did not affect the data meaning that endogenous adenosine is not interfering with the assay also demonstrating that it was not necessary to add ADA to further assays.

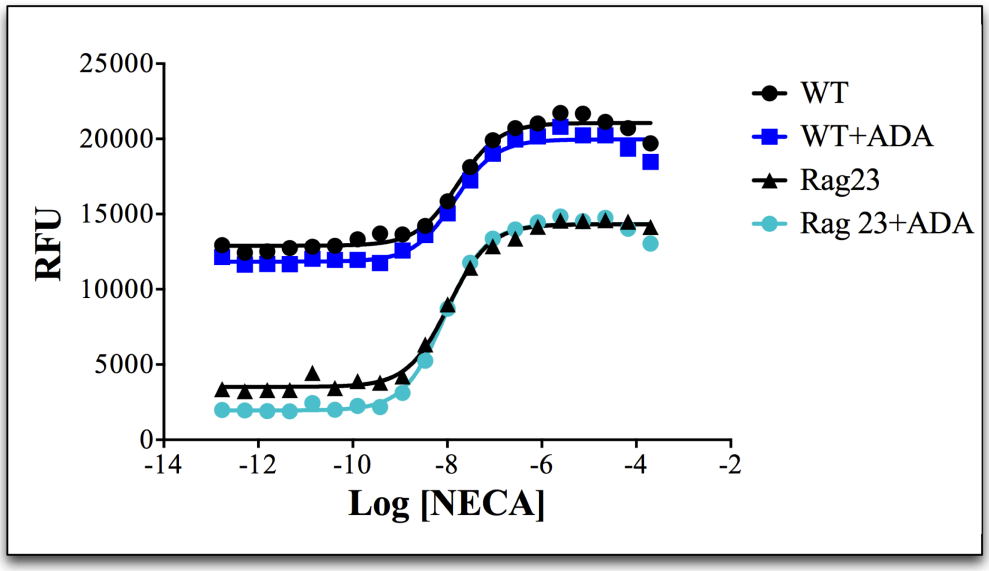


Figure 2-9 Effect of ADA on the activity profiles of the wild-type $A_{2A}R$ and the Rag23 with 5 mM of 3AT. Data points are the average of one experiment performed in triplicate.

2.4 Discussion

The yeast functional assay required optimization in order to be utilized for the studies of the WT and mutant A_{2A}Rs. The first step of assay optimization involved assessment of which expression vector resulted in adequate expression levels and correct localization of the receptors within the cells. The constructs containing the GFP were cloned in three different expression vectors. The quality of the protein expressed was monitored by in-gel fluorescence while localization was monitored by confocal microscopy. Incubation time with agonists, concentration of 3AT and role of endogenous adenosine were also investigated.

The p306GPD integrating vector gave the best expression levels and membrane localization. It is unclear why the integrating vector gave better results than the episomal vectors.

Investigation of the optimal incubation time with agonist was also assessed using the functional assay. The results confirmed the earlier finding indicating that using the p306GPD vector resulted in higher receptor expression. As shown in Figure 2-7, after 23 hours a dose-response curve is observed when the mutant was cloned into the p306GPD vector. When expressed using the p426GPD vector, although a dose-response curve is observed after 23 hours, the signal window is greatly reduced. This is mainly due to a very low efficacy achieved at saturating concentrations of agonist, consistent with low expression levels. When cloned into the p426GPD-L3 vector, the Rag23 shows no dose-response curve at all after 23 hours.

However, after 44 hours incubation time, the profiles observed are quite different. Indeed, the Rag23 cloned into the p306GPD vector still exhibits a dose-

response curve but with an increase noise signal. The Rag23 cloned into the p426GPD shows very high level of growth regardless of the concentration of agonist used.

In contrast, the Rag23 cloned into the p426GPD-L3 vector now shows a dose-response curve. This data indicate that when using the p426GPD-L3 expression vector, there is a delay in expression and trafficking of the receptor. Indeed, the in-gel fluorescence and confocal data were obtained after overnight cultures and showed no detectable expression of the protein. This was confirmed by the lack of signal in the functional assay. However, after 44 hours, the yeast seems to be expressing some functional protein as demonstrated by the dose-response curve obtained in the yeast growth assay.

Obtaining a clear signal window is important in order to achieve high assay sensitivity. Especially since it is expected that a range of different functional profiles will be observed. The 5 mM 3AT concentration was chosen for future assays for two reasons. Firstly, when using 5 mM of 3AT, the maximum response obtained at saturating concentrations of agonist is the same as obtained when using no 3AT. In contrast, both 10 and 20 mM 3AT reduced the maximum response. This means that the 3AT is not limiting the maximum response when using 5 mM. Secondly, when using 5 mM of 3AT, the signal window obtained was around two.

Finally, the addition of adenosine deaminase has no effect on the functional profiles of the wild-type and Rag23 receptor constructs in the yeast growth assay. This indicates that there is no interference from endogenous adenosine in this assay. Indeed, if adenosine had any effect at all, this should be reduced by the addition of

ADA, which metabolizes any adenosine present. Therefore ADA was not added when further assays were performed.

In summary, a yeast cell-based receptor-signalling assay was optimized to allow assessment of the functional profiles of the wild-type and thermostabilised mutant $A_{2A}R$ constructs. The p306GPD vector was chosen for expression since it gave the best results in terms of functional expression and localization of the receptors. In addition, the optimal incubation time used following this study was 23 hours in the presence of 5 mM of 3AT and no ADA. Using this set of conditions, this assay was optimized to provide a robust, high throughput and inexpensive tool to functionally characterize a set of thermostable $A_{2A}R$ mutants.

3 Functional characterizations of the Rag23, Rant5, Rant21 and some intermediate mutants

Part of the work presented here has been published in:

Br J Pharmacol. 2013 Jul; 169 (5): 988-98

Loss of constitutive activity is correlated with increased thermostability of the human adenosine $A_{2A}R$

Nicolas Bertheleme, Shweta Singh, Julia Hubbard, Simon Dowell, Bernadette Byrne

3.1 Introduction

Three of the most thermostable $A_{2A}R$ mutants generate by alanine-scanning mutagenesis (Magnani *et al.*, 2008) were investigated using both the yeast assay and a radioligand binding assay. One of these mutants is in a preferentially agonist-binding conformation (Rag23) and contains the following five mutations: F79A, A184L, R199A, L208A and L272A. The other two are preferentially in an antagonist-binding conformation (Rant5 and Rant21) and contain respectively the following three and four mutations: A54L, T88A and V239A; A54L, T88A, K122A and V239A.

Here the effects of these mutants on $A_{2A}R$ function are explored using the yeast cell growth assay described in the previous chapter. To further investigate the effect of individual mutations on the pharmacological profile of the receptor, intermediate mutants, between Rant5 and WT containing one or two mutations were generated and also characterized in the yeast cell growth assay.

In addition, Rag 23.1, an intermediate mutant between Rag 23 and WT in which the L208A was mutated back to the original leucine was characterised. The Rag 23.1 mutant was investigated because of the crucial localisation of L208 in ICL3.

Using the previously optimized yeast growth assay, three pharmacological parameters of the receptor constructs were examined. Firstly, the efficacy is a measure of the maximum response obtained when saturating concentrations of agonist are used (Fig 3-2). It represents how efficiently the receptor is able to activate its cognate G protein when fully activated by an agonist. Secondly, the constitutive activity is a measure of the activity of the receptor in the absence of agonist (Fig 3-2). It can be graphically illustrated as shown in figure 3-2 by the receptor activity at very

low concentrations of agonist. Finally, the potency is defined as the concentration of agonist necessary to obtain fifty percent of the maximum agonist-induced response (Fig 3-1). The potency is represented either by the EC_{50} or the pEC_{50}. Therefore, this assay allows us to make the distinction between agonist-induced activity and constitutive activity.

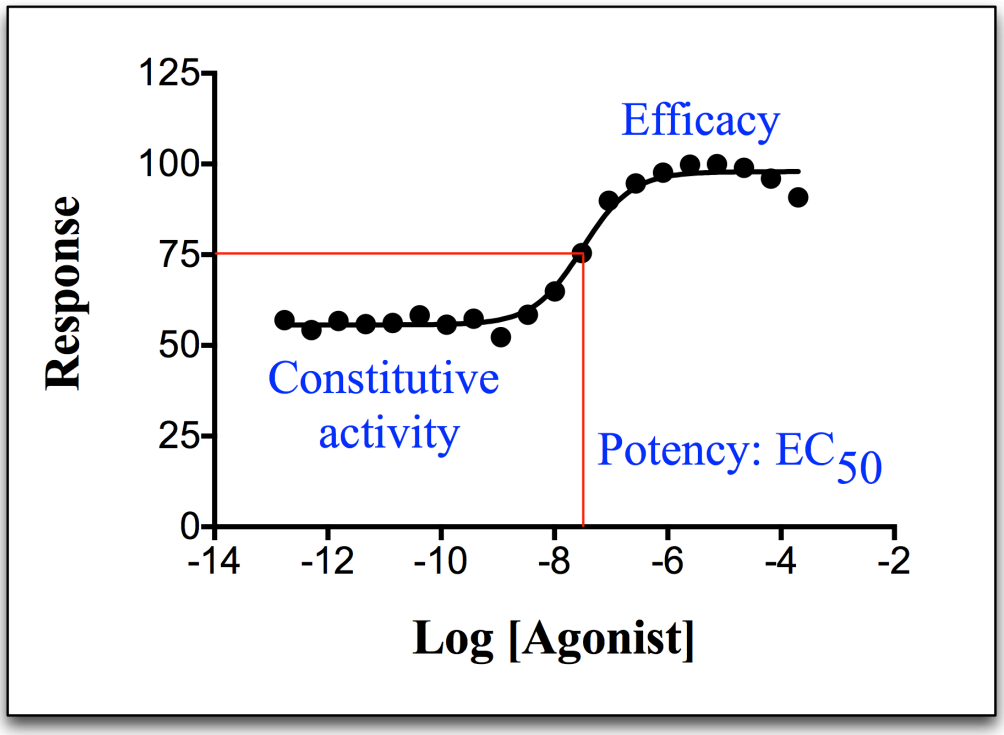


Figure 3-1 Dose-response curve illustrating the concepts of efficacy, potency and constitutive activity. The efficacy is graphically illustrated by the plateau reached at saturating concentrations of agonist. The constitutive activity is graphically illustrated by the plateau reached at very low concentrations of agonist. The potency is illustrated by the red lines.

The data presented in this chapter indicate that there is a correlation between loss of constitutive activity and thermostability. Furthermore, the data suggest that the agonist-induced and constitutively active conformations are distinct.

3.2 Material and Methods

3.2.1 Material

Yeast nitrogen base and yeast extract were purchased from Difco. Peptone, L-histidine, EDTA, EGTA, bovine serum albumin, Folin-Ciocalteau reagent, amino acids, 3AT, trichloro acetic acid, adenosine and theophylline were obtained from Sigma-Aldrich and dimethyl sulfoxide (DMSO) was purchased from Acros Organics (Geel, Belgium). Scintillation cocktail (Ultima Gold MV) and [^{3}H]NECA were obtained from PerkinElmer (Cambridge, UK). [^{3}H]ZM241385 was obtained from American Radiolabelled Chemicals Inc. (Royston, UK), while ZM241385 and NECA were obtained from Tocris (Abingdon, UK). GF/B filters were from Whatman (Little Chalfont, UK). The Lightning Quikchange site directed mutagenesis kit was obtained from Agilent technology (Wokingham, UK). Fluorescein Di-β-D-Glucopyranoside was purchased from Invitrogen (Paisley, UK).

3.2.2 Site-directed mutagenesis

The wild-type $A_{2A}R$ and most of the intermediate mutants were generated from the Rant5 synthetic gene by site-directed mutagenesis using the QuickChange Lightning Site-Directed Mutagenesis kit and the primers detailed in Table 3-1.

The Rag23.1 intermediate mutant (F79A, A184L, R199A, L272A), was obtained from the Rag23 synthetic gene by site-directed mutagenesis using the QuickChange Lightning Site-Directed mutagenesis kit and the primers detailed in Table 3-1.

Table 3-1 Mutagenic primers used to generate the intermediate mutant and wild-type $A_{2A}R$ constructs.

Primer	**Sequence (5' to 3')**
L54A_forward	cgttgtttctttggctgctgctgatattgcggttggtgttttagc
L54A_reverse	gctaaaacaccaaccgcaatatcagcagcagccaaagaaacaacg
A88T_forward	cttgcttcgttttggttttgactcaatcttctatcttctcc
A88T_reverse	ggagaagatagaagattgagtcaaaaccaaaacgaagcaag
A239V_forward	ctaagtccttggctattatagttggtttgttcgctttgtgttg
A239V_reverse	caacacaaagcgaacaaaccaactataatagccaaggacttag
A208L_forward	ctattttcttggctgccagaagacaactaaagcaaatggaatctcaacc
A208L_reverse	ggttgagattccatttgctttagttgtcttctggcagccaagaaaatag
V239I_forward	ctgccaagtcactggccatcattatagggctctttgcc
V239I_reverse	ggcaaagagccctataatgatggccagtgacttggcag

3.2.3 Expression

Since the level of constitutive activity as well as the efficacy of the different constructs will be compared, it is essential to estimate the expression levels of each mutant produced in the yeast system. Indeed, the levels of constitutive activity and efficacy are dependant on the number of functional receptors per cell. In contrast, the potency is not affected by expression levels. As described in chapter 2, all the $A_{2A}R$ constructs were fusions with a C-terminal GFP-8His tag in the p306GPD vector, transformed using the lithium-acetate procedure (Gietz & Schiestl, 2007) and chromosomally integrated at the *ura3* locus in the MMY24 (*MAT*a *fus1*::*FUS1-HIS3 LEU2*::*FUS1-lacZ far1 sst2 ste2 gpa1*::*ADE2 his3 ura3 TRP1*::*GPA1-Gai3*) yeast strain (Dowell & Brown, 2009). The wild-type and Rag23.1 constructs were also transformed into the MMY11 (*MATa fus1*::*FUS1-HIS3 LEU2*::*FUS1-lacZ far1 sst2*

ste2 gpa1::ADE2 his3 ura3 TRP1) yeast strain which has the same genotype as MMY24 but lacks the Gα protein. Estimation of the expression levels for all the constructs was obtained from the B_{max} values obtained from the saturation binding assays. In addition, the fluorescence of the GFP was also used as previously described (Drew *et al.*, 2008). Briefly, 10 ml of yeast culture expressing the desired protein were centrifuged at 4000 *g* for 10 minutes and resuspended in 200 µl of PBS. 200 µl were transferred into a black 96-well plate and the relative fluorescence units (RFU) were measured using a SpectraMax M2^e from Molecular Devices. The process was also performed with 10 ml of yeast culture not expressing the protein. The GFP concentration was obtained using the RFU of a known concentration of GFP in a final volume of 200 µl with the following formula:

$$\text{Conc GFP} = (RFU_{protein} - RFU_{no\ protein}) \times (\text{known Conc of GFP}) / RFU_{GFP}$$

This concentration was then divided by 40 and multiplied by 0.6 to determine the concentration in the 200 µl of buffer and to account for the recovery, which is typically 60%. This was then multiplied by the mass of the desired protein and divided by the mass of GFP to obtain the membrane protein overexpression in mg/L of culture.

3.2.4 Membrane preparation

Cells were resuspended in cold breaking buffer (50 mM Tris.HCl (pH7.6), 1 mM EDTA, 0.6 M sorbitol, 1 tablet of protease inhibitor for 100 ml). Glass beads were added to the suspension and cells were broken using a tissue lyser (Qiagen) set to 20 Mhz for 10 min. The suspension was then centrifuged at 4000 g for 1 min and the supernatant transferred to a new eppendorf tube. Cell debris and glass beads were resuspended and the same operation was repeated. Combined supernatants were then centrifuged at 13 000 g for 1 hour to collect the membranes. The supernatant was discarded and the membrane pellets resuspended in membrane buffer (20 mM Tris.HCl (pH7.5), 150 mM NaCl, 20% glycerol, 1 tablet of protease inhibitor for 100 ml), flash frozen in liquid nitrogen and stored at -80°C.

3.2.5 Protein concentration

All protein concentrations were determined as previously described (Lowry *et al.*, 1951; Singh *et al.*, 2010). A stock solution of BSA at 1 mg/ml was used to generate a standard curve. 0, 5 10, 20, 40, 60, 80, 100 μL of the stock solution were dispensed in eppendorfs in triplicate in addition to 5 and 10 μL of the test protein. 1 ml of 10% trichloro acetic acid (TCA) was added to all tubes, which were vortexed immediately. The tubes were centrifuged at 4000 g for 15 min. The supernatant was discarded and the precipitate dried for 10 min. 650 μl of a solution containing Lowry solution A (2% anhydrous Na_2CO_3, 0.1 M NaOH), Lowry solution B (4% $CuSO_4.5H_20$) and Lowry solution C (2% NAK tartrate) at a 100/1/1 ratio were added. The tubes were vortexed immediately and incubated at room temperature for 10 min.

The Folin-Ciocalteau reagent was diluted with an equal volume of water and 100 µl of this solution was added to each tube. The tubes were vortexed immediately and incubated at room temperature for 10 min. 650 µL of ddH_20 was added to each condition and the tubes were vortexed immediately. The OD_{760} absorbance values were plotted versus the BSA concentration. The amount of protein in the test sample was calculated from the standard curve using GraphPad Prism 5.0 (GraphPad Software, San Diego, CA, USA).

3.2.6 Saturation binding assay

For saturation assays membranes expressing the WT or mutant $A_{2A}R$ forms were incubated with [^{3}H]ZM241385 (0.036 – 20 nM) in binding buffer (20 mM HEPES pH 7.4, 1 mM EDTA,1 mM EGTA, 0.1% BSA). Non-specific binding was defined in the presence of 10 mM theophylline at each concentration. The WT and Rag23.1 membranes, prepared in the absence of NaCl, were also incubated with [^{3}H]NECA (0.3-300 nM) in an alternative binding buffer (20 mM HEPES pH 7.4, 1 mM EDTA, 1 mM EGTA, 0.1% BSA, 10 mM $MgCl_2$). Non-specific binding was defined in the presence of 10 mM theophylline at each concentration. Assays were performed at least in duplicate in a final volume of 1 ml containing 20 µg of membrane protein in each tube. The reactions were incubated for 3 h at room temperature. Following incubation, receptor bound radioligand was collected by filtration through Whatman glass micro-fibre GF/C filters which were then placed in individual scintillation vials containing 2 ml of Ultima GoldTM XR scintillation fluid. The filters were allowed to soak for at least six hours before the radioactivity was determined using an LS 6500 Beckman Coulter scintillation counter.

The data were obtained as Disintegration Per Minute (DPM), which were then converted in radioligand concentrations (pmol) using the specific activity of the ligand. Finally, the data were plotted as pmol of radioligand bound by mg of protein against the free concentration of radioligand added. The curves were fitted to a non-linear regression using a one-site binding model. This provided two parameters: the dissociation constant K_d and the B_{max}. The K_d is defined as the concentration of ligand needed to occupy half of the receptor binding sites and therefore is a measure of the affinity of the ligand for the protein. The B_{max} represents the maximum number of receptor binding sites occupied at saturating concentrations of ligand. Therefore, it is a measure of the number of functional binding sites.

3.2.7 Competition binding assay

Agonist competition binding profiles for the WT and mutant receptor forms were determined by competition binding assays. 20 μg of membrane protein containing WT and mutant $A_{2A}R$ were incubated with a fixed concentration of [^{3}H]ZM241385 (2 nM for Rant5, Rant21 and T88A and 9 nM for Rag23) and varying concentrations of competing NECA (100 μM to 1 nM for WT and Rag23 and 10 mM to 10 nM for Rant5, Rant21 and T88A) or Adenosine, in a final volume of 1 ml binding buffer. Non-specific binding was defined in the presence of 10 mM theophylline. Initiation, incubation and termination procedures were as described for the saturation binding assay.

3.2.8 Yeast cell growth assay

The yeast cell growth assay was performed as described in Chapter 2; Section 6. The RFU measured were normalised to the WT in each experiment. 100% represents the maximum response of the WT and 0% represents the response obtained in the absence of receptor.

3.3 Results

3.3.1 Expression levels

As mentioned previously, monitoring expression levels of each mutant form of the receptor is important in order to be able to accurately compare the constitutive activities and efficacies of the different constructs. This was done by measuring the fluorescence of GFP. The B_{max} values obtained from the saturation binding assays are also a measure of the expression levels. However, in the case of the B_{max}, the values are generated after membrane preparation. During this process, some of the protein may be degraded and the amount that is lost is likely to be construct-dependent. This may explain the discrepancies seen in the expression levels assessed by eGFP measurement and radioligand binding analysis. Results are summarized in table 3-2.

Table 3-2 Expression levels of the different $A_{2A}R$ + eGFP constructs in the MMY24 strain.

Constructs	**Expression (mg/ml)**	**B_{max}±SEM (pmol/mg)**
WT	0.8	1.1±0.2
Rag23	1.0	5.1±0.4
Rag23.1	1.1	1.8±0.7
Rant5	1.2	6.5±0.5
Rant21	1.6	5.8±0.7
A54L	1.1	ND
T88A	1.1	2.5±0.1
V239A	1.0	ND
A54L+T88A	0.7	ND
A54L+V239A	0.9	ND
T88A+V239A	1.2	ND

The expression levels of all constructs were calculated from the relative fluorescence units as described in Drew et al. (2008). The B_{max} values of the WT, Rant and Rag constructs were assessed by radioligand binding analysis of membrane bound receptor. ND: not determined.

In general, the expression levels expressed as mg/ml are similar for the different constructs. The major discrepancy concerns the wild-type and the Rant21. However, this does not influence our conclusions since the wild-type exhibits higher constitutive activity and efficacy than the Rant21 despite a lower expression level (see Fig 3-2).

3.3.2 Pharmacological profiles of the WT and mutants $A_{2A}R$

3.3.2.1 Wild-type, Rag23, Rant5 and Rant21

3.3.2.1.1 The Yeast cell growth assay

A summary of the pharmacological data for the constructs is given in Table 3-3. In the yeast cell assay, increases in fluorescence due to the production of fluorescein, report increases in cell growth driven by receptor activation. The wild-type receptor exhibits high levels of constitutive activity, observed as cell growth in the absence of any receptor agonist (Fig 3-2A, Table 3-3). The constitutive activity represents more than 50% of the total activity of the wild-type receptor. This is consistent with the high level of $A_{2A}R$ constitutive activity observed in a mammalian cell system as assessed by cAMP accumulation (Klinger *et al.*, 2002a). Addition of the $A_{2A}R$ agonist, NECA, further activates the receptor in a concentration dependent manner (pEC_{50} = 7.5 ± 0.1; Fig 3-2A; Table 3-3). The constitutive activity of the wild-type was partially inhibited by inverse agonists (Fig 3-3).

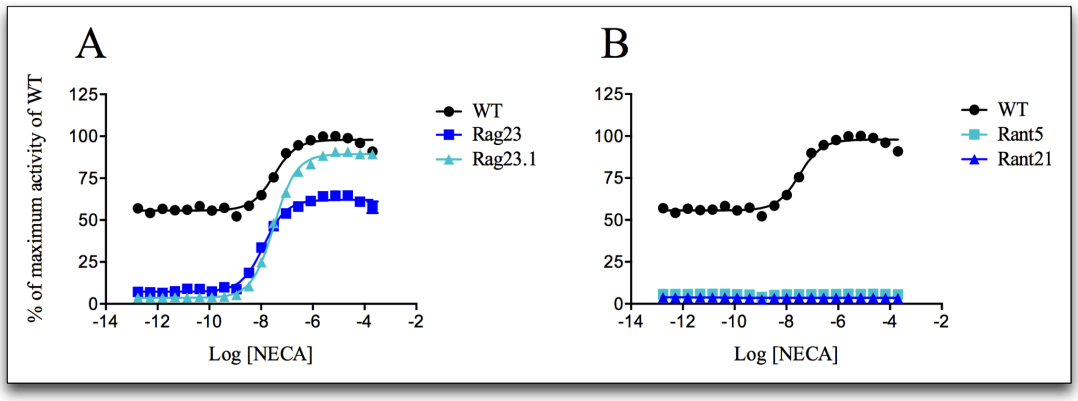


Figure 3-2 Functional data for the thermostabilised A_{2A} mutants Rag23, Rant5 and Rant21 compared to WT expressed in the MMY24 *S. cerevisae* strain as constructs in the p306GPD vector. Data points are the average of three different experiments performed in triplicate. (A) WT, Rag23, Rag23.1 (B) WT, Rant5, Rant21.

Table 3-3 Pharmacological characteristics of the wild-type and mutants A_{2A} forms.

Receptor form	NECA pEC_{50} ± SEM	Constitutive activity ± SEM (% of max activity of WT)
WT (n=3)	7.5 ± 0.1	54.8 ± 1.5
Rag23 (n=3)	7.9*	6.1 ± 0.9
Rant5 (n=3)	ND	5.3 ± 0.4
Rant21 (n=3)	ND	3.5 ± 0.2
Rag23.1 (n=2)	7.5*	3.6 ± 0.2

*SEM=0

Data are presented as mean ± standard error means of at least two independent experiments performed in triplicate.

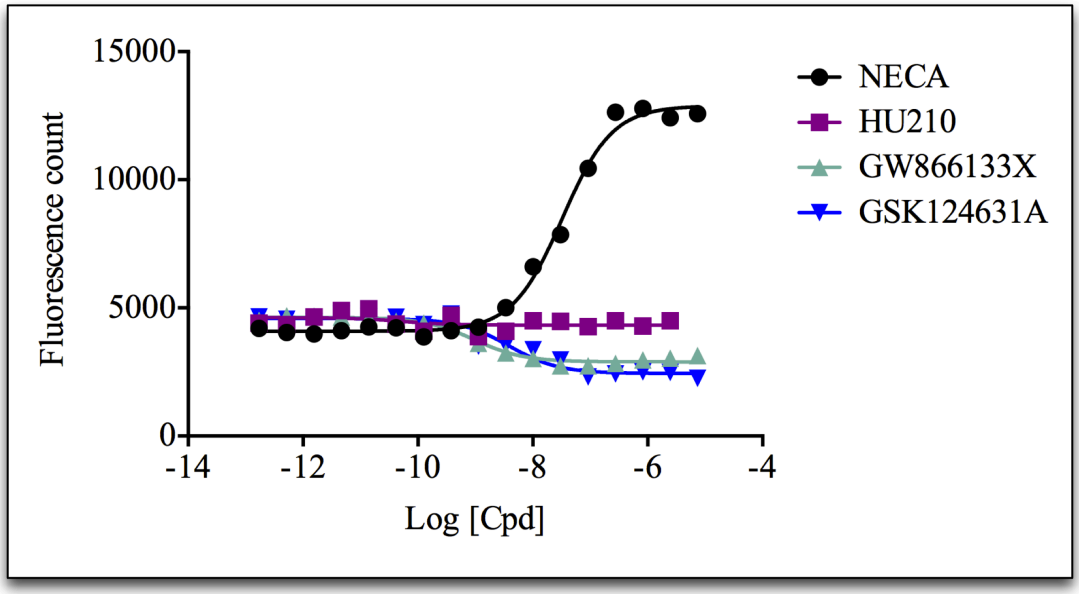


Figure 3-3 Pharmacological profiles of four different ligands using wild-type $A_{2A}R$. The agonist NECA activates the receptor in a dose-dependent manner. The inverse agonists GW866133X and GSK124631A partially inhibit the constitutive activity. HU210, a selective CB2 agonist, was used as a negative control and displays no effect on the receptor.

The Rag23, which is in a preferentially agonist-conformation exhibits a slight increase in potency compared with the wild-type and a decreased maximum efficacy (pEC_{50} = 7.9; Fig 3-2A; Table 3-3). The Rag23.1 intermediate mutant exhibits no constitutive activity and shows a similar potency to Rag23 with an

increased efficacy. Indeed, the efficacy of the Rag23.1 is similar to that of the wild-type (Fig 3-2A). The Rant5 and Rant21 mutants, which are in a preferentially antagonist-conformation show no agonist-induced receptor activity (Fig 3-2B). Interestingly, in contrast to the wild-type, the thermostabilised mutants also show no constitutive activity (Fig 3-2, Table 3-3).

3.3.2.1.2 Saturation and competition binding analysis in the MMY24 yeast strain

Saturation binding analysis of the wild-type, Rag23, Rant5 and Rant21 mutants reveals that all the receptor forms exhibit high affinity binding for the antagonist ZM241385 although the affinity of the Rag23, the thermostabilised agonist binding form is reduced by an order of magnitude compared to the other three receptor forms (Fig 3-4, Table 3-4). This is in agreement with the results reported for the expression of these receptor forms in *E. coli* (Magnani *et al.*, 2008).

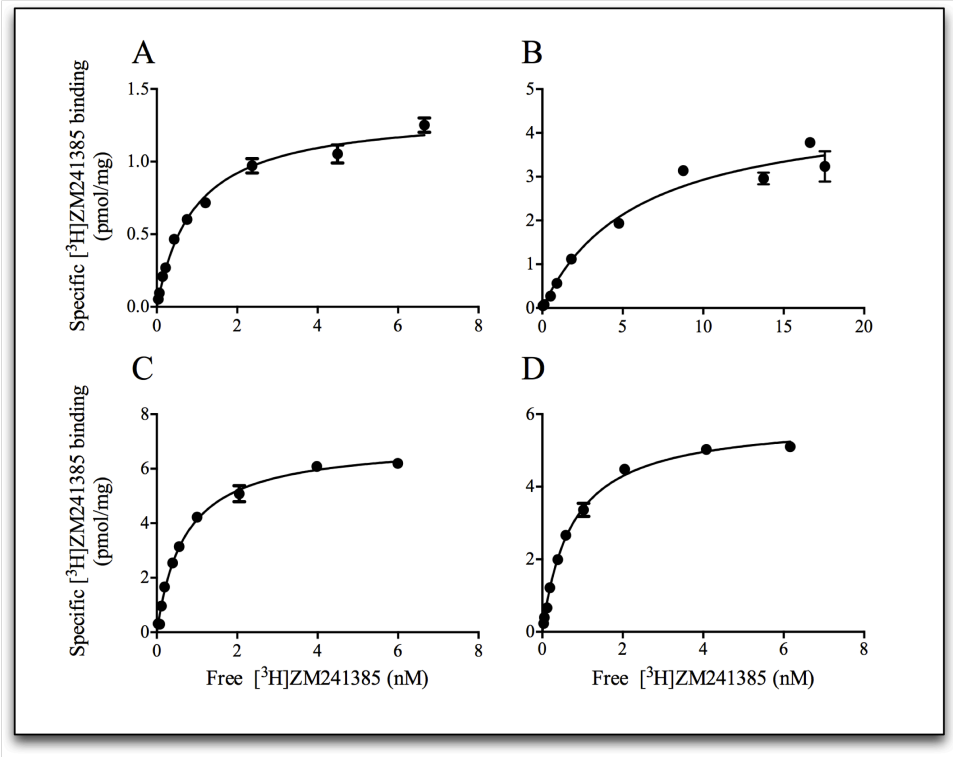


Figure 3-4 Saturation binding of [^{3}H]ZM241385 to *S. cerevisae* MMY24 membranes expressing the wild-type (A), Rag23 (B), Rant5 (C) and Rant21 (D) $A_{2A}R$ constructs. Data are representative of two independent experiments performed in triplicate. B_{max} and K_d values were derived by non-linear regression analysis. Mean data ± SEM are presented in Table 3-4.

However the precise K_d values obtained in the yeast expression described here are significantly lower than those reported for the same constructs expressed in *E. coli*. For example a K_d of 0.85 nM was obtained here (Fig 3-4A, Table 3-4) for the wild-type receptor compared to 12 nM for the receptor in *E. coli*. The value reported here is consistent with the $A_{2A}R$ heterologously expressed in *Pichia pastoris* (Fraser, 2006; Singh *et al.*, 2010), *S. cerevisiae* (O'Malley et al., 2007) CHO cells (Dionisotti *et al.*, 1997; Klotz *et al.*, 1998) and $A_{2A}R$ present in rat brain tissue (Alexander & Millns, 2001). Competition binding analysis, using NECA as an agonist, reveals that while Rag23 binds the agonist NECA with reduced K_i compared to the wild-type (Fig 3-5A and B, Table 3-4), the Rant5, Rant21 and T88A have dramatically increased K_i values (Fig 3-5C and D, Table 3-4). These results are consistent overall with those obtained for the same receptor constructs expressed in *E. coli* (Magnani *et al.*, 2008).

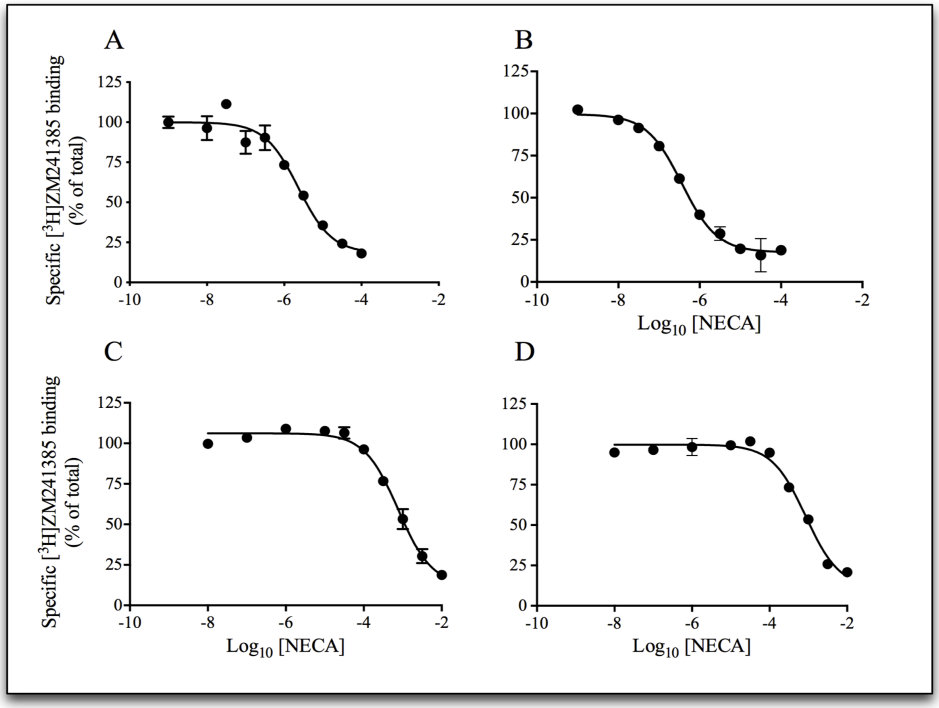


Figure 3-5 Binding of the low affinity agonist NECA to *S. cerevisae* MMY24 membranes expressing the wild-type (A), Rag23 (B), Rant5 (C) and Rant21 (D) $A_{2A}R$ constructs was assessed in competition with [^{3}H]ZM241385. Data were fitted best to a one binding site model and are representative of two independent experiments performed in triplicates. K_i values were derived from experimentally determined IC_{50} values. Mean data ± SEM are presented in Table 3-4.

3.3.2.1.3 Saturation binding assay of the wild-type and Rag23.1 $A_{2A}R$ in MMY11 and MMY24 yeast strain using [^{3}H]NECA

It is possible that the lack of constitutive activity of the Rag23 and Rag23.1 is the result of altered G-protein coupling for these mutants. The high efficacy of the Rag23.1 mutant following stimulation with ligand is strongly suggestive that the lack of constitutive activity seen in this mutant is not the result of reduced G-protein coupling. However, in order to investigate this further, binding of wild-type and Rag23.1 to [^{3}H]NECA in the presence and absence of G-protein was determined. This was achieved by also expressing the receptor variants in an alternative yeast strain, MMY11 (Olesnicky *et al.*, 1999), genetically identical to MMY24 but lacking the G protein alpha subunit. It is known that absence of G-protein reduces the affinity of a receptor for agonist (Ross *et al.*, 1977; Yao *et al.*, 2009). Thus if G-protein coupling has not been altered in the Rag23.1 mutant, the same level of reduction in affinity for [^{3}H]NECA in the absence of G-protein for both the mutant and wild-type receptor forms should be seen. Saturation binding assay using [^{3}H]NECA revealed that the binding affinity for the agonist of both the wild-type and Rag23.1 in the absence of G-protein was reduced by an order of magnitude compared with the binding affinities in the presence of G-protein (Fig 3-6, Table 3-4), demonstrating that the mutant does not have altered G-protein coupling.

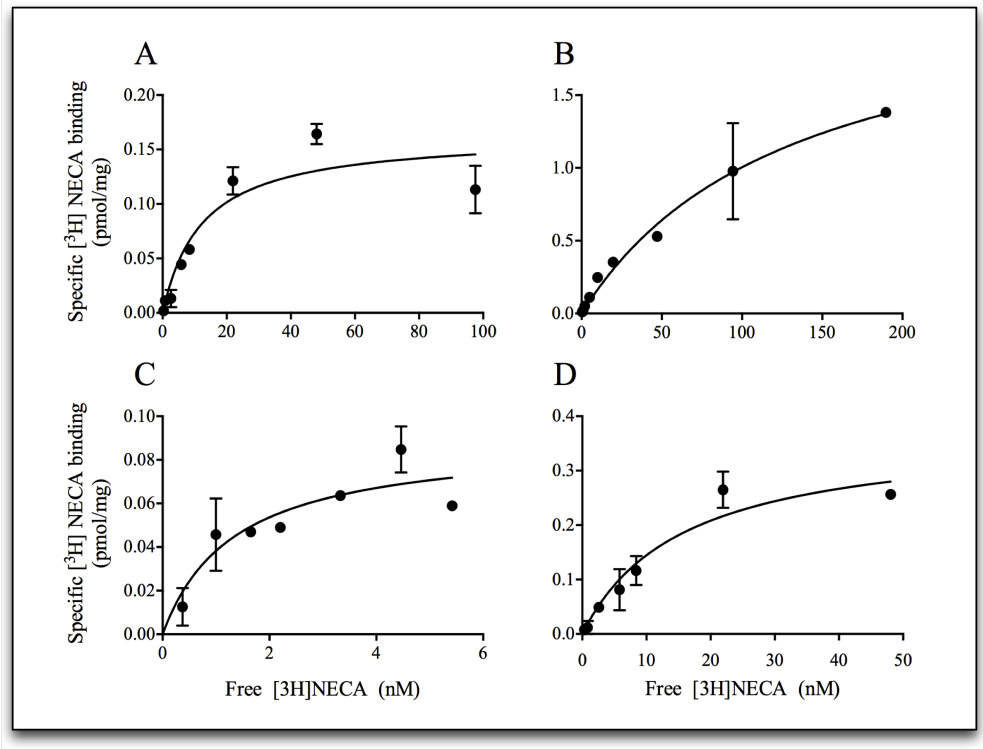


Figure 3-6 Saturation binding of [^{3}H]NECA to *S. cerevisae* membranes expressing the wild-type in MMY24 (A), wild-type in MMY11 (B), Rag23.1 in MMY24 (C) and Rag23.1 in MMY11 (D) $A_{2A}R$ constructs. Data are representative of two independent experiments performed in duplicate. K_d values were derived by non-linear regression analysis. Mean data ± SEM are presented in Table 3-3.

Table 3-4 K_d and K_i values for the different $A_{2A}R$ forms obtained from saturation and competition binding assay using [^{3}H] ZM235481 and [^{3}H]NECA as hot ligand and NECA and Adenosine as cold ligand.

Receptor form	**[^{3}H] ZM241385 K_d ± SEM (nM)**	**[^{3}H]NECA K_d ± SEM (nM)‡**		**NECA K_i ± SEM (μM)**	**Adenosine K_i ± SEM (μM)**
		+ G-protein	**- G-protein**		
WT	0.85 ± 0.08	8.6 ± 3.7	123.9±7.1	1.01 ± 0.23	0.36 ± 0.01
Rag23	6.32 ± 0.34	-	-	0.18 ± 0.02	-
Rag23.1	-	1.6 ± 0.2	14.4 ± 1.3	-	-
Rant5	0.74 ± 0.05	-	-	531 ± 300	-
Rant21	0.63 ± 0.09	-	-	247 ± 18	-

3.3.2.2 Intermediate mutants

The functional profiles of the mutants intermediate between Rant5 and wild-type show that the A54L mutant has reduced constitutive activity compared to wild-type (Table 3-4). In addition while this mutant exhibits agonist-dependent receptor activity, its potency is greatly reduced compared with the wild-type receptor or Rag23 (pEC_{50} = 7.0; Figure 3-7A; Table 3-5).

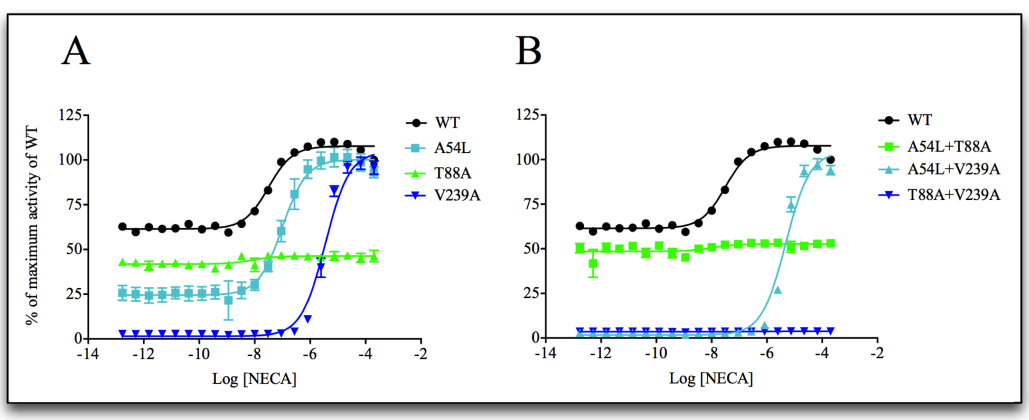


Figure 3-7 Functional data for the thermostabilised A_{2A} intermediate mutants expressed in the MMY24 *S. cerevisae* strain as constructs in the p306GPD vector. Data points are the average of three different experiments performed in triplicate. (A) Single mutants; (B) Double mutants.

In contrast, the T88A mutant displays high levels of constitutive activity but has no detectable agonist-induced activity, whereas the V239A mutant has no detectable constitutive activity and shows lower sensitivity to NECA than A54L (pEC_{50} = 5.5 ± 0.1; Figure 3-7A; Table 3-5).

Table 3-5 Pharmacological characteristics of the intermediate mutants. Data are presented as mean ± standard error means of at least two independent experiments performed in triplicate.

Receptor form	NECA pEC_{50} ± SEM	Constitutive activity ± SEM (% of max activity of WT)
A54L	7.0*	25.0 ± 1.1
T88A	ND	39.8 ± 2.3
V239	5.5 ± 0.1	2.5 ± 0.1
A54L+T88A	ND	46.4 ± 4.5
A54L+V239	5.3 ± 0.1	2.6 ± 0.1
T88A+V239	ND	3.4 ± 0.3

*SEM=0. ND: not determined.

The A54L + T88A and A54L + V239A mutants show almost identical activity profiles to that of the single T88A and V239A mutants respectively, while the T88A + V239A mutant shows a complete loss of both constitutive and agonist-dependent activity (Figure 3-7B; Table 3-5).

3.3.2.2.1 The effect of the T88A mutation

In order to further explore the complete lack of agonist-induced activity observed for the T88A mutant, the functional profile of that mutant was investigated using a different agonist, adenosine. While NECA is no longer able to activate the T88A mutant, adenosine is still able to stimulate the mutant but with reduced potency compared to the wild-type receptor. Furthermore, the efficacy of adenosine is maintained in the T88A mutant (Fig 3-8, Table 3-6). Competition binding analysis, using adenosine as an agonist, reveals that the T88A has increased K_i compared to the wild-type (~6 fold increase), consistent with the decrease in pEC_{50} observed in the yeast growth assay (Table 3-6).

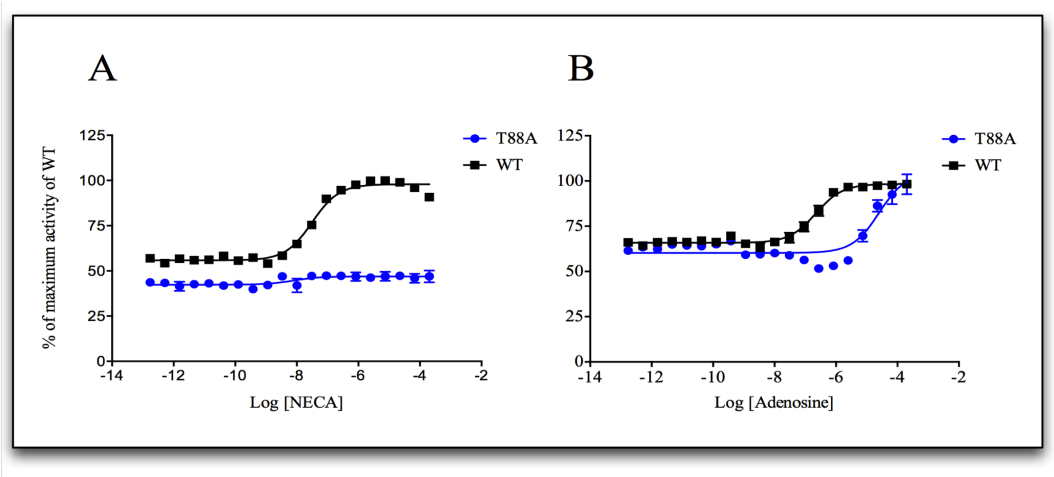


Figure 3-8 Activity of the T88A mutant compared to wild-type $A_{2A}R$. The different receptor forms were expressed in the MMY24 *S. cerevisae* strain as constructs in the p306GPD vector. The cells were treated with increasing concentrations of either NECA (A) or adenosine (B). Data points are the average of three different experiments performed in triplicate.

Table 3-6 Comparison of the NECA and adenosine binding and activation profile of T88A

Receptor form	**NECA pEC_{50} ± SEM**	**Adenosine pEC_{50} ± SEM**	**NECA K_i ± SEM (μM)**	**Adenosine K_i ± SEM (μM)**
WT	7.5 ± 0.1	6.4*	1.01 ± 0.23	0.36 ± 0.01
T88A	ND	4.5*	187 ± 54	2.75 ± 0.05

ND: no detectable activity, *SEM=0

As shown in Fig 3-8, the dose-response curve obtained for the T88A with adenosine as an agonist exhibits a biphasic nature. A possible explanation for this biphasic nature could be toxicity of the ligand at high concentrations. This was investigated by performing the assay with cells not expressing the receptor of interest but still containing the expression vector. Histidine was added to the assay media to a final concentration of 6 μg/ml in order to observe cell growth and potentially cell death at high concentration of adenosine. The results of this experiment showed no toxic effect on cell growth (Fig 3-9). The shape of the curve is therefore likely due to other pharmacological effects such as dimerisation of the receptor or allosteric binding of the adenosine. Further investigation would be needed to fully understand this phenomenon.

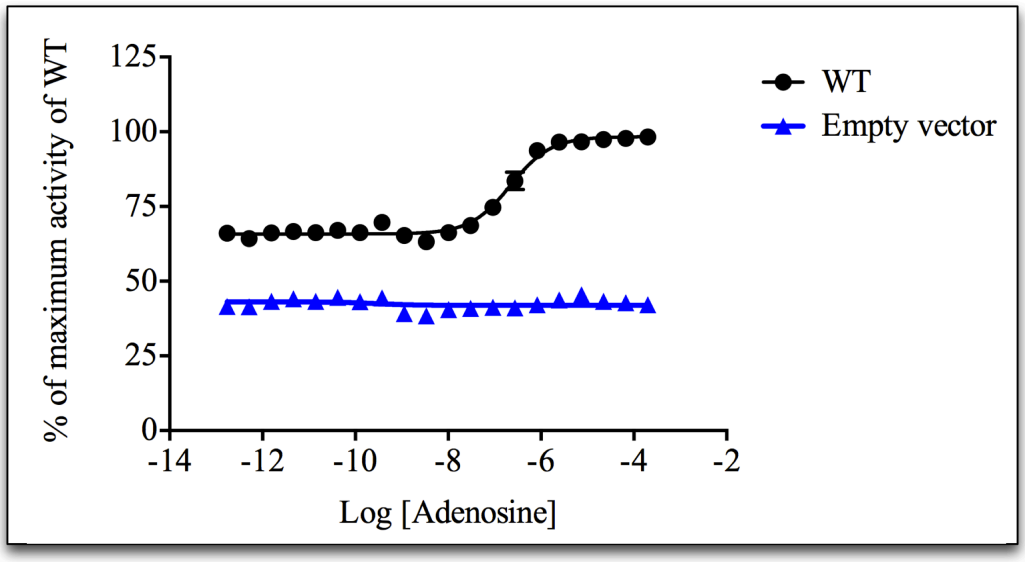


Figure 3-9 Effect of high concentrations of adenosine on cells not expressing the gene of interest but in the presence of histidine to observe a potential toxic effect of the ligand. Data points are the average of one experiment performed in triplicate.

3.3.2.2.2 The effect of the V239A mutation

Another interesting effect is the strong influence that the V239A mutation has on constitutive activity. Indeed, every mutant containing this particular substitution exhibits a complete loss of constitutive activity. Since the mutation involves changing one uncharged residues for another, it is likely that the effect observed is due to the reduction in size of the side chain. To further investigate the effect of the size of this residue, another mutant substituting V239 for a larger Ile residue (A54L+V239I) was generated and characterized (Fig 3-10).

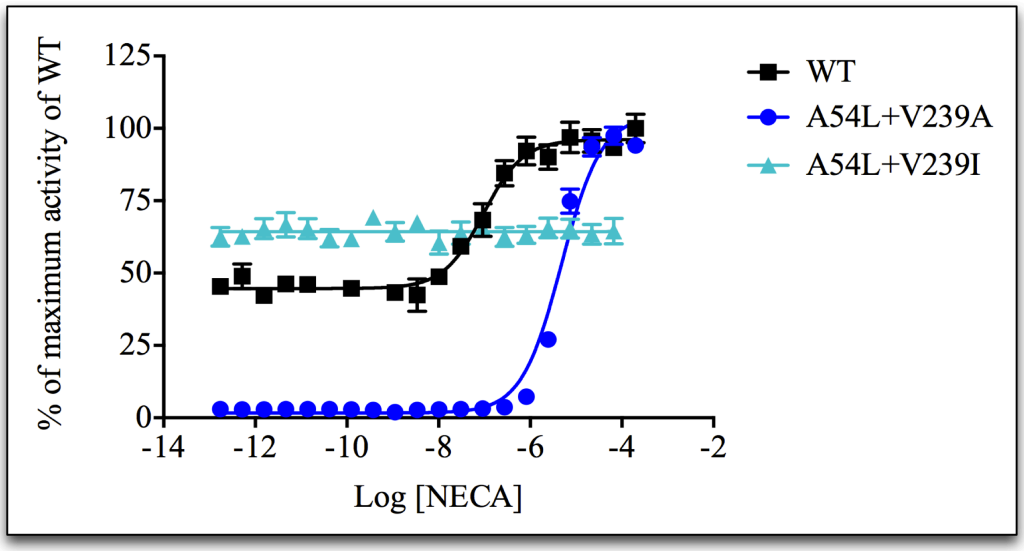


Figure 3-10 Functional characterization of the A54L+V239I mutant expressed in the MMY24 *S. cerevisae* strain as constructs in the p306GPD vector. Data points are the average of three different experiments performed in triplicate**.**

The A54L+V239A exhibited no constitutive activity and reduced potency compared to wild-type. In contrast, the A54L+V239I mutant exhibits higher constitutive activity than wild-type and shows a complete loss of NECA-induced activity.

3.4 Discussion

3.4.1 Thermostabilisation and functional profiles

The use of thermostable mutants of $A_{2A}R$ has been an important tool in facilitating the determination of high-resolution crystal structures (Lebon *et al.*, 2011b), but the effects of these mutations on receptor signalling function have not been described. The yeast cell growth assay allows simple and rapid assessment of the activation profile of different receptor forms. Here, the wild-type $A_{2A}R$ in addition to the previously reported Rag23, Rant5 and Rant21 mutants (Magnani *et al.*, 2008) were profiled in order to obtain a greater understanding of the molecular basis of their thermostabilization. The results of the analysis clearly demonstrate that while Rag23 retains high levels of agonist-induced receptor activity, the Rant mutants exhibit no discernable receptor activation. This is in agreement with the previous study using radioligand binding which showed that the Rant mutants have a significantly reduced affinity for the agonist NECA and a much stronger preference for the antagonist binding conformation than the wild-type receptor (Magnani *et al.*, 2008). One key observation was the total loss of constitutive activity for all three mutant forms. Constitutive activity accounts for approximately 50% of the overall activity of the wild-type $A_{2A}R$ in this assay. On the basis of these data, it seems likely that the loss of constitutive activity observed for all three mutant receptors is a major contributory factor in their increased thermostability.

Analysis of the Rant5 and intermediates revealed a clear trend in the characteristics of these mutants with differing degrees of reduced potency and reduced/no constitutive activity. One of the intermediate mutants T88A + V239A has

no constitutive activity and no signalling as observed for the Rant5 and Rant21 mutants. Another intermediate mutant A54L + V239A exhibits no constitutive activity and much lower potency compared with the wild-type receptor. The T_m for this receptor form in the presence of antagonist was measured as 42°C compared to 46°C for Rant5 and 49°C for Rant21 (Magnani *et al.*, 2008). There is no reported T_m for the T88A + V239A mutant receptor but given the lack of both constitutive and agonist induced signalling from this construct it is likely to be similar to the Rant5 and Rant21 mutants.

It is clear from the data that the effects of some of the intermediate mutations are additive. For example the T88A mutant has no agonist-induced activity but retains high levels of constitutive activity while the V239A mutant has reduced potency and no constitutive activity. The T88A + V239A double mutant has no agonist-induced activity and no constitutive activity as observed for Rant5. It should be noted that the Rant5 does bind NECA but with much reduced affinity. The conformation change induced by the mutations is sufficient to prevent receptor activation but still allows low affinity binding of NECA. Other mutant combinations do not appear to be additive eg. A54L + V239A, which has the same receptor activity profile as the V239A only mutant. It may be that there is a benefit conferred by the A54L that is not detectable by this assay.

3.4.2 Constitutive versus agonist-induced activity

The classical model of GPCR activity describes GPCRs as existing in an equilibrium between an active R* state and an inactive R state (Samama *et al.*, 1993). This model takes into account the constitutive activity of receptors by assuming the transition between the inactive R to active state R* carries a sufficiently low energetic cost that it is possible for some receptors to be in the R* state even in the absence of ligand. According to this model, the increase of agonist affinity should be accompanied by an increase of constitutive activity. However, the data presented here for Rag23 and Rag23.1 shows that it is possible to have very high levels of agonist-induced activity and ligand affinity even when constitutive activity has been abolished. By contrast, analysis of the T88A mutant revealed that significant constitutive activity was retained while the ability to be activated by NECA was lost. It is possible that the lack of constitutive activity observed for Rag23 and Rag23.1 is due to a decrease of G protein affinity for the mutated receptor. If that were the case the G protein would no longer be able to bind the active state of the receptor in the absence of ligand leading to the loss of constitutive activity. However, the presence of the agonist is known to increase the affinity of the G protein for the receptor and therefore enabling the G protein to bind the active state of the receptor to produce agonist-induced activity even if the overall affinity of the G protein for the receptor has been altered. The other possible explanation is that the agonist-induced conformation and the constitutive active conformation are distinct and somehow the mutations present in Rag23 and Rag23.1 prevent the formation of the constitutively active conformation without altering the agonist-induced conformation.

In order to investigate these possibilities further, the affinity of the G protein

for both wild-type and Rag23.1 was investigated indirectly. The fact that the Rag23.1 mutant exhibits maximal NECA-induced activity similar to wild-type receptor suggests that the loss of constitutive activity observed is not due to a reduction in G-protein coupling. This is supported by radioligand binding analysis performed with [^{3}H]NECA, which shows that the affinities of both the wild-type and Rag23.1 are reduced by the same amount in the absence of G-protein suggesting that the G protein binds both the wild-type and the Rag23.1 with a similar affinity.

Together, these results suggest that the constitutively active and agonist-induced active conformations of the $A_{2A}R$ are distinct. This is in accordance with previous studies that suggested a similar conclusion with the AT1 angiotensin receptor (Noda *et al.*, 1996) and the β_2-adrenergic receptor (Hannawacker *et al.*, 2002). This conclusion together with results presented by Kashai and coworkers showing that a GPCR is able to adopt different active conformations according to the agonist bound (Kahsai *et al.*, 2011) can be summarized in an extended cubic ternary complex model (Fig 3-11).

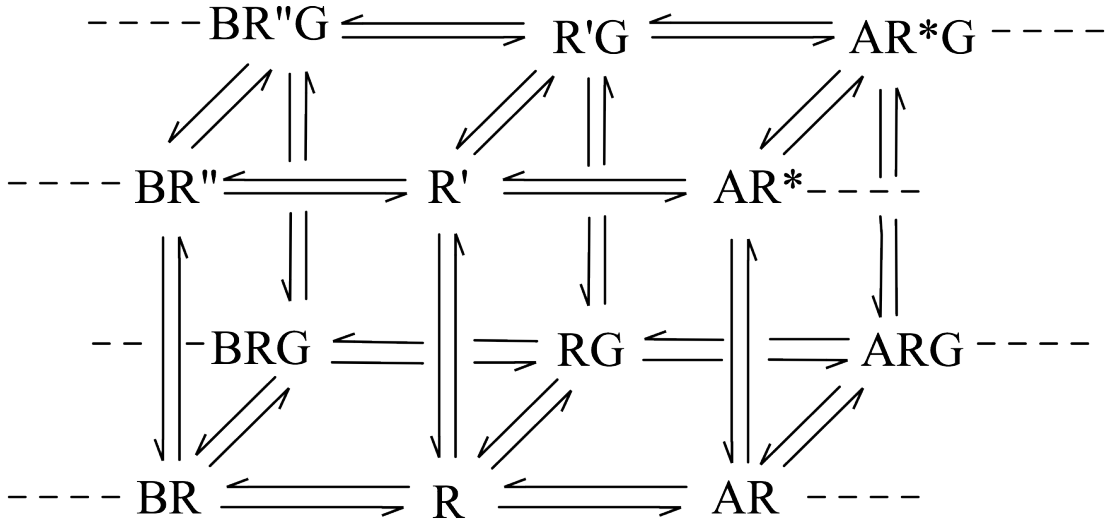


Figure 3-11 An extended cubic ternary complex model: the receptor is able to isomerize spontaneously to a constitutively active R' state which leads to constitutive activity when bound to the G protein. Once bound to an agonist (A or B), the receptor adopts a ligand specific active conformation (R* or R") leading to agonist-induced activity when bound to the G protein.

In addition, previous research on the 5-Hydroxytryptamine-4 receptor (5-HT_4R) indicates roles for a threonine residue in helix III (Thr104) and a tryptophan residue in helix VI (Trp272) in the formation of a so-called double toggle switch in stabilizing the constitutively active conformation but not the agonist-induced conformation of the receptor (Pellissier *et al.*, 2009). Mutation of the Thr104 to an Ala leads to a dramatic decrease in constitutive activity. A comparison of the primary sequences indicates that Thr88 of $A_{2A}R$ is equivalent to Thr104 of 5-HT_4R. However, in the case of the $A_{2A}R$, mutation of Thr88 to an Ala has little effect on the constitutive activity but a dramatic effect on agonist-induced activity both for NECA and adenosine. In addition, the T88A mutation is not present in either the Rag23 or Rag23.1 mutants, which do not exhibit constitutive activity. Therefore, the loss of constitutive activity observed in the $A_{2A}R$ mutants must have a different mechanism than the one proposed for 5-HT_4R.

3.4.3 The role of T88 in agonist binding and receptor activation

Previous research has shown that mutating T88A dramatically reduces both agonist binding and agonist-induced activity but does not significantly affect antagonist binding (Jiang *et al.*, 1996). The results presented here support these earlier findings and show that the degree to which agonist activity is reduced is dependent on the agonist. NECA fails to induce any receptor activity in the T88A mutant while adenosine induces low but detectable activity. Binding of the two ligands shows the same trend. The T88A mutant shows an ~8-fold decrease in affinity for adenosine and a ~200 fold decrease in affinity for NECA compared with the WT receptor. Clues to the precise molecular basis of the difference in the responsiveness of the mutant to the

two agonists can be obtained from the recent $A_{2A}R$ structures (Lebon *et al.*, 2011b). In the NECA bound structure the T88 forms a critical H-bond with the amide group of the ribose ring of the ligand (Fig 3-12A). In contrast the structure of the adenosine bound receptor reveals that the T88 is no longer able to form a H-bond with the ligand (Fig 3-12B). Rather this residue, together with a number of others, appears to play a role in stabilizing the protein via van der Waals interactions.

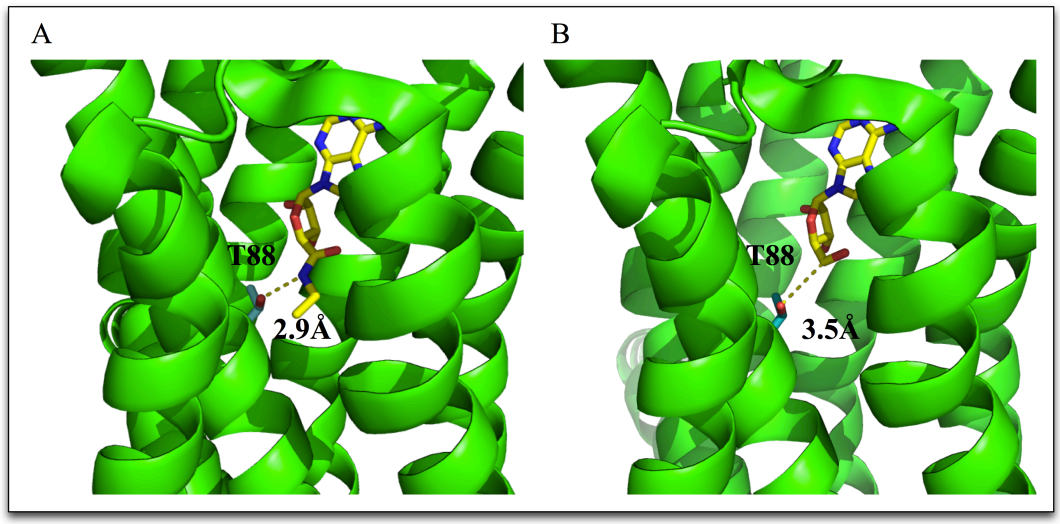


Figure 3-12 Interaction between the Thr88 of the $A_{2A}R$ and NECA which is forming an hydrogen bond with the hydroxyl group of the Threonine (pdb: 2YDV) (A) and Adenosine which is no longer able to form a hydrogen bond with the hydroxyl group (pdb: 2YDO) (B)

3.4.4 The role of V239 in the loss of constitutive activity

The data indicate that the V239A mutation has a strong effect on constitutive activity. V239 is located on helix VI, pointing towards helices III and V. It is possible that the reduction in size of this residue by introduction of the Ala mutation allows helices III and VI to come into closer proximity and thus form closer interactions. These interactions may then prevent the movements of helices III and VI required for constitutive activation. Superposition of inactive $A_{2A}R$ structures (Fig 3-13) reveals that there is a 1.1 Å movement of helix III towards helix VI in an inactive thermostabilised mutant (containing the V239A mutation) structure (PDB: 3PWH)

compared with the inactive $A_{2A}R$ bound to an antibody (PDB: 3VG9). This shift of helix III towards helix VI could explain the formation of the so-called ionic lock between the E/DRY motif and Glu228, which is not observed in the antibody-bound structure. The thermostabilised mutant contains other mutations but the only other one susceptible to play a role in this shift is the L235A, which is likely to have a similar effect to the V239A. However, a potential caveat to this hypothesis is that the presence of the antibody may induce the differences observed between the two structures.

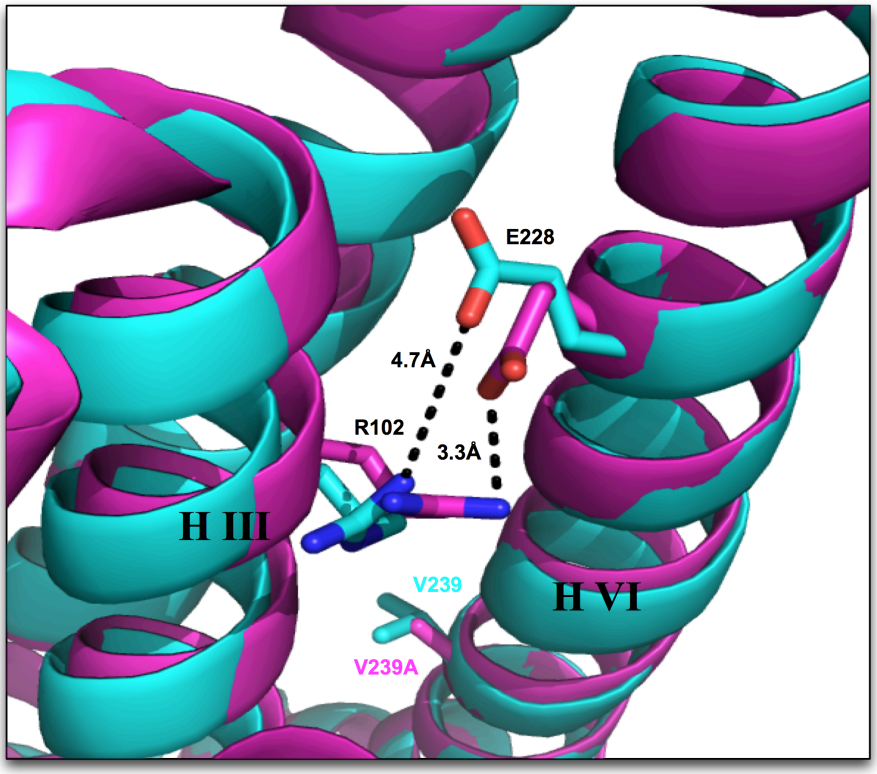


Figure 3-13 Superposition of helices III and VI of the inactive thermostabilized $A_{2A}R$ mutant (containing the V239A mutation) structure (pink, Pdb accession code 3PWH) and the inactive $A_{2A}R$ bound to an antibody (blue Pdb, accession code 3VG9). The V239 or V239A and E228 residues located on helix VI and the R102 residue located on helix III are shown as stick models. The distance between the charged interacting groups of E228 and R102 of the ionic lock in each case are indicated by the dotted lines.

In order to investigate this theory, a new mutant (A54L+V239I) was characterized in the yeast cell growth assay. Since the size of the residue seems to be a key factor, the V239 was replaced by a slightly bigger residue, an isoleucine. In

theory, this increase in size should keep helices III and VI further apart; facilitating the opening of the receptor needed for G protein binding and consequently increasing the constitutive activity. This is indeed what was observed (Fig 3-10) with the A54L+V239I mutant exhibiting a higher constitutive activity than the wild-type receptor. The lack of agonist-induced activity observed for this mutant remains unexplained.

In summary, the application of the yeast cell growth assay has allowed a detailed analysis of the pharmacological effects of receptor mutations since it discriminates between constitutive and agonist induced receptor-signalling events. The data presented here provide strong evidence that the agonist-induced and constitutively active conformations of the $A_{2A}R$ are distinct. This information is complementary to, and yet distinct from, that obtained from the recent high-resolution structures. In order to fully understand the mechanism of action of GPCRs it will be necessary to functionally and structurally characterize all the different active conformations. This data coupled with the high-resolution structure information may form the basis of rational design of receptor specific drugs that can antagonise basal activity with no effect on agonist-induced activity. In addition, this work suggests that increased receptor thermostability is correlated with the loss of constitutive activity. It may be that the yeast cell growth assay used in combination with either alanine-scanning mutagenesis or random mutagenesis methods would provide a powerful screening tool for the production of thermostable mutants of other GPCRs.

4 Functional characterization of the intermediate mutants between the Rag23 and the wild-type $A_{2A}R$

The work presented here has been submitted for publication in PlosOne and is under review at the time of writing.

4.1 Introduction

In the previous chapter, characterization of intermediate mutants between Rant5 and wild-type provided insights into the roles of individual amino acid residues in the function and stabilisation of the receptor. However, all the mutants explored were in a preferentially antagonist conformation. Functional analysis of the Rag23 and Rag23.1 constructs suggested that the constitutively active and agonist-induced active conformations are distinct. Interestingly, although they comprise a completely different set of mutations both the Rants and the Rags exhibited no constitutive activity. This suggests that there are at least two different mechanisms involved in constitutive activity.

Therefore in order to further investigate the differences between the agonist-induced and the constitutive active conformations, the intermediate mutants between Rag23 and the wild-type were explored. In addition, the characterization of these intermediate mutants should provide useful data concerning the role of individual amino acid residues on receptor function and stabilisation as well as insight into the different mechanisms involved in constitutive activity.

In this chapter, the mutants intermediate between the wild-type $A_{2A}R$ and Rag23, containing mutations (F79A, A184L, R199A, L208A and L272A) were explored. All possible combinations of the mutations were generated, leading to a total of 30 constructs, which were characterised in the yeast cell growth assay. The data showed that R199 and L208 have important roles in receptor function; substituting either of these residues for Ala abolishes constitutive activity. In addition the R199A mutation markedly reduces receptor potency while L208A reduces receptor efficacy. Furthermore, the A184L and L272A also reduce the constitutive

activity and the potency although to a lesser extent. In contrast, the F79A mutation increases constitutive activity, potency and efficacy of the receptor. These findings shed new light on the role individual residues have on stability of the receptor and also provide some clues as to the regions of the protein responsible for constitutive activity. Furthermore, the available adenosine A_{2A} receptor structures have allowed us to put these findings into a structural context.

4.2 Materials and methods

4.2.1 Materials

Materials have already been described in chapters 2 and 3; sections 2.2.1 and 3.2.1, respectively.

4.2.2 Site-directed mutagenesis

The 30 Rag intermediate mutants were obtained from the Rag23 synthetic gene by site-directed mutagenesis using the QuickChange Lightning Site-Directed mutagenesis kit and the primers detailed in Table 4-1.

Table 4-1 Mutagenic primers used to generate the Rag intermediate mutant $A_{2A}R$ constructs.

Primer	**Sequence (5' to 3')**
A79F_forward	gatgttgggtgtttacttgcgtattttcttggctgccaga
A79F_reverse	tctggcagccaagaaaatacgcaagtaaacacccaacatc
L184A_forward	catggtctacttcaatttcttcgcgtgtgttttggtccctttgttg
L184A_reverse	caacaaagggaccaaaacacacgcgaagaaattgaagtagaccatg
A199R_forward	ctaagtccttggctattatagttggtttgttcgctttgtgttg
A199R_reverse	caacacaaagcgaacaaaccaactataatagccaaggacttag
A208L_forward	ctattttcttggctgccagaagacaactaaagcaaatggaatctcaacc
A208L_reverse	ggttgagattccatttgctttagttgtcttctggcagccaagaaaatag
A272L_forward	tcatgctccattgtggttgatgtatctagctatagttttgtcccacac
A272L_reverse	gtgtgggacaaaactatagctagatacatcaaccacaatggagcatga

4.2.3 Expression

As described in chapter 2; section 2.2.2, all the $A_{2A}R$ constructs including the Rag intermediate mutants, were expressed as fusions with a C-terminal GFP-8His tag from the p306GPD vector. Estimation of the expression levels for all constructs was obtained from fluorescence of eGFP as previously described in chapter 3; section 3.2.3 (Drew *et al.*, 2008).

4.2.4 Yeast cell growth assay

The yeast cell growth assay was performed as described in Chapter 2; Section 2.2.6.

4.3 Results

4.3.1 Expression levels

Estimation of the expression levels for all the constructs using GFP gave values between 0.4-1.4 mg/ml (Table 4-2). The large variation observed in expression levels does not seem to affect the results of the assay. Indeed, Rag23.25 has the lowest level of expression while displaying the highest efficacy and the second highest level of constitutive activity. In contrast, Rag23.7 has the highest level of expression but exhibits no constitutive activity at all and an efficacy of only 53%. This suggests that the expression level is not responsible for the differences in efficacies and constitutive activities observed.

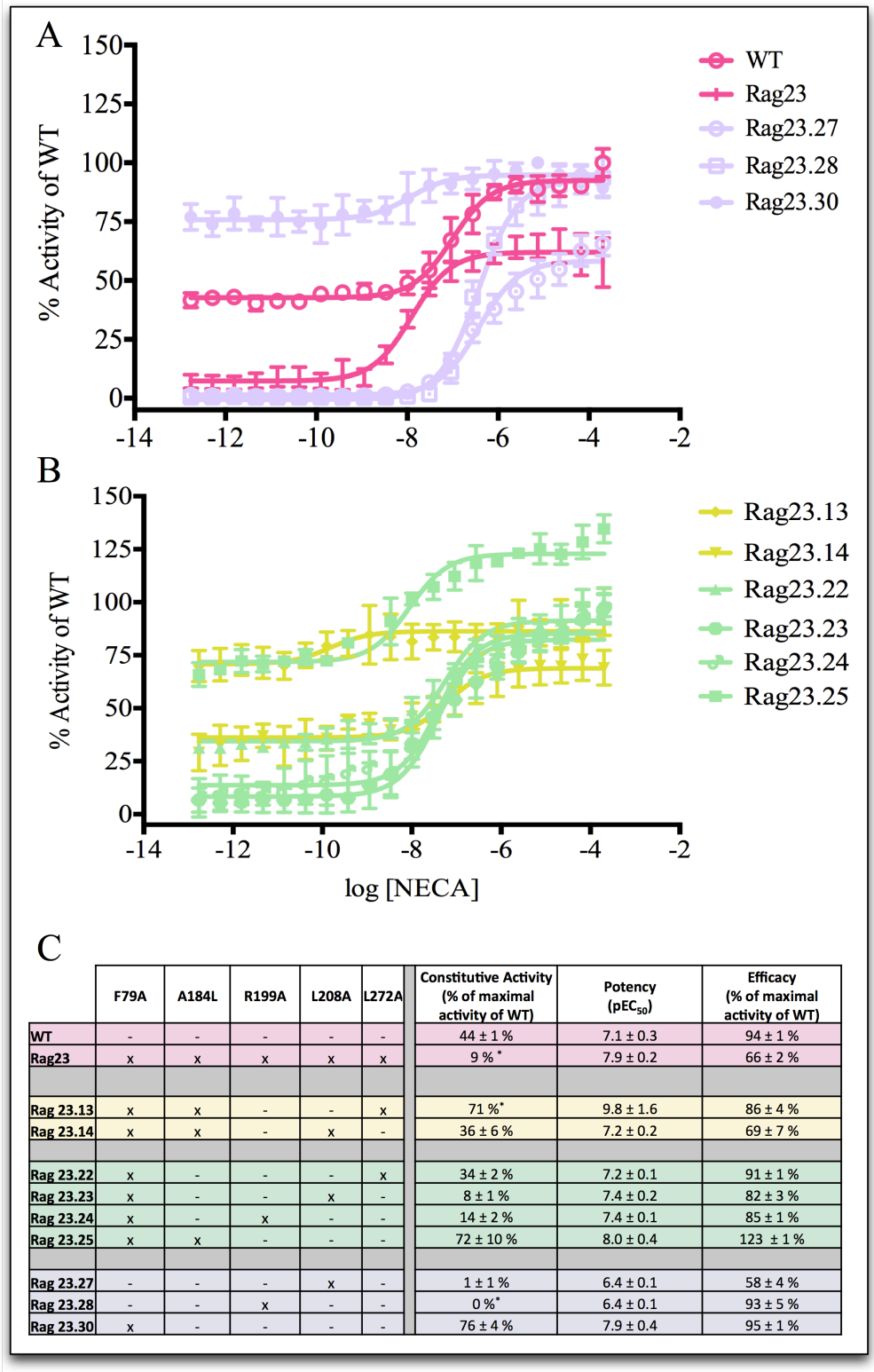
Table 4-2 Expression levels of the thirty mutants and the wild-type calculated using the eGFP fluorescence as described by Drew *et al.*

Construct	RFU	Level of Expression (mg/L)		Construct	RFU	Level of Expression (mg/L)
Rag 23.1	16,843	0.6		**Rag 23.16**	21,423	1.2
Rag 23.2	20,715	1.1		**Rag 23.17**	20,992	1.1
Rag 23.3	22,439	1.2		**Rag 23.18**	21,782	1.2
Rag 23.4	19,046	0.9		**Rag 23.19**	23,018	1.3
Rag 23.5	16,389	0.6		**Rag 23.20**	22,388	1.2
				Rag 23.21	16,312	0.6
Rag 23.6	20,479	1.0		**Rag 23.22**	14,803	0.4
Rag 23.7	23,799	1.4		**Rag 23.23**	15,874	0.5
Rag 23.8	14,547	0.4		**Rag 23.24**	19,569	0.9
Rag 23.9	19,162	0.9		**Rag 23.25**	14,356	0.4
Rag 23.10	17,677	0.7				
Rag 23.11	18,500	0.8		**Rag 23.26**	15,904	0.6
Rag 23.12	19,021	0.9		**Rag 23.27**	16,984	0.7
Rag 23.13	20,392	1.0		**Rag 23.28**	19,843	1.0
Rag 23.14	18,314	0.8		**Rag 23.29**	20,120	1.0
Rag 23.15	18,906	0.9		**Rag 23.30**	18,013	0.8
WT	19,954	1.0				

4.3.2 F79A enhances constitutive activity and potency

The activity of each of the receptor constructs is summarised in Table 4-3. The graphical data for all constructs is shown in Appendix 6-1.

The effects of the F79A mutation are illustrated by the single mutant Rag23.30. This has increased constitutive activity and potency compared to the wild-type while retaining similar efficacy (Figure 4-1A). These effects are also observed in constructs where F79A is combined with A184L and/or L272A (Rag23.13, Rag23.22 and Rag23.25; Figure 4-1B). All these constructs exhibit wild-type or higher levels of potency and constitutive activity. In contrast, constructs combining F79A with R199A or L208A (Rag23.23 and Rag23.24; Figure 4-1B), exhibit markedly lower constitutive activity than the wild-type. However, the presence of the F79A mutation still increases the constitutive activity of the receptor compared with the equivalent constructs containing R199A or L208A alone (Rag23.27 and Rag23.28; Figure 4-1A). The same trend is also observed for receptor potency demonstrating that the effects of F79A on potency and constitutive activity are antagonized by the presence of the R199A and L208A. One exception to that is Rag23.14, the combination of F79A, A184L and L208A produces an overall profile similar to wild-type. It is not clear from either the data presented here or the receptor structures why this wild-type-like behaviour is seen for this construct.



C

	F79A	A184L	R199A	L208A	L272A	Constitutive Activity (% of maximal activity of WT)	Potency (pEC_{50})	Efficacy (% of maximal activity of WT)
WT	-	-	-	-	-	44 ± 1 %	7.1 ± 0.3	94 ± 1 %
Rag23	x	x	x	x	x	9 % *	7.9 ± 0.2	66 ± 2 %
Rag 23.13	x	x	-	-	x	71 %*	9.8 ± 1.6	86 ± 4 %
Rag 23.14	x	x	-	x	-	36 ± 6 %	7.2 ± 0.2	69 ± 7 %
Rag 23.22	x	-	-	-	x	34 ± 2 %	7.2 ± 0.1	91 ± 1 %
Rag 23.23	x	-	-	x	-	8 ± 1 %	7.4 ± 0.2	82 ± 3 %
Rag 23.24	x	-	x	-	-	14 ± 2 %	7.4 ± 0.1	85 ± 1 %
Rag 23.25	x	x	-	-	-	72 ± 10 %	8.0 ± 0.4	123 ± 1 %
Rag 23.27	-	-	-	x	-	1 ± 1 %	6.4 ± 0.1	58 ± 4 %
Rag 23.28	-	-	x	-	-	0 %*	6.4 ± 0.1	93 ± 5 %
Rag 23.30	x	-	-	-	-	76 ± 4 %	7.9 ± 0.4	95 ± 1 %

Figure 4-1 Functional profiles of constructs illustrating the major effects of the F79A mutation. The F79A mutation increases constitutive activity, efficacy and potency, both alone (Rag23.30) and in combination with other mutations (Rag23.13, Rag23.14, Rag23.22, Rag23.23, Rag23.24, Rag23.25, Rag23.27, Rag23.28 and Rag23.30). The curves (A and B) are the average of two experiments performed in triplicate. The table (C) shows the pharmacological characteristics of each mutant characterized. The colours of the curves correspond to those in the table. The data for the wild-type and Rag23 constructs (pink) are also shown for comparison. *SEM=0

Interestingly, the F79A mutation is not thermostabilising but was included in the Rag23 because it was preferentially in an agonist-binding conformation (Magnani *et al.*, 2008). The increased constitutive activity and lack of thermostabilisation of the F79A mutation is consistent with the previous findings demonstrating a correlation between loss of constitutive activity and thermostabilisation.

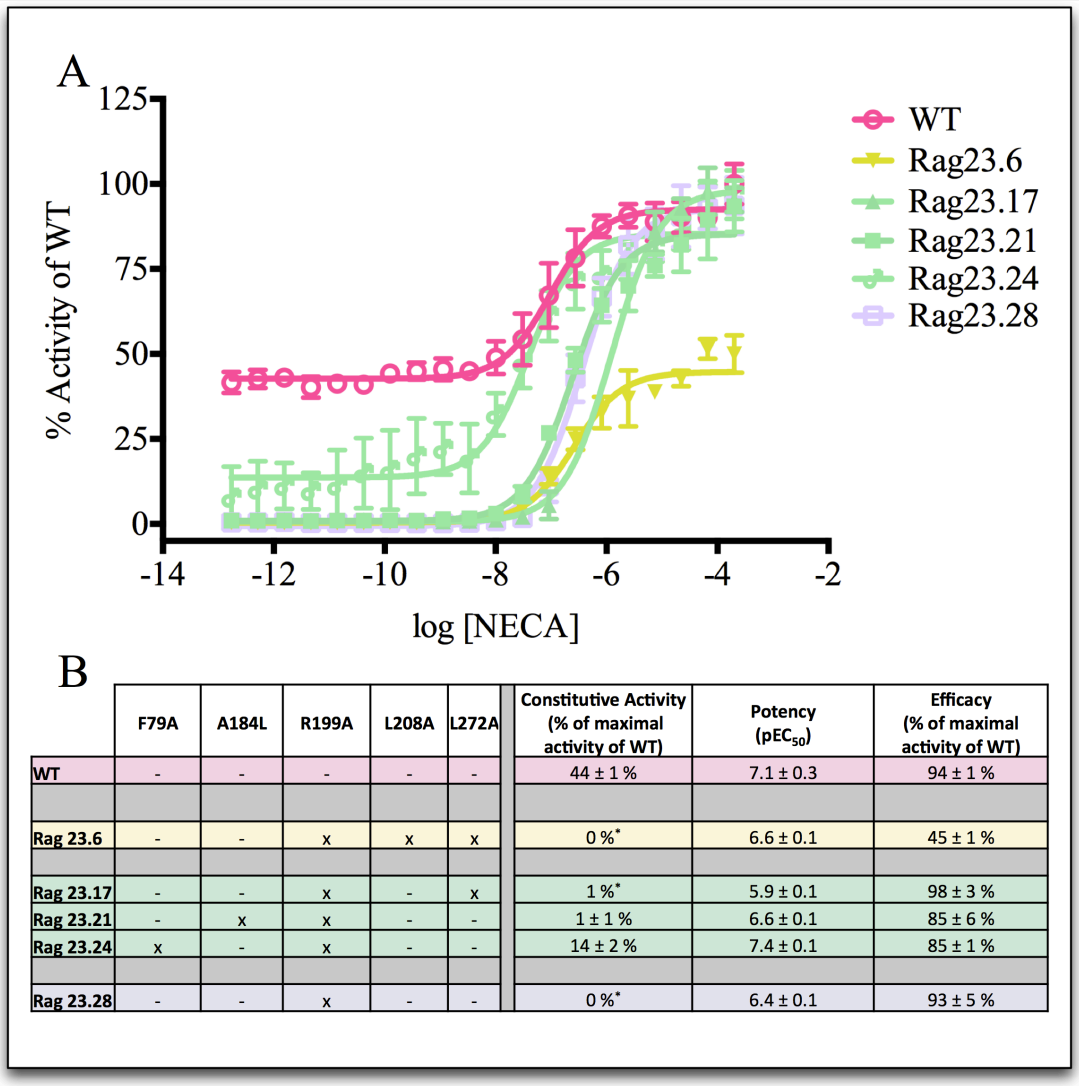
Table 4-3 Constitutive activities, potencies and efficacies of the Rag intermediate mutants.

	F79A	A184L	R199A	L208A	L272A	Constitutive Activity (% of maximal activity of WT)	Potency (pEC_{50})	Efficacy (% of maximal activity of WT)
WT	-	-	-	-	-	44 ± 1 %	7.1 ± 0.3	94 ± 1 %
Rag23	x	x	x	x	x	9 %*	7.9 ± 0.2	66 ± 2 %
Rag 23.1	x	x	x	-	x	4 ± 2 %	7.1 ± 0.2	88 ± 7 %
Rag 23.2	x	-	x	x	x	1 ± 1 %	6.6 ± 0.1	30 ± 3 %
Rag 23.3	-	x	x	x	x	0 %*	6.1 ± 0.1	43 ± 1 %
Rag 23.4	x	x	x	x	-	3 ± 1 %	6.9 ± 0.1	33 ± 2 %
Rag 23.5	x	x	-	x	x	3 %*	6.8 ± 0.1	46 ± 3 %
Rag 23.6	-	-	x	x	x	0 %*	6.6 ± 0.1	45 ± 1 %
Rag 23.7	-	x	-	x	x	1 %*	6.7 ± 0.1	53 ± 1 %
Rag 23.8	-	x	x	-	x	2 ± 2 %	6.7 ± 0.3	53 ± 5 %
Rag 23.9	-	x	x	x	-	0 %*	6.4 ± 0.2	59 ± 7 %
Rag 23.10	x	-	-	x	x	3 ± 2 %	6.9*	26 ± 3 %
Rag 23.11	x	-	x	-	x	2 ± 1 %	7.0 ± 0.2	79 ± 4 %
Rag 23.12	x	-	x	x	-	3 %*	6.8 ± 0.2	55 ± 12 %
Rag 23.13	x	x	-	-	x	71 %*	9.8 ± 1.6	86 ± 4 %
Rag 23.14	x	x	-	x	-	36 ± 6 %	7.2 ± 0.2	69 ± 7 %
Rag 23.15	x	x	x	-	-	1 %*	6.5 ± 0.1	67 ± 3 %
Rag 23.16	-	-	-	x	x	1 %*	6.3 ± 0.3	58 ± 7 %
Rag 23.17	-	-	x	-	x	1 %*	5.9 ± 0.1	98 ± 3 %
Rag 23.18	-	-	x	x	-	0 %*	6.1 ± 0.2	60 ± 10 %
Rag 23.19	-	x	-	-	x	2 ± 1 %	6.7 ± 0.1	88 ± 5 %
Rag 23.20	-	x	-	x	-	4 ± 3 %	7.2 ± 0.2	47 ± 4 %
Rag 23.21	-	x	x	-	-	1 ± 1 %	6.6 ± 0.1	85 ± 6 %
Rag 23.22	x	-	-	-	x	34 ± 2 %	7.2 ± 0.1	91 ± 1 %
Rag 23.23	x	-	-	x	-	8 ± 1 %	7.4 ± 0.2	82 ± 3 %
Rag 23.24	x	-	x	-	-	14 ± 2 %	7.4 ± 0.1	85 ± 1 %
Rag 23.25	x	x	-	-	-	72 ± 10 %	8.0 ± 0.4	123 ± 1 %
Rag 23.26	-	-	-	-	x	15± 1 %	6.4 ± 0.1	95 ± 5 %
Rag 23.27	-	-	-	x	-	1 ± 1 %	6.4 ± 0.1	58 ± 4 %
Rag 23.28	-	-	x	-	-	0 %*	6.4 ± 0.1	93 ± 5 %
Rag 23.29	-	x	-	-	-	0 %*	6.3 ± 0.1	63 ± 4 %
Rag 23.30	x	-	-	-	-	76 ± 4 %	7.9 ± 0.4	95 ± 1 %

For each of the constructs shown an "x" indicates the presence of a specific mutation while a "-" indicates the presence of the WT amino acid. The quadruple, triple, double and single mutants are indicated in the blue, yellow, green and purple sections of the table respectively. The Rag23 and WT receptor forms are indicated in the pink sections. The constitutive activity, potency and efficacy values for each receptor are shown. Each parameter is an average of two independent experiments performed in triplicate. *No errors are given in these examples as the data obtained from different experiments was so consistent as to preclude their calculation.

4.3.3 R199A reduces constitutive activity and potency

All constructs containing the R199A mutation exhibited an almost complete lack of constitutive activity and reduced potency compared to the wild-type (Figure 4-2). For clarity, Figure 4-2 only shows these effects for some examples of the intermediate single, double and triple mutants. However the same characteristics are clearly seen in all constructs with the R199A mutation (Table 4-3). The data strongly indicate that R199 has a key role in the constitutive activity of the $A_{2A}R$. This is further illustrated by Rag23.24, which contains both F79A and R199A mutations. The profile of this mutant shows that the increase of constitutive activity due to the F79A mutation is almost completely overcome by the R199A mutation (Figure 4-2) and as mentioned above the R199A further reduces the overall constitutive activity of this construct compared to wild-type. The R199A also reduces receptor potency compared to wild-type, however the effects are less dominant than those observed for the constitutive activity. F79A alone increases potency but in combination with R199A produces a construct with wild-type potency. These findings indicate that the R199A cancels out the increase in potency caused by F79A but has no further effect on potency in this construct compared to wild-type.



B

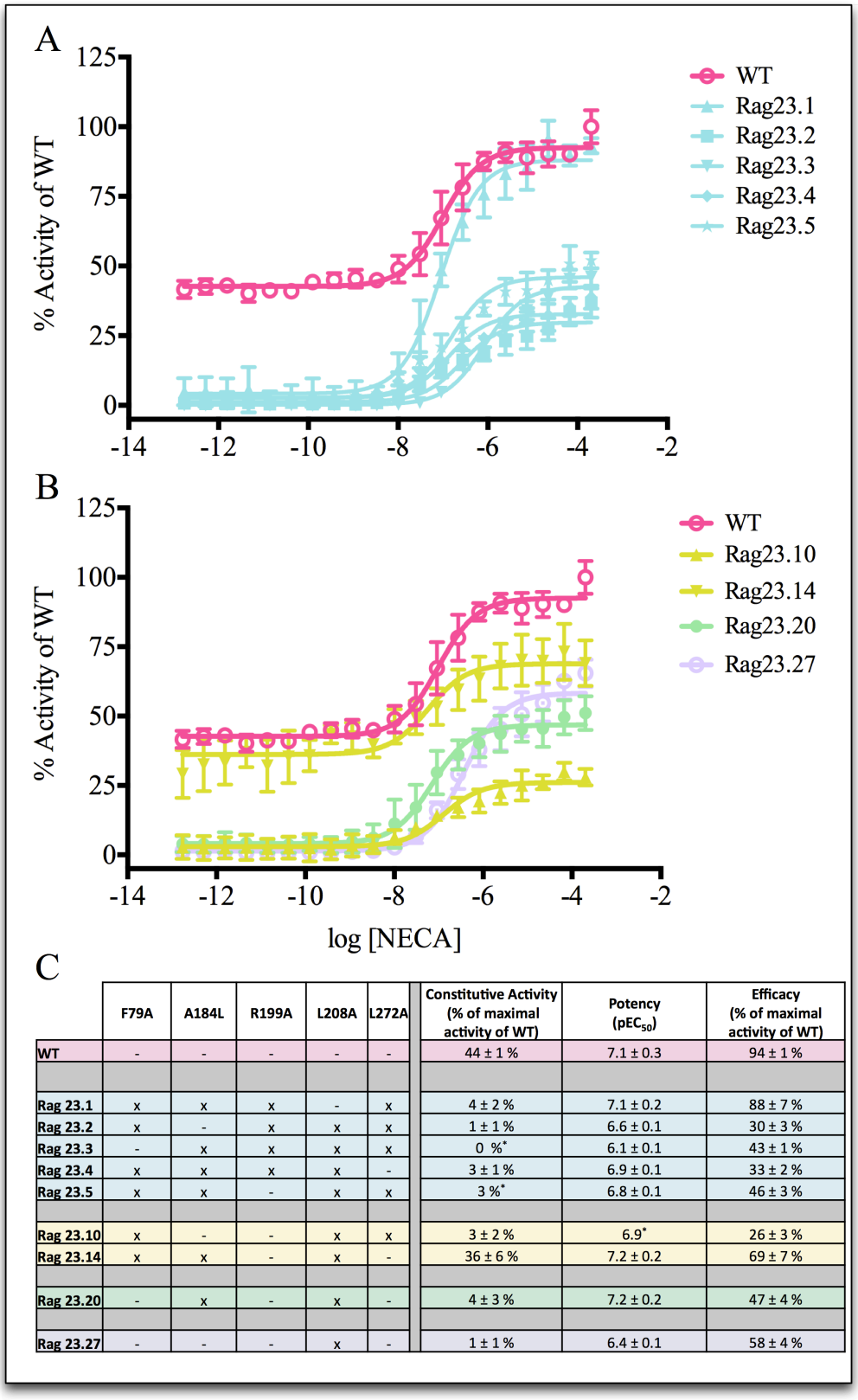
	F79A	A184L	R199A	L208A	L272A	Constitutive Activity (% of maximal activity of WT)	Potency (pEC_{50})	Efficacy (% of maximal activity of WT)
WT	-	-	-	-	-	44 ± 1 %	7.1 ± 0.3	94 ± 1 %
Rag 23.6	-	-	x	x	x	0 %*	6.6 ± 0.1	45 ± 1 %
Rag 23.17	-	-	x	-	x	1 %*	5.9 ± 0.1	98 ± 3 %
Rag 23.21	-	x	x	-	-	1 ± 1 %	6.6 ± 0.1	85 ± 6 %
Rag 23.24	x	-	x	-	-	14 ± 2 %	7.4 ± 0.1	85 ± 1 %
Rag 23.28	-	-	x	-	-	0 %*	6.4 ± 0.1	93 ± 5 %

Figure 4-2 Functional profiles of constructs illustrating the major effects of the R199A mutation. The R199A mutation reduces constitutive activity and potency, both alone (Rag23.28) and in combination with other mutations (Rag23.6, Rag23.17, Rag23.21, Rag23.24 and Rag23.28). The curves (A) are the average of two experiments performed in triplicate. The table (B) shows the precise details of each mutant characterized. The colours of the curves correspond to those in the table. The data for the wild-type (pink) are also shown for comparison. *SEM=0

4.3.4 L208A mutation reduces constitutive activity and efficacy

Almost all the constructs containing the L208A mutations exhibited very low or undetectable constitutive activity and markedly reduced efficacy compared with wild-type (Figure 4-3). As for the R199A mutation, the effect of the L208A mutation almost completely overcomes the enhancing effect of the F79A on constitutive activity, except in the presence of A184L, Rag23.14 (Figure 4-3B).

The effects of L208A on efficacy are illustrated by the quadruple mutant, Rag23.1. Rag23.1 lacks the L208A substitution and has markedly increased efficacy compared to all the constructs containing L208A. This indicates that the low levels of efficacy observed in the Rag23.2, 3, 4 and 5 as well as Rag23 are due to the presence of the L208A mutation (Figure 4-3A). The L208A influences the potency in a similar way to the R199A.



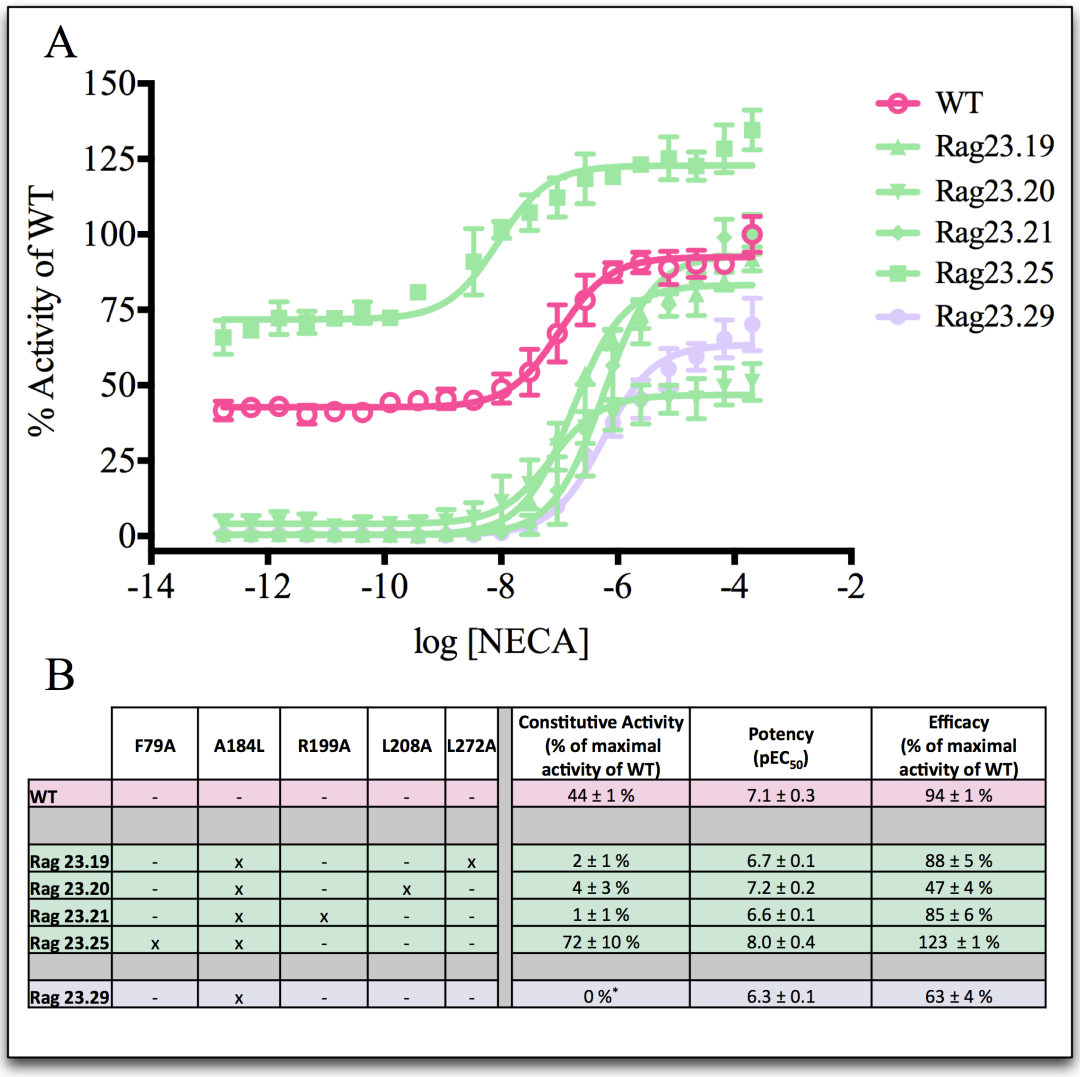
C

	F79A	A184L	R199A	L208A	L272A	Constitutive Activity (% of maximal activity of WT)	Potency (pEC_{50})	Efficacy (% of maximal activity of WT)
WT	-	-	-	-	-	44 ± 1 %	7.1 ± 0.3	94 ± 1 %
Rag 23.1	x	x	x	-	x	4 ± 2 %	7.1 ± 0.2	88 ± 7 %
Rag 23.2	x	-	x	x	x	1 ± 1 %	6.6 ± 0.1	30 ± 3 %
Rag 23.3	-	x	x	x	x	0 %*	6.1 ± 0.1	43 ± 1 %
Rag 23.4	x	x	x	x	-	3 ± 1 %	6.9 ± 0.1	33 ± 2 %
Rag 23.5	x	x	-	x	x	3 %*	6.8 ± 0.1	46 ± 3 %
Rag 23.10	x	-	-	x	x	3 ± 2 %	6.9*	26 ± 3 %
Rag 23.14	x	x	-	x	-	36 ± 6 %	7.2 ± 0.2	69 ± 7 %
Rag 23.20	-	x	-	x	-	4 ± 3 %	7.2 ± 0.2	47 ± 4 %
Rag 23.27	-	-	-	x	-	1 ± 1 %	6.4 ± 0.1	58 ± 4 %

Figure 4-3 Functional profiles of constructs illustrating the major effects of the L208A mutation. The L208A mutation reduces constitutive activity and efficacy, both alone (Rag23.27) and in combination with other mutations (Rag23.1, Rag23.2, Rag23.3, Rag23.4, Rag23.5, Rag23.10, Rag23.14, Rag23.20 and Rag23.27). The curves are the average of two experiments performed in triplicate. The table (C) shows the pharmacological characteristics of each mutant characterized. The colours of the curves correspond to those in the table. The data for the wild-type (pink) are also shown for comparison. *SEM=0

4.3.5 The effects of A184L and L272A are overcome by the other mutations

As can be seen from the data for the A184L single mutant construct, Rag23.29, this substitution has effects on the three key functional parameters assessed here (Figure 4-4). It reduces the constitutive activity, potency and efficacy of the receptor (0 %, 6.3, and 63 %, respectively; Figure 4-4B). An almost identical functional profile is seen for the Rag23.19 (Figure 4-4), which combines the A184L and L272A mutations. However, these effects are not observed in those constructs, which combine the A184L with L208A, R199A and/or F79A. For example, when A184L (Rag23.29) is combined with the strong positive effects of F79A on constitutive activity, potency and efficacy (Rag23.30), this leads to an increase in all three parameters of the resulting mutant (Rag23.25; Figure 4-4) relative to wild-type. In contrast, addition of A184L with R199A (Rag 23.21; Figure 4-4) or L208A (Rag23.20; Figure 4-4) results in reduced potency (with R199A) and efficacy (with L208A).



B

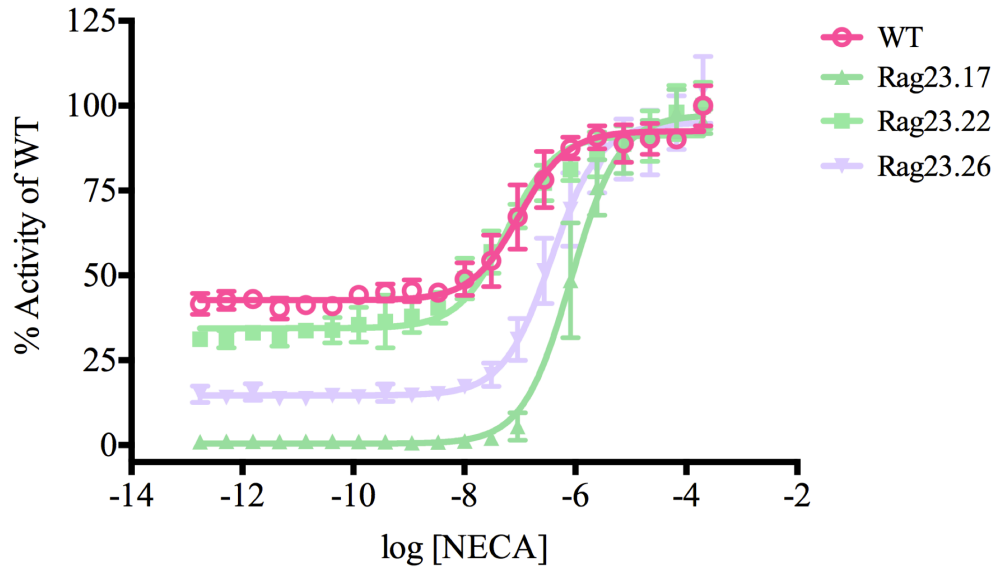
	F79A	A184L	R199A	L208A	L272A	Constitutive Activity (% of maximal activity of WT)	Potency (pEC_{50})	Efficacy (% of maximal activity of WT)
WT	-	-	-	-	-	44 ± 1 %	7.1 ± 0.3	94 ± 1 %
Rag 23.19	-	x	-	-	x	2 ± 1 %	6.7 ± 0.1	88 ± 5 %
Rag 23.20	-	x	-	x	-	4 ± 3 %	7.2 ± 0.2	47 ± 4 %
Rag 23.21	-	x	x	-	-	1 ± 1 %	6.6 ± 0.1	85 ± 6 %
Rag 23.25	x	x	-	-	-	72 ± 10 %	8.0 ± 0.4	123 ± 1 %
Rag 23.29	-	x	-	-	-	0 %*	6.3 ± 0.1	63 ± 4 %

Figure 4-4 Functional profiles of constructs illustrating the major effects of the A184L mutation. The A184L mutation alone abolishes constitutive activity (Rag23.29) but this is overcome by the dominant effect of F79A (Rag23.25). The curves (A) are the average of two experiments performed in triplicate. The table (B) shows the precise details of each mutant characterized. The colours of the curves correspond to those in the table. The data for the wild-type (pink) are also shown for comparison. *SEM=0

L272A alone has a moderate negative effect on the constitutive activity and potency of the $A_{2A}R$ (Rag23.26, Figure 4-5). Much like A184L, these effects are markedly influenced by the presence of other more dominant mutations. For example, when L272A is combined with F79A in Rag23.22 (Figure 4-5), this mutant still has increased constitutive activity and potency compared to wild-type, as a result of the strong influence of F79A. In contrast, when L272A is combined with R199A in

Rag23.17, this mutant has very low levels of constitutive activity and reduced potency compared to wild-type due to the influence of R199A.

A



B

	F79A	A184L	R199A	L208A	L272A	Constitutive Activity (% of maximal activity of WT)	Potency (pEC_{50})	Efficacy (% of maximal activity of WT)
WT	-	-	-	-	-	44 ± 1 %	7.1 ± 0.3	94 ± 1 %
Rag 23.17	-	-	x	-	x	1 %*	5.9 ± 0.1	98 ± 3 %
Rag 23.22	x	-	-	-	x	34 ± 2 %	7.2 ± 0.1	91 ± 1 %
Rag 23.26	-	-	-	-	x	15± 1 %	6.4 ± 0.1	95 ± 5 %

Figure 4-5 Functional profiles of constructs illustrating the major effects of the L272A mutation. The L272A mutation alone decreases constitutive activity on its own (Rag23.26) but this effect is overcome by the dominant effect of the F79A (Rag23.22). In the case of the combination with the R199A (Rag23.17) mutation there is an almost complete loss of constitutive activity. The curves (A) are the average of two experiments performed in triplicate. The table (B) shows the precise details of each mutant characterized. The colours of the curves correspond to those in the table. The data for the wild-type (pink) are also shown for comparison. *SEM=0

4.4 Discussion

4.4.1 Structural basis of the effects of the F79A mutation

There are a number of high resolution $A_{2A}R$ structures which have been obtained using a variety of techniques and in the presence of different ligands (Dore *et al.*, 2011; Hino *et al.*, 2012; Jaakola *et al.*, 2008; Lebon *et al.*, 2011b; Xu *et al.*, 2011). Given that here the roles of mutations in a thermostabilised receptor in the preferentially agonist-bound conformation (Magnani *et al.*, 2008) are explored, the structure of a thermostabilised $A_{2A}R$ containing 5 point mutations in complex with the agonist NECA (Lebon *et al.*, 2011b) was used to provide further context to the results of this study (pdb access code: 2YVD).

In this structure, F79 is located in helix III (Figure 4-6A and 4-6B), a region of the protein with key roles in GPCR function. "A consensus network of 24 inter-helices contacts mediated by 36 topologically equivalent amino acids" has been identified by Venkatakrishnan and colleagues when comparing the known structures of GPCRs (Venkatakrishnan *et al.*, 2013). They noted that helix III plays a major role in this network of contacts by interacting with all the other helices except helices I and VII. Therefore, helix III seems to be central for maintaining the scaffold of GPCRs. Furthermore, topologically equivalent residues in helix III have been shown to interact with the ligand in nearly all the receptors for which a high-resolution structure is available (Venkatakrishnan *et al.*, 2013). Moreover, once the receptor is activated, helix III forms a critical interaction with the G-protein as exemplified by the $Arg^{3.50}$ of the β_2AR interacting with a backbone carbonyl of the C terminus of the G_s protein (Rasmussen *et al.*, 2011a). It is therefore not a surprise that GPCR activity

is very sensitive to mutations in helix III, since these often lead to a complete loss of function or markedly increased constitutive activity (Jiang *et al.*, 1997; Jiang *et al.*, 1996; Venkatakrishnan *et al.*, 2013).

In addition, when comparing the structure of the $A_{2A}R$ bound to NECA (pdb accession code: 2YDV) with the structure of the $A_{2A}R$-T4L bound to ZM241385 (pdb accession code: 3EML), Lebon and colleagues observed a 2 Å upward movement of helix III in the active-like conformation of the receptor (Lebon *et al.*, 2011b). In the inactive conformation (pdb access code: 3PWH), F79 forms van der Waals interactions with a number of surrounding residues including F62 and L137. These interactions are lost when F79 is mutated to an Ala possibly resulting in a less stable inactive conformation. The receptor is then more likely to adopt an active conformation, with the associated 2 Å upward movement of helix III, explaining the increase in constitutive activity observed in our study.

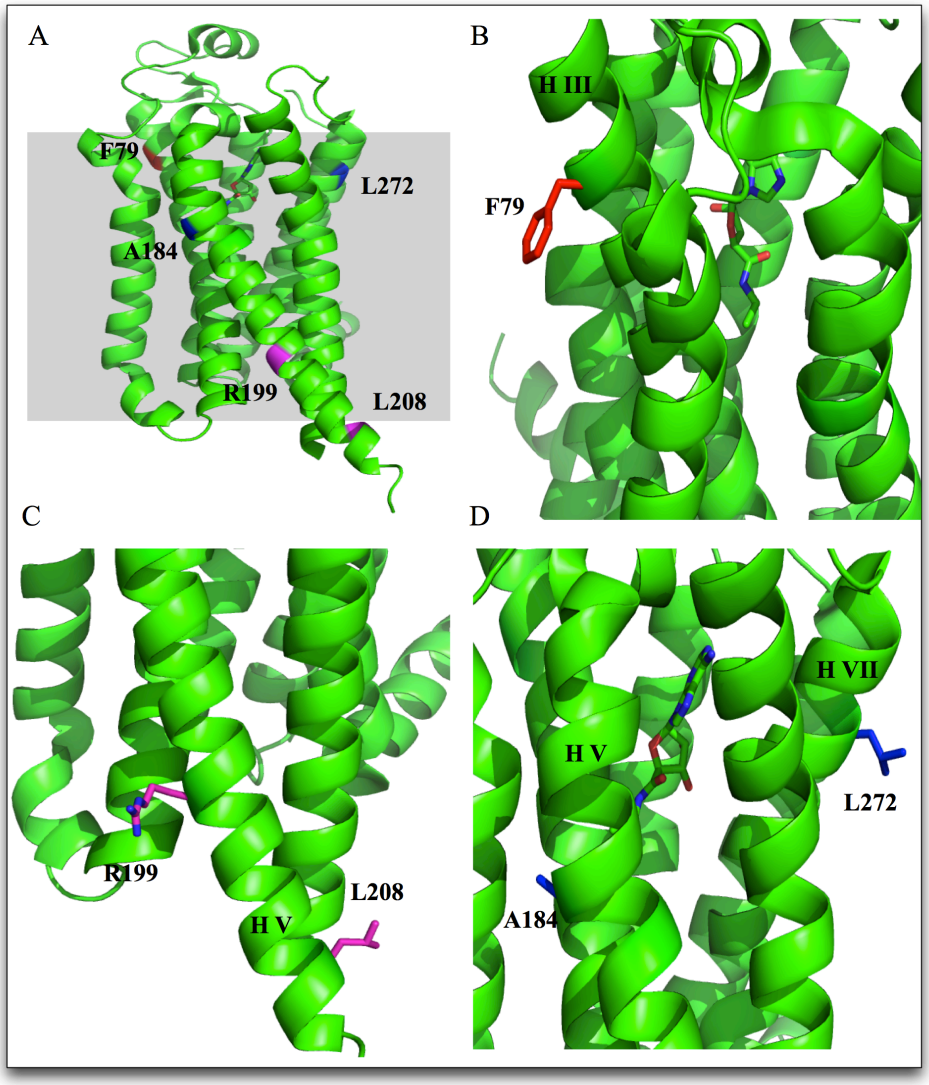


Figure 4-6 Position of the F79 (red), R199A and L208 (magenta), A184 and L272 (blue) residues in the high-resolution crystal structure of the $A_{2A}R$ GL31 thermostable mutant (2YVD) (A). F79 is located on helix III (B) while R199 and L208 are both located at the cytoplasmic end of helix V (C) and A184 and L272 are located at the extracellular end of helix V and helix VII respectively (D) The agonist NECA is shown in B and D.

4.4.2 Structural basis of the effects of the R199A and L208A mutations

Both the R199A and L208A mutations affect constitutive activity dramatically. However, only the L208A mutation affects efficacy. The structures of the $A_{2A}R$ and the β_2AR in complex with G_s provide clues to explain this difference. In the structure of the $A_{2A}R$, R199 and L208 are both located in the cytoplasmic portion of transmembrane helix V (H V; Figure 6A and 6C). This region of helix V is involved in the interaction between the β_2AR and the $G\alpha_s$ (Rasmussen *et al.*, 2011a) and is thus likely to be involved in the interaction of the $A_{2A}R$ with the $G\alpha_i$-related chimera protein used in the yeast cell growth assay.

The R199 and the L208 residues are conserved in the β_2 adrenergic receptor, corresponding to R221 and L230 respectively. Due to the lack of a structure of the $A_{2A}R$ in an active conformation, the structure of the β_2 adrenergic receptor in complex with the G_s protein was used to aid interpretation of our data. In this structure, R221 of the β_2AR forms a hydrogen bond with a threonine (equivalent to an arginine in the $A_{2A}R$) on helix III when the receptor is in complex with the G_s protein. This hydrogen bond no longer exists when R221 is mutated to an alanine. Here it was demonstrated that the R199A mutation completely abolishes constitutive activity of the $A_{2A}R$ without affecting efficacy suggesting that the interaction between helix III and helix V is crucial for constitutive activity but not for agonist-induced activity.

The L230 residue of β_2AR forms a direct interaction with the leucine at the extreme C-terminal end of the G protein. Mutating the equivalent residue of $A_{2A}R$, L208, seems to prevent activation of the G protein in the absence of ligand but only reduces receptor activation in the presence of agonist. This suggests that this

interaction is crucial for formation of a constitutively active complex but it is of less importance in the formation of the agonist-induced active complex.

The fact that L208 is in direct contact with the G protein whilst R199 is involved in making intra-receptor contacts, could explain why the L208A mutation has an effect on both constitutive activity and efficacy while the R199A mutation affects only the constitutive activity.

The data presented in chapter 3 suggested that the agonist induced and constitutively active conformations of the $A_{2A}R$ are distinct, thus inhibiting constitutive activity of the receptor does not necessarily have any negative effects on agonist-induced activity.

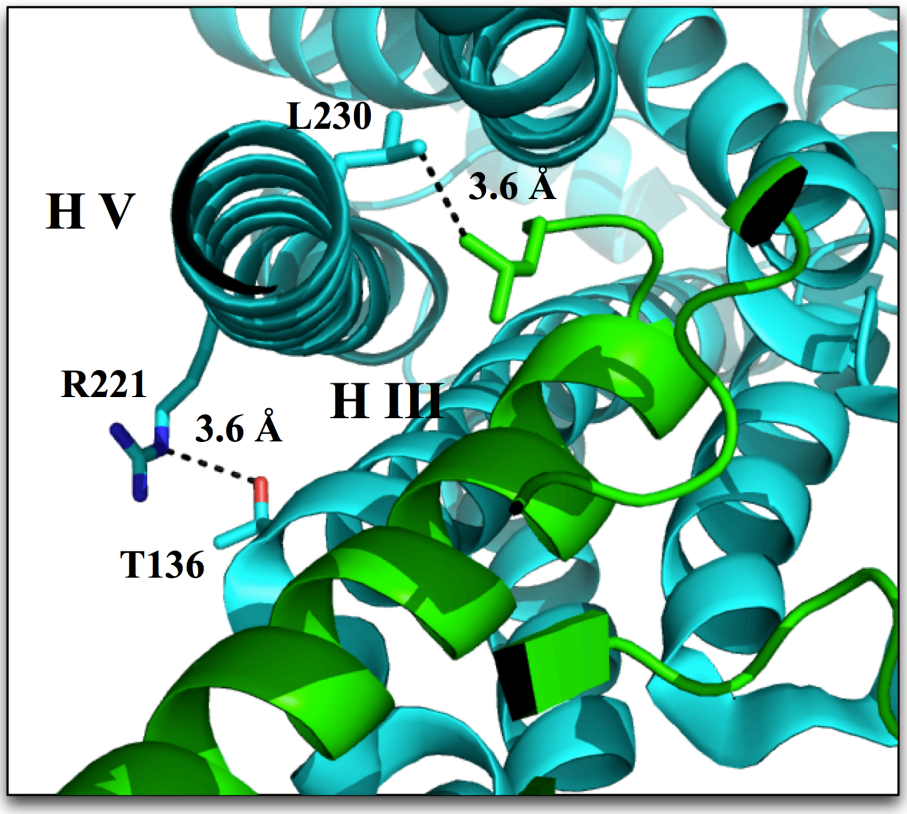


Figure 4-7 Structure of the β_2AR (cyan) in complex with G_S protein (green) (pdb access code: 3SN6) viewed from the cytoplasmic face. The L230 residue of the receptor forms Van der Waals contact with the leucine at the extreme C-terminal end of the G protein. The R221 residue forms a hydrogen bond with the T136 residue on helix III

4.4.3 Structural Basis for the Effects of the A184L and L272A Mutations

A184L and L272A are located on the extracellular ends of helices V and VII respectively (Figure 6A and 6D). Both of these residues are a significant distance away from both the ligand-binding pocket and the G protein-binding region. Based on their location in the crystal structure (Lebon *et al.*, 2011b) these residues are unlikely to be directly involved in G protein coupling or ligand binding (Figure 6D). The data presented here, together with the available structural data, are not sufficient to explain why A184L and L272A have the observed functional effects in the constructs with these single mutations (i.e. Rag23.29 and Rag23.26). However, this does provide clues as to why F79A, R199A and L208A have more dominant effects on the function of the receptor. Interestingly, the level of the effect the mutations have on the pharmacological profile of the receptor is in accordance with the stabilisation effects of the individual mutations observed by Magnani and colleagues when they generated these mutants. One exception is the F79A mutation, which is not thermostabilising (Magnani *et al.*, 2008). For example, the R199A (Rag23.28) and L208A (Rag23.27) single mutants retain 101% and 108% of the wild-type binding activity after heating at 30°C for 30 minutes respectively while the A184L (Rag23.29) and L272A (Rag23.26) retained 75% and 79% respectively. In this analysis, wild-type binding activity after heating is 50%. The F79A mutant shows similar levels of activity after heating as the wild-type receptor.

In conclusion, the R199A and L208A mutations inhibit constitutive activity of the $A_{2A}R$ receptor while F79A enhances constitutive activity. In addition, the L208A mutation also affects the efficacy of the receptor. The effects of A184L and L272A are overcome by the more dominant F79A, R199A and L208A mutations. Analysis of the mutations alone and in combination using the yeast assay, together with the known $A_{2A}R$ structures provides information on the role of individual amino acids in receptor function. However as with all types of analysis of this kind, it can be difficult to fully dissect the activity of an individual amino acid from the contributions of all others. A full understanding of the roles of all the amino acid residues will only be revealed through multiple crystal structures in a range of different conformations coupled with detailed dynamics studies.

5 Discussion and future outlook

GPCRs are essential integral membrane proteins that respond to a wide range of stimuli such as hormones, peptides and neurotransmitters. As such they are the targets of many modern drugs. For many years, our understanding of GPCR mechanism of action was limited by the lack of high-resolution structural information. This was due to several reasons including the difficulties in expressing the protein of interest in quantities large enough for structural studies (Andre *et al.*, 2006; Grisshammer, 2006; McCusker *et al.*, 2007; Sarramegna *et al.*, 2003), the highly dynamic nature of GPCRs (Kobilka & Deupi, 2007), which makes them difficult to isolate in a relevant conformation, and finally their low propensity to crystallize (Rosenbaum *et al.*, 2007). However, recent progress in the field of GPCR overexpression, stabilization and crystallization has resulted in the publication of 58 high-resolution structures of 22 different GPCRs, excluding Rhodopsin, in the last few years. These are essential to furthering our understanding of GPCR function and to facilitate drug design. However, these structures are of highly engineered receptors and little is known about the effect these modifications have on receptor signalling function. One successful method for GPCR structure determination is the introduction of thermostabilising mutations through alanine scanning mutagenesis. Through this method, it is possible to isolate receptors in either a preferentially agonist-binding or antagonist-binding conformation. This reduces the conformational flexibility of the receptor, resulting in increased thermostability. Investigation of the signalling properties of several thermostable mutants of the $A_{2A}R$ using a functional yeast assay revealed several important findings.

5.1 Agonist-induced and constitutive active conformations are distinct

The results from our studies showed that Rag23 and Rag23.1, both of which are in agonist-binding conformations, exhibit increased potencies and affinities for NECA compared with the wild-type while displaying a complete loss of constitutive activity. These findings are not explained by the extended ternary complex model (Samama *et al.*, 1993). Further investigation revealed that the interaction between the receptor and its G protein has not been altered by the mutations in Rag23.1. A possible explanation to these observations could be that the agonist-induced and constitutive active conformations are distinct. Pellisier and coworkers showed that different conformational rearrangements occur during the stabilization of the active states of the 5-HT4 receptor according to the agonist used. In addition, they also showed that different residues were involved in the formation of constitutive and agonist-induced active conformations, reinforcing the idea of distinct conformations (Pellissier *et al.*, 2009).

These findings have major implications for drug design, since it may be possible to design allosteric drugs that would block unwanted constitutive activity of a specific receptor without having any effect of receptor activation through endogenous ligands. This could dramatically reduce side effects since it would allow the receptor to function normally upon release of endogenous ligand.

5.2 Role of individual residues in receptor function and stabilisation

The analysis of the mutants intermediate between Rag23 and the wild-type and between Rant5 and the wild-type revealed the role of individual residues in receptor function and stabilisation. In that regard, the yeast functional assay provides a powerful tool in combination with high-resolution structures, since it is difficult to identify the role of individual residues on receptor function and stabilisation using high-resolution structural information alone.

5.2.1 T88 plays a crucial role for agonist-induced activity

The results presented here are in accordance with previous findings showing that Thr88 plays a crucial role in ligand binding and in agonist-induced activity (Jiang *et al.*, 1997) of the $A_{2A}R$. In addition, the data show that this effect is agonist-dependant. Indeed, while NECA is no longer able to activate the T88A mutant, adenosine still activates T88A with a reduced potency. This T88 residue (3.36 in the Ballestros-Weinstein numbering) seems to be important in most GPCRs, as it is part of the "ligand-binding cradle" described earlier. However, the effect of mutating this residue is receptor specific. Indeed, replacing S3.36 in the H_1 receptor by a threonine dramatically increased the constitutive activity while replacing it with an alanine completely abolishes it (Jongejan *et al.*, 2005). In addition, replacing T3.36 in the 5-HT_4R with an alanine also abolishes constitutive activity (Pellissier *et al.*, 2009). Therefore it is obvious that the 3.36 residue plays a crucial role across GPCRs either on the ligand-binding properties or on the constitutive activity.

5.2.2 Role of individual residues on constitutive activity

The functional characterisation of the intermediate mutants revealed that there are several mechanisms to block constitutive activity, highlighting the complexity of receptor activation. Indeed, the reduction in size of the residue when mutating V239 to an alanine, seems to bring helices III and VI closer to each other, strengthening their interaction and blocking the outward movement of helix VI needed for GPCR activation.

The loss of constitutive activity observed in the R199A mutant involves a different mechanism. It is possible to speculate about the mechanism involved in the loss of constitutive activity by looking at the structures of the $A_{2A}R$ in an inactive conformation, in a partially active conformation and the structure of the β_2AR in complex with G_s. However, it is important to bear in mind that the structures of the partially active $A_{2A}R$ and the active β_2AR are in agonist-induced conformations, which limits interpretation of why the R199A mutation abolishes constitutive activity. In the structure of the $A_{2A}R$ in an inactive conformation, R199 does not seem to be interacting with any other residues within the receptor and is 4.6 Å away from R107 located on helix III (Fig 5-1A). However, the structure of this receptor bound to an agonist and in a partially active conformation reveals that R199 is now 3.9 Å away from R107 (Fig 5-1B). In the β_2AR structure, T136 (equivalent to $A_{2A}R$ R107) forms a hydrogen bond with R221, (equivalent to $A_{2A}R$ R199) (Fig 5-1C). Therefore, it seems that upon activation of the receptor, the movement of helices III and V brings R107 and R199 in close proximity, stabilising the active conformation. Clearly, this interaction is not crucial for the stabilisation of the agonist-induced active

conformation but is necessary for the stabilisation of the constitutive active conformation.

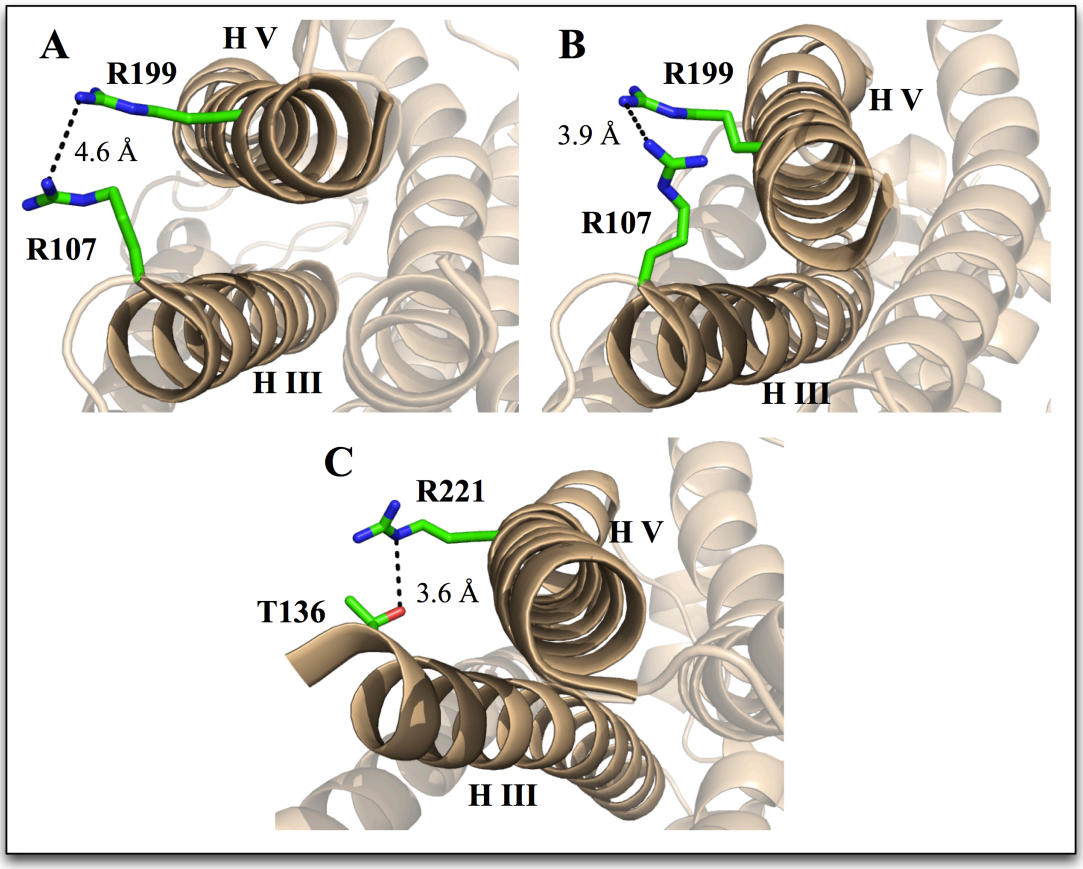


Figure 5-1 Position of the R199 residue of the $A_{2A}R$ or its equivalent R221 of the β_2AR in an inactive conformation (A), in a partially active conformation (B) and in a fully active conformation (C), looking down from the extracellular face.

Finally, the L208 residue, equivalent to L230 in the β_2AR, is involved in both constitutive activity and efficacy. This is certainly due to the direct interaction of this residue with the C-terminal tail for the G_s protein in the β_2AR structure in complex with G_s. However, mutating this residue to an alanine completely abolishes constitutive activity while it only partially reduces efficacy. It is possible that when an agonist is bound to the receptor extra stabilising interactions, not occurring in the constitutively active conformation, allow the formation of an active complex between the receptor and the G protein which involves residues other than L208.

5.3 The yeast functional assay as a screening tool

The data presented here demonstrates that there is a correlation between thermostability and loss of constitutive activity. In addition, this assay allows the distinction between agonist-binding and antagonist-binding conformations. This means that this yeast functional assay could be used to screen stable mutants that would preferentially be in an active or inactive conformation. Indeed, this assay is high throughput, inexpensive and has been demonstrated to work with other GPCRs such as the cannabinoid CB_1 and CB_2 receptors (Dowell & Brown, 2009), GPR41 and GPR43 (Brown *et al.*, 2003) in addition to the $A_{2A}R$ reported here, demonstrating the broad applicability of this method. This method would also offer the advantage of knowing that the stable construct generated is in a functionally relevant conformation.

Furthermore, previous studies on other GPCRs gave no evidence that the pharmacology in yeast is 'wrong' compared with mammalian cell systems, based on such criteria as rank orders of potency of ligands and the translation of compound activities into more complex systems. Indeed, in many cases, yeast data have been more predictive of phenotypic or in vivo studies than data from recombinant mammalian cell assays (GSK unpublished data). This highlights the relevance of using the yeast system as a screening tool.

5.4 Future outlook

Although, the yeast functional assay provides useful data on GPCRs function and stabilisation, it has limitations. Indeed, while this assay provides information on the role of individual residues on the function of receptor, it is difficult to identify the mechanisms underlying this effect without a high-resolution structure. In order to fully understand the complexity of the activation mechanism of GPCRs, high-resolution structures of native receptors in all the different conformations and bound to β-arrestin as well as G protein would be needed.

Another limitation of this assay that it shares with crystal structures of GPCRs, is that it is impossible to investigate the dynamics of the receptor in their native environment. This can be achieved by using solid-state NMR technique since NMR can describe both overall and local protein dynamics. In addition, structures of unmodified receptors can be obtained in phospholipids bilayer, as demonstrated by the structure of the CXCR1 chemokine receptor (Park *et al.*, 2012). Furthermore, NMR technique was used to study the dynamics of the β_2AR by labelling strategically positioned methionines (Nygaard *et al.*, 2013). Nygaard and co-workers were able to observe an alternative inactive state that slowly exchanges with the crystallographically observed inactive state in the absence of ligand or upon inverse agonist binding. They also demonstrated that upon agonist binding the receptor is structurally heterogeneous and that the most populated conformation is distinct from the inactive states. Finally, when the receptor is bound to both an agonist and the Nb80 nanobody, which mimics the G protein, the receptor adopts a more homogeneous conformation corresponding to the fully active state, different from the intermediate active states observed upon agonist binding only.

It seems that only a combination of biochemical studies, X-ray crystallography and NMR spectroscopy will allow researchers to fully understand the dynamics and detailed mechanism of action of GPCRs.

References

Ahn S, Shenoy SK, Wei H, Lefkowitz RJ (2004). Differential kinetic and spatial patterns of beta-arrestin and G protein-mediated ERK activation by the angiotensin II receptor. *J Biol Chem* **279**(34)**:** 35518-35525.

Alexander SP, Millns PJ (2001). [(3)H]ZM241385--an antagonist radioligand for adenosine A(2A) receptors in rat brain. *Eur J Pharmacol* **411**(3)**:** 205-210.

Anborgh PH, Seachrist JL, Dale LB, Ferguson SS (2000). Receptor/beta-arrestin complex formation and the differential trafficking and resensitization of beta2-adrenergic and angiotensin II type 1A receptors. *Mol Endocrinol* **14**(12)**:** 2040-2053.

Andre N, Cherouati N, Prual C, Steffan T, Zeder-Lutz G, Magnin T*, et al.* (2006). Enhancing functional production of G protein-coupled receptors in Pichia pastoris to levels required for structural studies via a single expression screen. *Protein Sci* **15**(5)**:** 1115-1126.

Aris L, Gilchrist A, Rens-Domiano S, Meyer C, Schatz PJ, Dratz EA*, et al.* (2001). Structural requirements for the stabilization of metarhodopsin II by the C terminus of the alpha subunit of transducin. *J Biol Chem* **276**(4)**:** 2333-2339.

Atwood BK, Lopez J, Wager-Miller J, Mackie K, Straiker A (2011). Expression of G protein-coupled receptors and related proteins in HEK293, AtT20, BV2, and N18 cell lines as revealed by microarray analysis. *BMC Genomics* **12:** 14.

Bae H, Cabrera-Vera TM, Depree KM, Graber SG, Hamm HE (1999). Two amino acids within the alpha4 helix of Galphai1 mediate coupling with 5-hydroxytryptamine1B receptors. *J Biol Chem* **274**(21)**:** 14963-14971.

Barnes WG, Reiter E, Violin JD, Ren XR, Milligan G, Lefkowitz RJ (2005). beta-Arrestin 1 and Galphaq/11 coordinately activate RhoA and stress fiber formation following receptor stimulation. *J Biol Chem* **280**(9)**:** 8041-8050.

Beaulieu JM, Sotnikova TD, Marion S, Lefkowitz RJ, Gainetdinov RR, Caron MG (2005). An Akt/beta-arrestin 2/PP2A signaling complex mediates dopaminergic neurotransmission and behavior. *Cell* **122**(2)**:** 261-273.

Bertin B, Freissmuth M, Breyer RM, Schutz W, Strosberg AD, Marullo S (1992). Functional expression of the human serotonin 5-HT1A receptor in Escherichia coli. Ligand binding properties and interaction with recombinant G protein alpha-subunits. *J Biol Chem* **267**(12)**:** 8200-8206.

Beukers MvO, J. van der Hoorn, P. Blad, C. den Dulk, H. Brouwer, J. and IJzerman, A. (2004). Random Mutagenesis of the Human Adenosine A2B Receptor Followed by Growth Selection in Yeast. Identification of Constitutively Active and Gain of Function Mutations. *Mol. Pharmacol.* **65**(3)**:** 702-710.

Bockaert J, Pin JP (1999). Molecular tinkering of G protein-coupled receptors: an evolutionary success. *EMBO J* **18**(7)**:** 1723-1729.

Bohn LM, Lefkowitz RJ, Gainetdinov RR, Peppel K, Caron MG, Lin FT (1999). Enhanced morphine analgesia in mice lacking beta-arrestin 2. *Science* **286**(5449)**:** 2495-2498.

Bourne HR (1997). How receptors talk to trimeric G proteins. *Curr Opin Cell Biol* **9**(2)**:** 134-142.

Bremnes T, Paasche JD, Mehlum A, Sandberg C, Bremnes B, Attramadal H (2000). Regulation and intracellular trafficking pathways of the endothelin receptors. *J Biol Chem* **275**(23)**:** 17596-17604.

Brown AJ, Goldsworthy SM, Barnes AA, Eilert MM, Tcheang L, Daniels D*, et al.* (2003). The Orphan G Protein-coupled Receptors GPR41 and GPR43 Are Activated by Propionate and Other Short Chain Carboxylic Acids. *J Biol Chem* **278:** 11312-11319.

Bruchas MR, Macey TA, Lowe JD, Chavkin C (2006). Kappa opioid receptor activation of p38 MAPK is GRK3- and arrestin-dependent in neurons and astrocytes. *J Biol Chem* **281**(26)**:** 18081-18089.

Buchanan FG, Gorden DL, Matta P, Shi Q, Matrisian LM, DuBois RN (2006). Role of beta-arrestin 1 in the metastatic progression of colorectal cancer. *Proc Natl Acad Sci U S A* **103**(5)**:** 1492-1497.

Cabrera-Vera TM, Vanhauwe J, Thomas TO, Medkova M, Preininger A, Mazzoni MR*, et al.* (2003). Insights into G protein structure, function, and regulation. *Endocr Rev* **24**(6)**:** 765-781.

Cai K, Itoh Y, Khorana HG (2001). Mapping of contact sites in complex formation between transducin and light-activated rhodopsin by covalent crosslinking: use of a photoactivatable reagent. *Proc Natl Acad Sci U S A* **98**(9)**:** 4877-4882.

Chen CA, Manning DR (2001). Regulation of G proteins by covalent modification. *Oncogene* **20**(13)**:** 1643-1652.

Chen JF, Huang Z, Ma J, Zhu J, Moratalla R, Standaert D*, et al.* (1999). A(2A) adenosine receptor deficiency attenuates brain injury induced by transient focal ischemia in mice. *J Neurosci* **19**(21)**:** 9192-9200.

Cherezov V, Rosenbaum DM, Hanson MA, Rasmussen SGF, Thian FS, Kobilka TS*, et al.* (2007). High-Resolution Crystal Structure of an Engineered Human 2-Adrenergic G Protein Coupled Receptor. *Science* **318**(5854)**:** 1258-1265.

Chien EY, Liu W, Zhao Q, Katritch V, Han GW, Hanson MA*, et al.* (2010). Structure of the human dopamine D3 receptor in complex with a D2/D3 selective antagonist. *Science* **330**(6007)**:** 1091-1095.

Chun E, Thompson AA, Liu W, Roth CB, Griffith MT, Katritch V*, et al.* (2012). Fusion partner toolchest for the stabilization and crystallization of g protein-coupled receptors. *Structure* **20**(6)**:** 967-976.

Congreve M, Andrews SP, Dore AS, Hollenstein K, Hurrell E, Langmead CJ*, et al.* (2012). Discovery of 1,2,4-triazine derivatives as adenosine A(2A) antagonists using structure based drug design. *J Med Chem* **55**(5)**:** 1898-1903.

Conklin BR, Bourne HR (1993). Structural elements of G alpha subunits that interact with G beta gamma, receptors, and effectors. *Cell* **73**(4)**:** 631-641.

Conklin BR, Herzmark P, Ishida S, Voyno-Yasenetskaya TA, Sun Y, Farfel Z*, et al.* (1996). Carboxyl-terminal mutations of Gq alpha and Gs alpha that alter the fidelity of receptor activation. *Mol Pharmacol* **50**(4)**:** 885-890.

De Lean A, Stadel JM, Lefkowitz RJ (1980). A ternary complex model explains the agonist-specific binding properties of the adenylate cyclase-coupled beta-adrenergic receptor. *J Biol Chem* **255**(15)**:** 7108-7117.

de Lera Ruiz M, Lim YH, Zheng J (2013). The Adenosine A2A Receptor as a Drug Discovery Target. *J Med Chem*.

DeFea KA, Vaughn ZD, O'Bryan EM, Nishijima D, Dery O, Bunnett NW (2000a). The proliferative and antiapoptotic effects of substance P are facilitated by formation of a beta -arrestin-dependent scaffolding complex. *Proc Natl Acad Sci U S A* **97**(20)**:** 11086-11091.

DeFea KA, Zalevsky J, Thoma MS, Dery O, Mullins RD, Bunnett NW (2000b). beta-arrestin-dependent endocytosis of proteinase-activated receptor 2 is required for intracellular targeting of activated ERK1/2. *J Cell Biol* **148**(6)**:** 1267-1281.

DeWire SM, Ahn S, Lefkowitz RJ, Shenoy SK (2007). Beta-arrestins and cell signaling. *Annu Rev Physiol* **69:** 483-510.

Dionisotti S, Ongini E, Zocchi C, Kull B, Arslan G, Fredholm BB (1997). Characterization of human A2A adenosine receptors with the antagonist radioligand [3H]-SCH 58261. *Br J Pharmacol* **121**(3)**:** 353-360.

Dodevski I, Pluckthun A (2011). Evolution of three human GPCRs for higher expression and stability. *J Mol Biol* **408**(4)**:** 599-615.

Dore AS, Robertson N, Errey JC, Ng I, Hollenstein K, Tehan B*, et al.* (2011). Structure of the adenosine A(2A) receptor in complex with ZM241385 and the xanthines XAC and caffeine. *Structure* **19**(9)**:** 1283-1293.

Dowell SJ, Brown AJ (2009). Yeast assays for G protein-coupled receptors. *Methods Mol Biol* **552:** 213-229.

Downes GB, Gautam N (1999). The G protein subunit gene families. *Genomics* **62**(3)**:** 544-552.

Drew D, Newstead S, Sonoda Y, Kim H, von Heijne G, Iwata S (2008). GFP-based optimization scheme for the overexpression and purification of eukaryotic membrane proteins in Saccharomyces cerevisiae. *Nat Protoc* **3**(5)**:** 784-798.

Eason MG, Kurose H, Holt BD, Raymond JR, Liggett SB (1992). Simultaneous coupling of alpha 2-adrenergic receptors to two G-proteins with opposing effects. Subtype-selective coupling of alpha 2C10, alpha 2C4, and alpha 2C2 adrenergic receptors to Gi and Gs. *J Biol Chem* **267**(22)**:** 15795-15801.

Enjalbert A, Bockaert J (1983). Pharmacological characterization of the D2 dopamine receptor negatively coupled with adenylate cyclase in rat anterior pituitary. *Mol Pharmacol* **23**(3)**:** 576-584.

Ferguson SS (2001). Evolving concepts in G protein-coupled receptor endocytosis: the role in receptor desensitization and signaling. *Pharmacol Rev* **53**(1)**:** 1-24.

Ferre S, Goldberg SR, Lluis C, Franco R (2009). Looking for the role of cannabinoid receptor heteromers in striatal function. *Neuropharmacology* **56 Suppl 1:** 226-234.

Ferre S, Karcz-Kubicha M, Hope BT, Popoli P, Burgueno J, Gutierrez MA*, et al.* (2002). Synergistic interaction between adenosine A2A and glutamate mGlu5 receptors: implications for striatal neuronal function. *Proc Natl Acad Sci U S A* **99**(18)**:** 11940-11945.

Fisher A, Heldman E, Gurwitz D, Haring R, Barak D, Meshulam H*, et al.* (1993). Selective signaling via unique M1 muscarinic agonists. *Ann N Y Acad Sci* **695:** 300-303.

Ford CE, Skiba NP, Bae H, Daaka Y, Reuveny E, Shekter LR*, et al.* (1998). Molecular basis for interactions of G protein betagamma subunits with effectors. *Science* **280**(5367)**:** 1271-1274.

Fozard JR, Ellis KM, Villela Dantas MF, Tigani B, Mazzoni L (2002). Effects of CGS 21680, a selective adenosine A2A receptor agonist, on allergic airways inflammation in the rat. *Eur J Pharmacol* **438**(3)**:** 183-188.

Fraser NJ (2006). Expression and functional purification of a glycosylation deficient version of the human adenosine 2a receptor for structural studies. *Protein Expr Purif* **49**(1)**:** 129-137.

Fredholm BB, Ijzerman A, Jacobson KA, Klotz KN, Linden J (2001). International Union of Pharmacology. XXV. Nomenclature and classification of adenosine receptors. *Pharmacol Rev* **53**(4)**:** 527-552.

Fredriksson R (2005). The Repertoire of G-Protein-Coupled Receptors in Fully Sequenced Genomes. *Molecular Pharmacology* **67**(5)**:** 1414-1425.

Fredriksson R, Lagerstrom M, Lundin LG, Schioth HB (2003). The G-Protein-Coupled Receptors in the Human Genome Form Five Main Families. Phylogenetic

Analysis, Paralogon Groups, and Fingerprints. *Molecular Pharmacology* **63**(6)**:** 1256-1272.

Fukada Y, Kokame K (1994). [Covalent lipid modifications of heterotrimeric G proteins]. *Nihon Yakurigaku Zasshi* **103**(6)**:** 263-272.

Fuxe K, Ferre S, Canals M, Torvinen M, Terasmaa A, Marcellino D*, et al.* (2005). Adenosine A2A and dopamine D2 heteromeric receptor complexes and their function. *J Mol Neurosci* **26**(2-3)**:** 209-220.

Gao H, Sun Y, Wu Y, Luan B, Wang Y, Qu B*, et al.* (2004). Identification of beta-arrestin2 as a G protein-coupled receptor-stimulated regulator of NF-kappaB pathways. *Mol Cell* **14**(3)**:** 303-317.

Garritsen A, van Galen PJ, Simonds WF (1993). The N-terminal coiled-coil domain of beta is essential for gamma association: a model for G-protein beta gamma subunit interaction. *Proc Natl Acad Sci U S A* **90**(16)**:** 7706-7710.

Ge L, Ly Y, Hollenberg M, DeFea K (2003). A beta-arrestin-dependent scaffold is associated with prolonged MAPK activation in pseudopodia during protease-activated receptor-2-induced chemotaxis. *J Biol Chem* **278**(36)**:** 34418-34426.

Gietz RD, Schiestl RH (2007). High-efficiency yeast transformation using the LiAc/SS carrier DNA/PEG method. *Nature Protocols* **2**(1)**:** 31-34.

Gimpl G, Klein U, Reilander H, Fahrenholz F (1995). Expression of the human oxytocin receptor in baculovirus-infected insect cells: high-affinity binding is induced by a cholesterol-cyclodextrin complex. *Biochemistry* **34**(42)**:** 13794-13801.

Gloriam DE, Fredriksson R, Schiöth HB (2007). The G protein-coupled receptor subset of the rat genome. *BMC Genomics* **8**(1)**:** 338.

Goodman OB, Jr., Krupnick JG, Santini F, Gurevich VV, Penn RB, Gagnon AW*, et al.* (1996). Beta-arrestin acts as a clathrin adaptor in endocytosis of the beta2-adrenergic receptor. *Nature* **383**(6599)**:** 447-450.

Granier S, Manglik A, Kruse AC, Kobilka TS, Thian FS, Weis WI*, et al.* (2012). Structure of the delta-opioid receptor bound to naltrindole. *Nature* **485**(7398)**:** 400-404.

Grisshammer R (2006). Understanding recombinant expression of membrane proteins. *Current Opinion in Biotechnology* **17**(4)**:** 337-340.

Grisshammer R, Duckworth R, Henderson R (1993). Expression of a rat neurotensin receptor in Escherichia coli. *Biochem J* **295 (Pt 2):** 571-576.

Gui L, Duan W, Tian H, Li C, Zhu J, Chen JF*, et al.* (2009). Adenosine A 2A receptor deficiency reduces striatal glutamate outflow and attenuates brain injury induced by transient focal cerebral ischemia in mice. *Brain Res* **1297:** 185-193.

Gurwitz D, Haring R, Heldman E, Fraser CM, Manor D, Fisher A (1994). Discrete activation of transduction pathways associated with acetylcholine m1 receptor by several muscarinic ligands. *Eur J Pharmacol* **267**(1)**:** 21-31.

Haga K, Kruse AC, Asada H, Yurugi-Kobayashi T, Shiroishi M, Zhang C*, et al.* (2012). Structure of the human M2 muscarinic acetylcholine receptor bound to an antagonist. *Nature* **482**(7386)**:** 547-551.

Hamm HE, Deretic D, Arendt A, Hargrave PA, Koenig B, Hofmann KP (1988). Site of G protein binding to rhodopsin mapped with synthetic peptides from the alpha subunit. *Science* **241**(4867)**:** 832-835.

Han X, Tachado SD, Koziel H, Boisvert WA (2012). Leu128(3.43) (l128) and Val247(6.40) (V247) of CXCR1 are critical amino acid residues for g protein coupling and receptor activation. *PLoS One* **7**(8)**:** e42765.

Hannawacker A, Krasel C, Lohse MJ (2002). Mutation of Asn293 to Asp in transmembrane helix VI abolishes agonist-induced but not constitutive activity of the beta(2)-adrenergic receptor. *Mol Pharmacol* **62**(6)**:** 1431-1437.

Hanson MA, Roth CB, Jo E, Griffith MT, Scott FL, Reinhart G*, et al.* (2012). Crystal structure of a lipid G protein-coupled receptor. *Science* **335**(6070)**:** 851-855.

Hasegawa J, Loh HH, Lee NM (1987). Lipid requirement for mu opioid receptor binding. *J Neurochem* **49**(4)**:** 1007-1012.

Hauser RA, Schwarzschild MA (2005). Adenosine A2A receptor antagonists for Parkinson's disease: rationale, therapeutic potential and clinical experience. *Drugs Aging* **22**(6)**:** 471-482.

Hein P, Frank M, Hoffmann C, Lohse MJ, Bunemann M (2005). Dynamics of receptor/G protein coupling in living cells. *EMBO J* **24**(23)**:** 4106-4114.

Hepler JR, Gilman AG (1992). G proteins. *Trends Biochem Sci* **17**(10)**:** 383-387.

Hermans E (2003). Biochemical and pharmacological control of the multiplicity of coupling at G-protein-coupled receptors. *Pharmacol Ther* **99**(1)**:** 25-44.

Hide I, Padgett WL, Jacobson KA, Daly JW (1992). A2A adenosine receptors from rat striatum and rat pheochromocytoma PC12 cells: characterization with radioligand binding and by activation of adenylate cyclase. *Mol Pharmacol* **41**(2)**:** 352-359.

Hino T, Arakawa T, Iwanari H, Yurugi-Kobayashi T, Ikeda-Suno C, Nakada-Nakura Y*, et al.* (2012). G-protein-coupled receptor inactivation by an allosteric inverse-agonist antibody. *Nature* **482**(7384)**:** 237-240.

Hofmann KP, Scheerer P, Hildebrand PW, Choe HW, Park JH, Heck M*, et al.* (2009). A G protein-coupled receptor at work: the rhodopsin model. *Trends Biochem Sci* **34**(11)**:** 540-552.

Hollenstein K, Kean J, Bortolato A, Cheng RK, Dore AS, Jazayeri A*, et al.* (2013). Structure of class B GPCR corticotropin-releasing factor receptor 1. *Nature* **499**(7459)**:** 438-443.

Hopkins A, Groom C (2002). The druggable genome. *Nat Rev Drug Discov* **1**(9)**:** 727-730.

Howard A, McAllister G, Feighner S, Liu Q, Nargund R, Van der Ploeg L*, et al.* (2001). Orphan G-protein-coupled receptors and natural ligand discovery. *Trends Pharmacol Sci* **22**(3)**:** 132-139.

Huang J, Chen S, Zhang JJ, Huang XY (2013). Crystal structure of oligomeric beta1-adrenergic G protein-coupled receptors in ligand-free basal state. *Nat Struct Mol Biol* **20**(4)**:** 419-425.

Jaakola V-P, Griffith MT, Hanson MA, Cherezov V, Chien EYT, Lane JR*, et al.* (2008). The 2.6 Angstrom Crystal Structure of a Human A2a adenosine Receptor Bound to an Antagonist. *Science* **322**(5905)**:** 1211-1217.

Jiang Q, Lee BX, Glashofer M, van Rhee AM, Jacobson KA (1997). Mutagenesis reveals structure-activity parallels between human A2A adenosine receptors and biogenic amine G protein-coupled receptors. *J Med Chem* **40**(16)**:** 2588-2595.

Jiang Q, Van Rhee AM, Kim J, Yehle S, Wess J, Jacobson KA (1996). Hydrophilic side chains in the third and seventh transmembrane helical domains of human A2A adenosine receptors are required for ligand recognition. *Mol Pharmacol* **50**(3)**:** 512-521.

Jongejan A, Bruysters M, Ballesteros JA, Haaksma E, Bakker RA, Pardo L*, et al.* (2005). Linking agonist binding to histamine H1 receptor activation. *Nature Chemical Biology* **1**(2)**:** 98-103.

Kahsai AW, Xiao K, Rajagopal S, Ahn S, Shukla AK, Sun J*, et al.* (2011). Multiple ligand-specific conformations of the beta(2)-adrenergic receptor. *Nat Chem Biol* **7**(10)**:** 692-700.

Kang J, Shi Y, Xiang B, Qu B, Su W, Zhu M*, et al.* (2005). A nuclear function of beta-arrestin1 in GPCR signaling: regulation of histone acetylation and gene transcription. *Cell* **123**(5)**:** 833-847.

Kaushal S, Khorana HG (1994). Structure and function in rhodopsin. 7. Point mutations associated with autosomal dominant retinitis pigmentosa. *Biochemistry* **33**(20)**:** 6121-6128.

Kenakin T (2007). Functional selectivity through protean and biased agonism: who steers the ship? *Mol Pharmacol* **72**(6)**:** 1393-1401.

Klabunde T, Hessler G (2002). Drug design strategies for targeting G-protein-coupled receptors. *Chembiochem* **3**(10)**:** 928-944.

Klinger M, Freissmuth M, Nanoff C (2002a). Adenosine receptors: G protein-mediated signalling and the role of accessory proteins. *Cell Signal* **14**(2)**:** 99-108.

Klinger M, Kuhn M, Just H, Stefan E, Palmer T, Freissmuth M*, et al.* (2002b). Removal of the carboxy terminus of the A2A-adenosine receptor blunts constitutive activity: differential effect on cAMP accumulation and MAP kinase stimulation. *Naunyn Schmiedebergs Arch Pharmacol* **366**(4)**:** 287-298.

Klotz KN, Hessling J, Hegler J, Owman C, Kull B, Fredholm BB*, et al.* (1998). Comparative pharmacology of human adenosine receptor subtypes - characterization of stably transfected receptors in CHO cells. *Naunyn Schmiedebergs Arch Pharmacol* **357**(1)**:** 1-9.

Kobilka BK, Deupi X (2007). Conformational complexity of G-protein-coupled receptors. *Trends in Pharmacological Sciences* **28**(8)**:** 397-406.

Kobilka BK, Kobilka TS, Daniel K, Regan JW, Caron MG, Lefkowitz RJ (1988). Chimeric alpha 2-,beta 2-adrenergic receptors: delineation of domains involved in effector coupling and ligand binding specificity. *Science* **240**(4857)**:** 1310-1316.

Kostenis E, Degtyarev MY, Conklin BR, Wess J (1997). The N-terminal extension of Galphaq is critical for constraining the selectivity of receptor coupling. *J Biol Chem* **272**(31)**:** 19107-19110.

Krupnick JG, Goodman OB, Jr., Keen JH, Benovic JL (1997). Arrestin/clathrin interaction. Localization of the clathrin binding domain of nonvisual arrestins to the carboxy terminus. *J Biol Chem* **272**(23)**:** 15011-15016.

Kruse AC, Hu J, Pan AC, Arlow DH, Rosenbaum DM, Rosemond E*, et al.* (2012). Structure and dynamics of the M3 muscarinic acetylcholine receptor. *Nature* **482**(7386)**:** 552-556.

Lagane B, Gaibelet G, Meilhoc E, Masson JM, Cezanne L, Lopez A (2000). Role of sterols in modulating the human mu-opioid receptor function in Saccharomyces cerevisiae. *J Biol Chem* **275**(43)**:** 33197-33200.

Laporte SA, Oakley RH, Holt JA, Barak LS, Caron MG (2000). The interaction of beta-arrestin with the AP-2 adaptor is required for the clustering of beta 2-adrenergic receptor into clathrin-coated pits. *J Biol Chem* **275**(30)**:** 23120-23126.

Laporte SA, Oakley RH, Zhang J, Holt JA, Ferguson SS, Caron MG*, et al.* (1999). The beta2-adrenergic receptor/betaarrestin complex recruits the clathrin adaptor AP-2 during endocytosis. *Proc Natl Acad Sci U S A* **96**(7)**:** 3712-3717.

Lebon G, Bennett K, Jazayeri A, Tate CG (2011a). Thermostabilisation of an agonist-bound conformation of the human adenosine A(2A) receptor. *J Mol Biol* **409**(3)**:** 298-310.

Lebon G, Warne T, Edwards PC, Bennett K, Langmead CJ, Leslie AG*, et al.* (2011b). Agonist-bound adenosine A2A receptor structures reveal common features of GPCR activation. *Nature* **474**(7352)**:** 521-525.

Li J, Edwards PC, Burghammer M, Villa C, Schertler GF (2004). Structure of bovine rhodopsin in a trigonal crystal form. *J Mol Biol* **343**(5)**:** 1409-1438.

Liu W, Chun E, Thompson AA, Chubukov P, Xu F, Katritch V*, et al.* (2012). Structural Basis for Allosteric Regulation of GPCRs by Sodium Ions. *Science* **337**(6091)**:** 232-236.

Lowry OH, Rosebrough NJ, Farr AL, Randall RJ (1951). Protein measurement with the Folin phenol reagent. *J Biol Chem* **193**(1)**:** 265-275.

Luttrell LM, Ferguson SS, Daaka Y, Miller WE, Maudsley S, Della Rocca GJ*, et al.* (1999). Beta-arrestin-dependent formation of beta2 adrenergic receptor-Src protein kinase complexes. *Science* **283**(5402)**:** 655-661.

Luttrell LM, Gesty-Palmer D (2010). Beyond desensitization: physiological relevance of arrestin-dependent signaling. *Pharmacol Rev* **62**(2)**:** 305-330.

Luttrell LM, Roudabush FL, Choy EW, Miller WE, Field ME, Pierce KL*, et al.* (2001). Activation and targeting of extracellular signal-regulated kinases by beta-arrestin scaffolds. *Proc Natl Acad Sci U S A* **98**(5)**:** 2449-2454.

Ma L, Pei G (2007). Beta-arrestin signaling and regulation of transcription. *J Cell Sci* **120**(Pt 2)**:** 213-218.

Magnani F, Shibata Y, Serrano-Vega MJ, Tate CG (2008). Co-evolving stability and conformational homogeneity of the human adenosine A2a receptor. *Proceedings of the National Academy of Sciences* **105**(31)**:** 10744-10749.

Manglik A, Kruse AC, Kobilka TS, Thian FS, Mathiesen JM, Sunahara RK*, et al.* (2012). Crystal structure of the micro-opioid receptor bound to a morphinan antagonist. *Nature* **485**(7398)**:** 321-326.

Martin EL, Rens-Domiano S, Schatz PJ, Hamm HE (1996). Potent peptide analogues of a G protein receptor-binding region obtained with a combinatorial library. *J Biol Chem* **271**(1)**:** 361-366.

McCusker EC, Bane SE, O'Malley MA, Robinson AS (2007). Heterologous GPCR expression: a bottleneck to obtaining crystal structures. *Biotechnol Prog* **23**(3)**:** 540-547.

McDonald PH, Chow CW, Miller WE, Laporte SA, Field ME, Lin FT*, et al.* (2000). Beta-arrestin 2: a receptor-regulated MAPK scaffold for the activation of JNK3. *Science* **290**(5496)**:** 1574-1577.

McKnight AJ, Gordon S (1998). The EGF-TM7 family: unusual structures at the leukocyte surface. *J Leukoc Biol* **63**(3)**:** 271-280.

Miller WE, McDonald PH, Cai SF, Field ME, Davis RJ, Lefkowitz RJ (2001). Identification of a motif in the carboxyl terminus of beta -arrestin2 responsible for activation of JNK3. *J Biol Chem* **276**(30)**:** 27770-27777.

Milligan G, Bond RA, Lee M (1995). Inverse agonism: pharmacological curiosity or potential therapeutic strategy? *Trends Pharmacol Sci* **16**(1)**:** 10-13.

Milligan G, Kostenis E (2006). Heterotrimeric G-proteins: a short history. *Br J Pharmacol* **147 Suppl 1:** S46-55.

Moukhametzianov R, Warne T, Edwards PC, Serrano-Vega MJ, Leslie AG, Tate CG*, et al.* (2011). Two distinct conformations of helix 6 observed in antagonist-bound structures of a beta1-adrenergic receptor. *Proc Natl Acad Sci U S A* **108**(20)**:** 8228-8232.

Mumberg D, Muller R, Funk M (1995). Yeast vectors for the controlled expression of heterologous proteins in different genetic backgrounds. *Gene* **156**(1)**:** 119-122.

Nakamichi H, Okada T (2006). Local peptide movement in the photoreaction intermediate of rhodopsin. *Proc Natl Acad Sci U S A* **103**(34)**:** 12729-12734.

Nelson CD, Perry SJ, Regier DS, Prescott SM, Topham MK, Lefkowitz RJ (2007). Targeting of diacylglycerol degradation to M1 muscarinic receptors by beta-arrestins. *Science* **315**(5812)**:** 663-666.

Newstead S, Kim H, von Heijne G, Iwata S, Drew D (2007). High-throughput fluorescent-based optimization of eukaryotic membrane protein overexpression and purification in Saccharomyces cerevisiae. *Proc Natl Acad Sci U S A* **104**(35)**:** 13936-13941.

Noda K, Feng YH, Liu XP, Saad Y, Husain A, Karnik SS (1996). The active state of the AT1 angiotensin receptor is generated by angiotensin II induction. *Biochemistry* **35**(51)**:** 16435-16442.

Noma T, Lemaire A, Naga Prasad SV, Barki-Harrington L, Tilley DG, Chen J*, et al.* (2007). Beta-arrestin-mediated beta1-adrenergic receptor transactivation of the EGFR confers cardioprotection. *J Clin Invest* **117**(9)**:** 2445-2458.

Nygaard R, Zou Y, Dror RO, Mildorf TJ, Arlow DH, Manglik A*, et al.* (2013). The dynamic process of beta(2)-adrenergic receptor activation. *Cell* **152**(3)**:** 532-542.

O'Malley MA, Lazarova T, Britton ZT, Robinson AS (2007). High-level expression in Saccharomyces cerevisiae enables isolation and spectroscopic characterization of functional human adenosine A2a receptor. *J Struct Biol* **159**(2)**:** 166-178.

Oakley RH, Laporte SA, Holt JA, Caron MG, Barak LS (2000). Differential affinities of visual arrestin, beta arrestin1, and beta arrestin2 for G protein-coupled receptors delineate two major classes of receptors. *J Biol Chem* **275**(22)**:** 17201-17210.

Okada T, Sugihara M, Bondar A-N, Elstner M, Entel P, Buss V (2004). The Retinal Conformation and its Environment in Rhodopsin in Light of a New 2.2Å Crystal Structure†. *Journal of Molecular Biology* **342**(2)**:** 571-583.

Oldham WM, Hamm HE (2006). Structural basis of function in heterotrimeric G proteins. *Q Rev Biophys* **39**(2)**:** 117-166.

Olesnicky NS, Brown AJ, Dowell SJ, Casselton LA (1999). A constitutively active G-protein-coupled receptor causes mating self-compatibility in the mushroom Coprinus. *EMBO J* **18**(10)**:** 2756-2763.

Onrust R, Herzmark P, Chi P, Garcia PD, Lichtarge O, Kingsley C*, et al.* (1997). Receptor and betagamma binding sites in the alpha subunit of the retinal G protein transducin. *Science* **275**(5298)**:** 381-384.

Osawa S, Weiss ER (1995). The effect of carboxyl-terminal mutagenesis of Gt alpha on rhodopsin and guanine nucleotide binding. *J Biol Chem* **270**(52)**:** 31052-31058.

Palczewski K (2000). Crystal Structure of Rhodopsin: A G Protein-Coupled Receptor. *Science* **289**(5480)**:** 739-745.

Park JH, Scheerer P, Hofmann KP, Choe HW, Ernst OP (2008). Crystal structure of the ligand-free G-protein-coupled receptor opsin. *Nature* **454**(7201)**:** 183-187.

Park SH, Das BB, Casagrande F, Tian Y, Nothnagel HJ, Chu M*, et al.* (2012). Structure of the chemokine receptor CXCR1 in phospholipid bilayers. *Nature* **491**(7426)**:** 779-783.

Parthier C, Reedtz-Runge S, Rudolph R, Stubbs MT (2009). Passing the baton in class B GPCRs: peptide hormone activation via helix induction? *Trends Biochem Sci* **34**(6)**:** 303-310.

Peeters MC, van Westen GJP, Guo D, Wisse LE, Muller CE, Beukers MW*, et al.* (2010). GPCR structure and activation: an essential role for the first extracellular loop in activating the adenosine A2B receptor. *The FASEB Journal* **25**(2)**:** 632-643.

Pellissier LP, Sallander J, Campillo M, Gaven F, Queffeulou E, Pillot M*, et al.* (2009). Conformational Toggle Switches Implicated in Basal Constitutive and Agonist-Induced Activated States of 5-Hydroxytryptamine-4 Receptors. *Molecular Pharmacology* **75**(4)**:** 982-990.

Perry SJ, Baillie GS, Kohout TA, McPhee I, Magiera MM, Ang KL*, et al.* (2002). Targeting of cyclic AMP degradation to beta 2-adrenergic receptors by beta-arrestins. *Science* **298**(5594)**:** 834-836.

Pierce KL, Premont RT, Lefkowitz RJ (2002). Seven-transmembrane receptors. *Nat Rev Mol Cell Biol* **3**(9)**:** 639-650.

Povsic TJ, Kohout TA, Lefkowitz RJ (2003). Beta-arrestin1 mediates insulin-like growth factor 1 (IGF-1) activation of phosphatidylinositol 3-kinase (PI3K) and anti-apoptosis. *J Biol Chem* **278**(51)**:** 51334-51339.

Qin K, Dong C, Wu G, Lambert NA (2011). Inactive-state preassembly of G(q)-coupled receptors and G(q) heterotrimers. *Nat Chem Biol* **7**(10)**:** 740-747.

Raehal KM, Walker JK, Bohn LM (2005). Morphine side effects in beta-arrestin 2 knockout mice. *J Pharmacol Exp Ther* **314**(3)**:** 1195-1201.

Rajagopal S, Rajagopal K, Lefkowitz RJ (2010). Teaching old receptors new tricks: biasing seven-transmembrane receptors. *Nat Rev Drug Discov* **9**(5)**:** 373-386.

Rasmussen SG, DeVree BT, Zou Y, Kruse AC, Chung KY, Kobilka TS*, et al.* (2011a). Crystal structure of the beta2 adrenergic receptor-Gs protein complex. *Nature* **477**(7366)**:** 549-555.

Rasmussen SGF, Choi H-J, Fung JJ, Pardon E, Casarosa P, Chae PS*, et al.* (2011b). Structure of a nanobody-stabilized active state of the β2 adrenoceptor. *Nature* **469**(7329)**:** 175-180.

Rasmussen SGF, Choi H-J, Rosenbaum DM, Kobilka TS, Thian FS, Edwards PC*, et al.* (2007). Crystal structure of the human β2 adrenergic G-protein-coupled receptor. *Nature* **450**(7168)**:** 383-387.

Reilander H, Boege F, Vasudevan S, Maul G, Hekman M, Dees C*, et al.* (1991). Purification and functional characterization of the human beta 2-adrenergic receptor produced in baculovirus-infected insect cells. *FEBS Lett* **282**(2)**:** 441-444.

Riitano D, Werge TM, Costa T (1997). A mutation changes ligand selectivity and transmembrane signaling preference of the neurokinin-1 receptor. *J Biol Chem* **272**(12)**:** 7646-7655.

Rosenbaum DM, Cherezov V, Hanson MA, Rasmussen SGF, Thian FS, Kobilka TS*, et al.* (2007). GPCR Engineering Yields High-Resolution Structural Insights into 2-Adrenergic Receptor Function. *Science* **318**(5854)**:** 1266-1273.

Rosenbaum DM, Rasmussen SGF, Kobilka BK (2009). The structure and function of G-protein-coupled receptors. *Nature* **459**(7245)**:** 356-363.

Ross EM, Maguire ME, Sturgill TW, Biltonen RL, Gilman AG (1977). Relationship between the beta-adrenergic receptor and adenylate cyclase. *J Biol Chem* **252**(16)**:** 5761-5775.

Ross EM, Wilkie TM (2000). GTPase-activating proteins for heterotrimeric G proteins: regulators of G protein signaling (RGS) and RGS-like proteins. *Annu Rev Biochem* **69:** 795-827.

Salom D, Lodowski DT, Stenkamp RE, Le Trong I, Golczak M, Jastrzebska B*, et al.* (2006). Crystal structure of a photoactivated deprotonated intermediate of rhodopsin. *Proc Natl Acad Sci U S A* **103**(44)**:** 16123-16128.

Samama P, Cotecchia S, Costa T, Lefkowitz RJ (1993). A mutation-induced activated state of the beta 2-adrenergic receptor. Extending the ternary complex model. *J Biol Chem* **268**(7)**:** 4625-4636.

Sarramegna V, Talmont F, Demange P, Milon A (2003). Heterologous expression of G-protein-coupled receptors: comparison of expression systems from the standpoint of large-scale production and purification. *Cell Mol Life Sci* **60**(8)**:** 1529-1546.

Satoh S, Matsumura H, Hayaishi O (1998). Involvement of adenosine A2A receptor in sleep promotion. *Eur J Pharmacol* **351**(2)**:** 155-162.

Scaramellini C, Leff P (1998). A three-state receptor model: predictions of multiple agonist pharmacology for the same receptor type. *Ann N Y Acad Sci* **861:** 97-103.

Scheerer P, Park JH, Hildebrand PW, Kim YJ, Krauss N, Choe HW*, et al.* (2008). Crystal structure of opsin in its G-protein-interacting conformation. *Nature* **455**(7212)**:** 497-502.

Serrano-Vega MJ, Magnani F, Shibata Y, Tate CG (2008). Conformational thermostabilization of the beta 1-adrenergic receptor in a detergent-resistant form. *Proceedings of the National Academy of Sciences* **105**(3)**:** 877-882.

Serrano-Vega MJ, Tate CG (2009). Transferability of thermostabilizing mutations between β-adrenergic receptors. *Molecular Membrane Biology* **26**(8)**:** 385-396.

Shi L, Javitch JA (2002). THE BINDING SITE OF AMINERGIC G PROTEIN–COUPLED RECEPTORS: The Transmembrane Segments and Second Extracellular Loop. *Annu. Rev. Pharmacol. Toxicol.* **42:** 437-467.

Shibata Y, White JF, Serrano-Vega MJ, Magnani F, Aloia AL, Grisshammer R*, et al.* (2009). Thermostabilization of the Neurotensin Receptor NTS1. *Journal of Molecular Biology* **390**(2)**:** 262-277.

Shimamura T, Shiroishi M, Weyand S, Tsujimoto H, Winter G, Katritch V*, et al.* (2011). Structure of the human histamine H1 receptor complex with doxepin. *Nature* **475**(7354)**:** 65-70.

Shukla AK, Manglik A, Kruse AC, Xiao K, Reis RI, Tseng WC*, et al.* (2013). Structure of active beta-arrestin-1 bound to a G-protein-coupled receptor phosphopeptide. *Nature* **497**(7447)**:** 137-141.

Sikorski RS, Hieter P (1989). A system of shuttle vectors and yeast host strains designed for efficient manipulation of DNA in Saccharomyces cerevisiae. *Genetics* **122**(1)**:** 19-27.

Simon MI, Strathmann MP, Gautam N (1991). Diversity of G proteins in signal transduction. *Science* **252**(5007)**:** 802-808.

Singh S, Hedley D, Kara E, Gras A, Iwata S, Ruprecht J*, et al.* (2010). A purified C-terminally truncated human adenosine A(2A) receptor construct is functionally stable and degradation resistant. *Protein Expr Purif* **74**(1)**:** 80-87.

Siu FY, He M, de Graaf C, Han GW, Yang D, Zhang Z*, et al.* (2013). Structure of the human glucagon class B G-protein-coupled receptor. *Nature* **499**(7459)**:** 444-449.

Smotrys JE, Linder ME (2004). Palmitoylation of intracellular signaling proteins: regulation and function. *Annu Rev Biochem* **73:** 559-587.

Stacey M, Lin HH, Gordon S, McKnight AJ (2000). LNB-TM7, a group of seven-transmembrane proteins related to family-B G-protein-coupled receptors. *Trends Biochem Sci* **25**(6)**:** 284-289.

Standfuss J, Xie G, Edwards PC, Burghammer M, Oprian DD, Schertler GF (2007). Crystal structure of a thermally stable rhodopsin mutant. *J Mol Biol* **372**(5)**:** 1179-1188.

Stevens B, Porta S, Haak LL, Gallo V, Fields RD (2002). Adenosine: a neuron-glial transmitter promoting myelination in the CNS in response to action potentials. *Neuron* **36**(5)**:** 855-868.

Stoffel RH, 3rd, Pitcher JA, Lefkowitz RJ (1997). Targeting G protein-coupled receptor kinases to their receptor substrates. *J Membr Biol* **157**(1)**:** 1-8.

Strange PG (2002). Mechanisms of inverse agonism at G-protein-coupled receptors. *Trends Pharmacol Sci* **23**(2)**:** 89-95.

Sullivan KA, Miller RT, Masters SB, Beiderman B, Heideman W, Bourne HR (1987). Identification of receptor contact site involved in receptor-G protein coupling. *Nature* **330**(6150)**:** 758-760.

Sun Y, Cheng Z, Ma L, Pei G (2002). Beta-arrestin2 is critically involved in CXCR4-mediated chemotaxis, and this is mediated by its enhancement of p38 MAPK activation. *J Biol Chem* **277**(51)**:** 49212-49219.

Tan Q, Zhu Y, Li J, Chen Z, Han GW, Kufareva I*, et al.* (2013). Structure of the CCR5 chemokine receptor-HIV entry inhibitor maraviroc complex. *Science* **341**(6152)**:** 1387-1390.

Tesmer JJ, Sunahara RK, Gilman AG, Sprang SR (1997). Crystal structure of the catalytic domains of adenylyl cyclase in a complex with Gsalpha.GTPgammaS. *Science* **278**(5345)**:** 1907-1916.

Thompson AA, Liu W, Chun E, Katritch V, Wu H, Vardy E*, et al.* (2012). Structure of the nociceptin/orphanin FQ receptor in complex with a peptide mimetic. *Nature* **485**(7398)**:** 395-399.

Tohgo A, Pierce KL, Choy EW, Lefkowitz RJ, Luttrell LM (2002). beta-Arrestin scaffolding of the ERK cascade enhances cytosolic ERK activity but inhibits ERK-mediated transcription following angiotensin AT1a receptor stimulation. *J Biol Chem* **277**(11)**:** 9429-9436.

Torvinen M, Marcellino D, Canals M, Agnati LF, Lluis C, Franco R*, et al.* (2005). Adenosine A2A receptor and dopamine D3 receptor interactions: evidence of functional A2A/D3 heteromeric complexes. *Mol Pharmacol* **67**(2)**:** 400-407.

Trejo J, Coughlin SR (1999). The cytoplasmic tails of protease-activated receptor-1 and substance P receptor specify sorting to lysosomes versus recycling. *J Biol Chem* **274**(4)**:** 2216-2224.

Van Dop C, Yamanaka G, Steinberg F, Sekura RD, Manclark CR, Stryer L*, et al.* (1984). ADP-ribosylation of transducin by pertussis toxin blocks the light-stimulated hydrolysis of GTP and cGMP in retinal photoreceptors. *J Biol Chem* **259**(1)**:** 23-26.

van Rhee AM, Jacobson K (1996). Molecular architecture of G protein-coupled receptors. *Drug Development Research* **37**(1)**:** 1-38.

Venkatakrishnan A, Deupi X, Lebon G, Tate C, Schertler G, Babu M (2013). Molecular signatures of G-protein-coupled receptors. *Nature* **494**(7436)**:** 185-194.

Volpini R, Dal Ben D, Lambertucci C, Marucci G, Mishra RC, Ramadori AT*, et al.* (2009). Adenosine A2A receptor antagonists: new 8-substituted 9-ethyladenines as tools for in vivo rat models of Parkinson's disease. *ChemMedChem* **4**(6)**:** 1010-1019.

Wacker D, Wang C, Katritch V, Han GW, Huang XP, Vardy E*, et al.* (2013). Structural features for functional selectivity at serotonin receptors. *Science* **340**(6132)**:** 615-619.

Wang C, Jiang Y, Ma J, Wu H, Wacker D, Katritch V*, et al.* (2013a). Structural basis for molecular recognition at serotonin receptors. *Science* **340**(6132)**:** 610-614.

Wang C, Wu H, Katritch V, Han GW, Huang XP, Liu W*, et al.* (2013b). Structure of the human smoothened receptor bound to an antitumour agent. *Nature* **497**(7449)**:** 338-343.

Warne T, Edwards PC, Leslie AG, Tate CG (2012). Crystal structures of a stabilized beta1-adrenoceptor bound to the biased agonists bucindolol and carvedilol. *Structure* **20**(5)**:** 841-849.

Warne T, Moukhametzianov R, Baker JG, Nehmé R, Edwards PC, Leslie AGW*, et al.* (2011). The structural basis for agonist and partial agonist action on a β1-adrenergic receptor. *Nature* **469**(7329)**:** 241-244.

Warne T, Serrano-Vega MJ, Baker JG, Moukhametzianov R, Edwards PC, Henderson R*, et al.* (2008). Structure of a β1-adrenergic G-protein-coupled receptor. *Nature* **454**(7203)**:** 486-491.

Weiss HM, Grisshammer R (2002). Purification and characterization of the human adenosine A(2a) receptor functionally expressed in Escherichia coli. *Eur J Biochem* **269**(1)**:** 82-92.

Weiss JM, Morgan PH, Lutz MW, Kenakin TP (1996). The cubic Ternary Complex Receptor-Occupancy Model I. Model Description. *J. theor. Biol.* **178:** 151-167.

Wess J (1997). G-protein-coupled receptors: molecular mechanisms involved in receptor activation and selectivity of G-protein recognition. *FASEB J* **11**(5)**:** 346-354.

West RE, Jr., Moss J, Vaughan M, Liu T, Liu TY (1985). Pertussis toxin-catalyzed ADP-ribosylation of transducin. Cysteine 347 is the ADP-ribose acceptor site. *J Biol Chem* **260**(27)**:** 14428-14430.

Wheatley M, Wootten D, Conner MT, Simms J, Kendrick R, Logan RT*, et al.* (2012). Lifting the lid on GPCRs: the role of extracellular loops. *Br J Pharmacol* **165**(6)**:** 1688-1703.

White JF, Noinaj N, Shibata Y, Love J, Kloss B, Xu F*, et al.* (2012). Structure of the agonist-bound neurotensin receptor. *Nature* **490**(7421)**:** 508-513.

Witherow DS, Garrison TR, Miller WE, Lefkowitz RJ (2004). beta-Arrestin inhibits NF-kappaB activity by means of its interaction with the NF-kappaB inhibitor IkappaBalpha. *Proc Natl Acad Sci U S A* **101**(23)**:** 8603-8607.

Wu B, Chien EY, Mol CD, Fenalti G, Liu W, Katritch V*, et al.* (2010). Structures of the CXCR4 chemokine GPCR with small-molecule and cyclic peptide antagonists. *Science* **330**(6007)**:** 1066-1071.

Wu H, Wacker D, Mileni M, Katritch V, Han GW, Vardy E*, et al.* (2012). Structure of the human kappa-opioid receptor in complex with JDTic. *Nature* **485**(7398)**:** 327-332.

Xu F, Wu H, Katritch V, Han GW, Jacobson KA, Gao ZG*, et al.* (2011). Structure of an agonist-bound human A2A adenosine receptor. *Science* **332**(6027)**:** 322-327.

Xu K, Bastia E, Schwarzschild M (2005). Therapeutic potential of adenosine A(2A) receptor antagonists in Parkinson's disease. *Pharmacol Ther* **105**(3)**:** 267-310.

Yao XJ, Velez Ruiz G, Whorton MR, Rasmussen SGF, DeVree BT, Deupi X*, et al.* (2009). The effect of ligand efficacy on the formation and stability of a GPCR-G protein complex. *Proceedings of the National Academy of Sciences* **106**(23)**:** 9501-9506.

Yeliseev AA, Wong KK, Soubias O, Gawrisch K (2005). Expression of human peripheral cannabinoid receptor for structural studies. *Protein Sci* **14**(10)**:** 2638-2653.

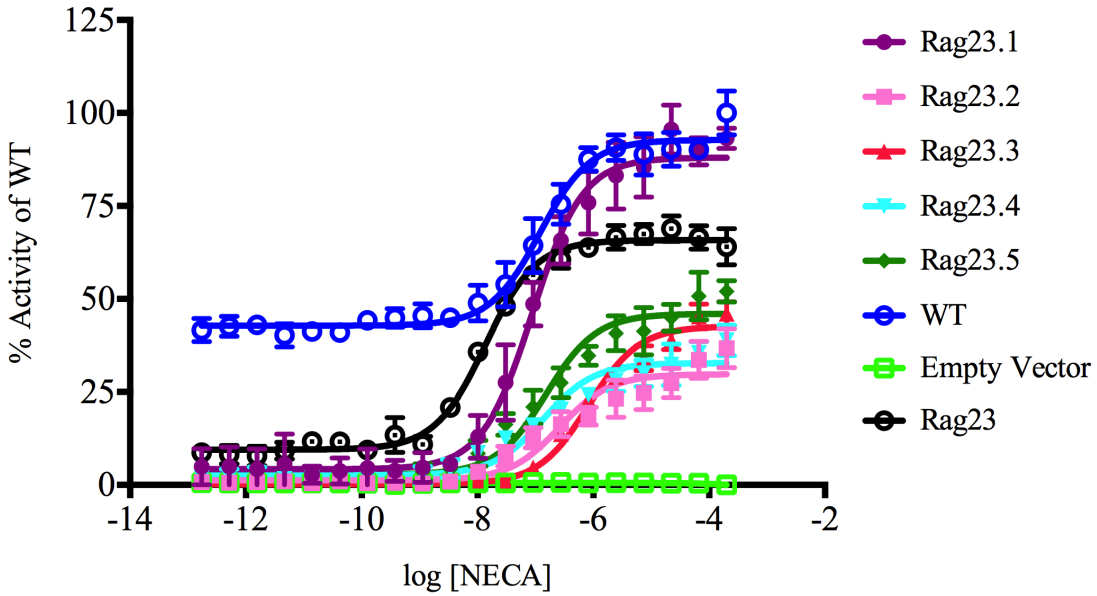
Zhang C, Srinivasan Y, Arlow DH, Fung JJ, Palmer D, Zheng Y*, et al.* (2012). High-resolution crystal structure of human protease-activated receptor 1. *Nature* **492**(7429)**:** 387-392.

Zhang J, Barak LS, Anborgh PH, Laporte SA, Caron MG, Ferguson SS (1999). Cellular trafficking of G protein-coupled receptor/beta-arrestin endocytic complexes. *J Biol Chem* **274**(16)**:** 10999-11006.

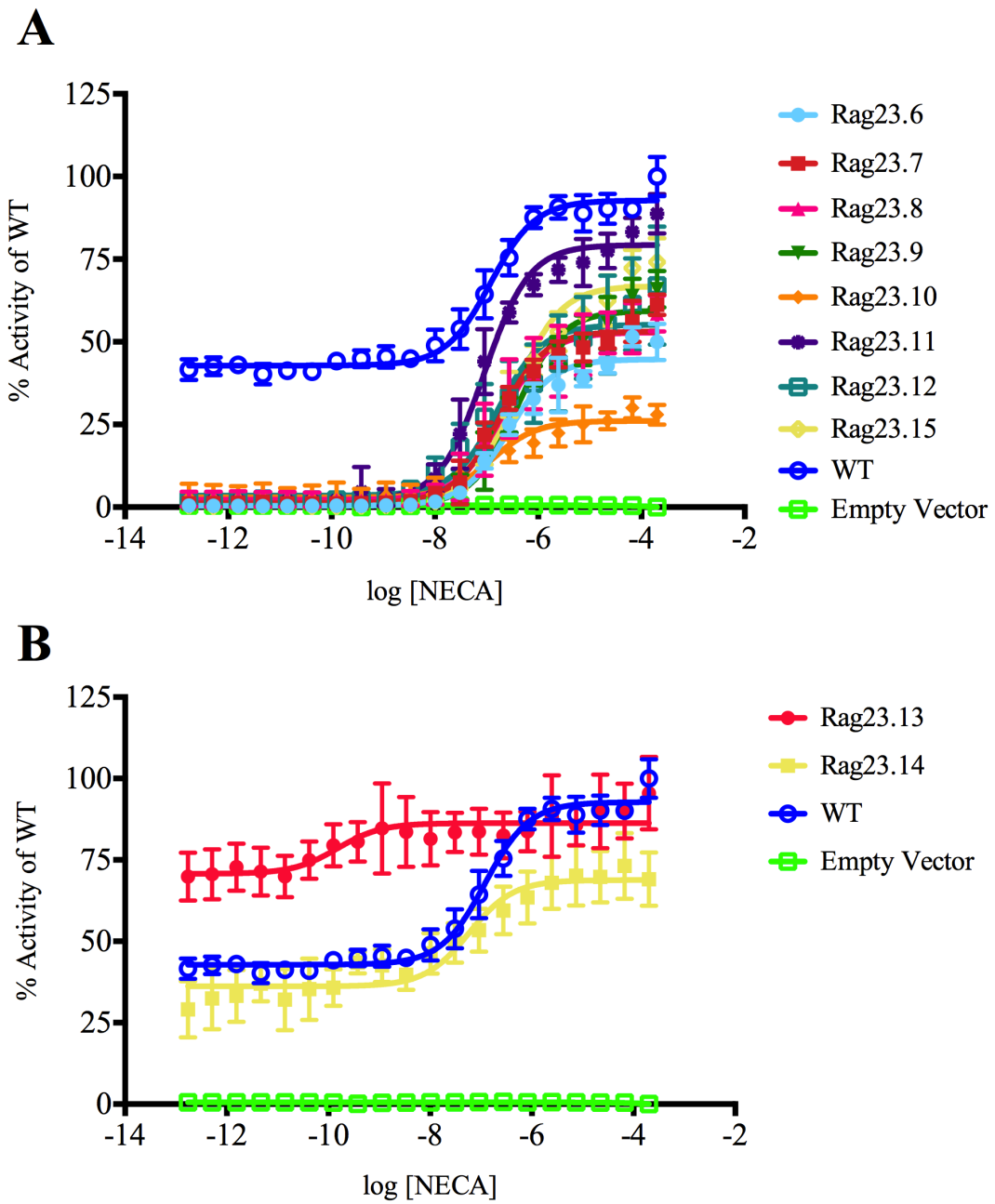
Zou Y, Weis WI, Kobilka BK (2012). N-terminal T4 lysozyme fusion facilitates crystallization of a G protein coupled receptor. *PLoS One* **7**(10)**:** e46039.

6 Appendix

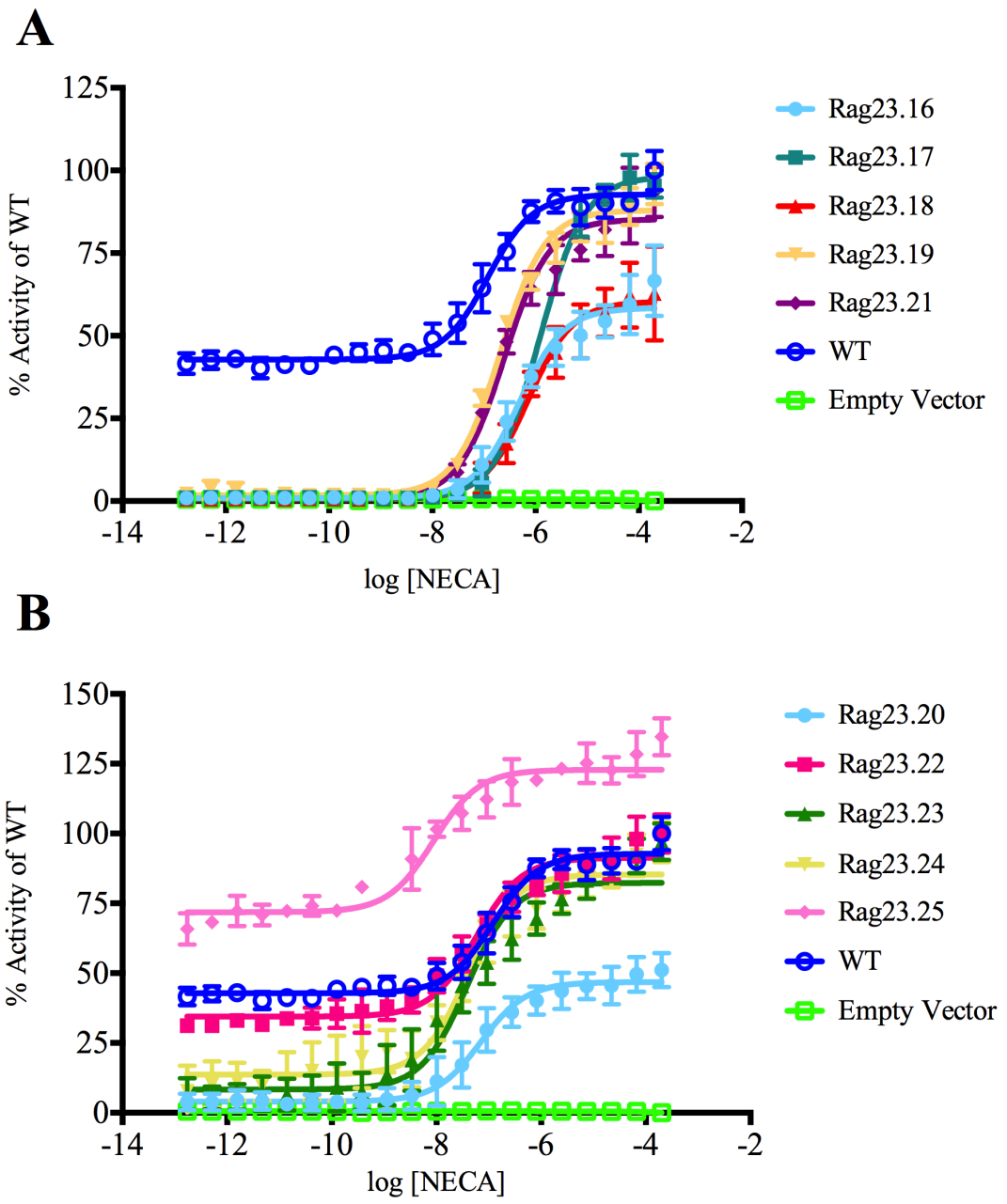
6.1 Graphical data for all the Rag23 intermediate mutants



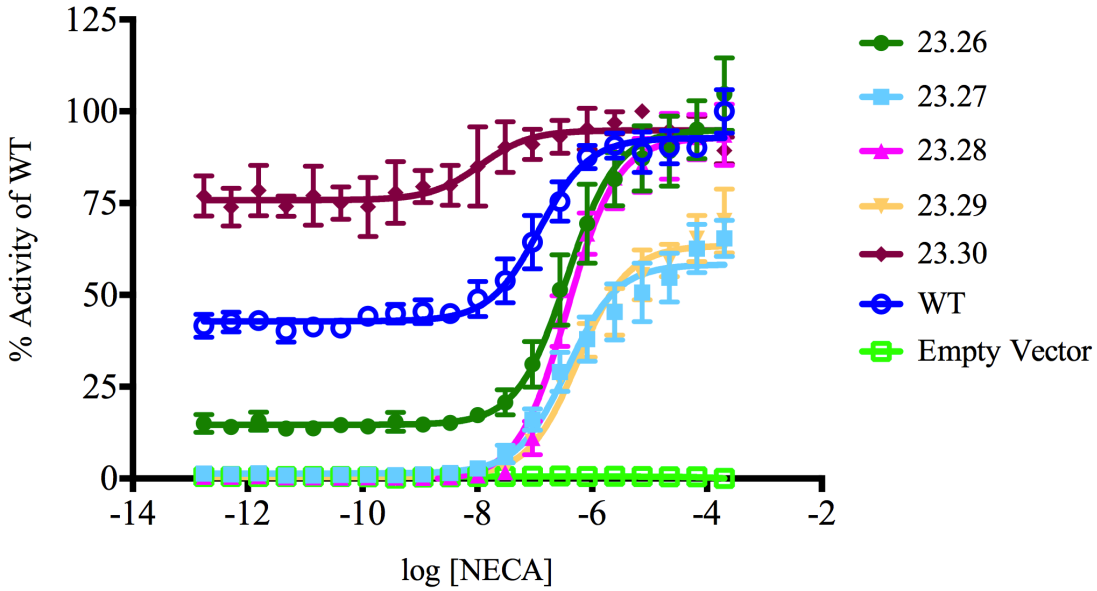
NECA-induced activity of the WT $A_{2A}R$, Rag23 and the quadruple mutants intermediate between the WT and Rag23. See Table 4-3 for the precise details of each mutant. The receptor constructs were expressed in the MMY24 *S. cerevisiae* strain using the p306GPD vector. The activity of cells containing empty vector is shown as a control.



NECA-induced activity of the WT $A_{2A}R$ and the triple mutants intermediate between the WT and Rag23. See Table 4-3 for the precise details of each mutant. The receptor constructs were expressed in the MMY24 *S. cerevisiae* strain using the p306GPD vector. The activity of cells containing empty vector is shown as a control.



NECA-induced activity of the WT $A_{2A}R$ and the double mutants intermediate between the WT and Rag23. See Table 4-3 for the precise details of each mutant. The receptor constructs were expressed in the MMY24 *S. cerevisiae* strain using the p306GPD vector. The activity of cells containing empty vector is shown as a control.



NECA-induced activity of the WT $A_{2A}R$ and the single mutants intermediate between the WT and Rag23. See Table 4-3 for the precise details of each mutant. The receptor constructs were expressed in the MMY24 *S. cerevisiae* strain using the p306GPD vector. The activity of cells containing empty vector is shown as a control.

6.2 Permission to republish third party copyrighted work from chapter 3

RightsLink | Copyright Clearance Center

Thank You For Your Order!

Dear Mr. Nicolas Bertheleme,

Thank you for placing your order through Copyright Clearance Center's RightsLink service. John Wiley and Sons has partnered with RightsLink to license its content. This notice is a confirmation that your order was successful.

Your order details and publisher terms and conditions are available by clicking the link below:
http://s100.copyright.com/CustomerAdmin/PLF.jsp?ref=bd165095-63e4-48ee-92fa-5ce6ad19f551

Order Details
Licensee: Nicolas Bertheleme
License Date: Nov 13, 2013
License Number: 3267011437485
Publication: British Journal of Pharmacology
Title: Loss of constitutive activity is correlated with increased thermostability of the human adenosine A2A receptor
Type Of Use: Dissertation/Thesis
Total: 0.00 USD

To access your account, please visit https://myaccount.copyright.com.

Please note: Online payments are charged immediately after order confirmation; invoices are issued daily and are payable immediately upon receipt.

To ensure we are continuously improving our services, please take a moment to complete our customer satisfaction survey.

B.1:v4.2



+1-877-622-5543 / Tel: +1-978-646-2777

6.3 Yeast transformation protocol

1. Pick a single yeast colony and grow in 5mls medium overnight (shaking at 30^{o}C) which should give a saturated culture (approx. 1x10^{8} cells/ml).

2. Next morning, make a 1/100 dilution into 100mls and grow for 4-8 hours (approx. 2-3 generations; final density approx. 1x10^{7} cells/ml).

3. Spin at 4000 r.p.m. for 1 min. to harvest.

4. Wash in sterile water, and reharvest.

5. Resuspend cells in 1ml LiAc-TE (approx. 1x10^{9} cells/ml).

6. Take 50ml cells per transformation, and add 5ml ssDNA.

7. Add 1mg DNA to be transformed.

8. Add 300ml LiAc/PEG/TE and mix.

9. Incubate either at R.T. or 30^{o}C with occasional (or gentle) agitation for 10 min.

10. Heat shock in 42^{o}C water bath for 20 min.

11. Remove, and plate 50ml directly onto selective plates.

The method is so efficient, you don't need to plate out the whole transformation onto a small petri dish.

12. For chromosomal integrations, use ~5 ug DNA and linearize in the selectable marker gene (using eg. *Nsi*I or *Stu*I for *URA3*); you may need to plate out all the transformation mixture as the efficiency is lower than for episomal plasmids.

Solutions

Make up: 1) 1M LiAc

2) 50% PEG3350

3) 10xTE pH7.5 (0.1M Tris-Cl pH7.5, 0.01M EDTA)

LiAcTE is 5mls 1M LiAc, 5mls 10xTE, 40mls H_2O

LiPEG-TE is 5mls 1M LiAc, 5mls 10xTE, 40mls 50% PEG

ssDNA	Sigma D-9156 Salmon Testes DNA aliquoted into microfuge tubes, boiled for 10 min, cooled immediately in ice and frozen (for best efficiency, don't use aliquots more than twice).